AIAA 80-0665R

Buckling of Shells—Pitfall for Designers

David Bushnell
Lockheed Palo Alto Research Laboratory, Palo Alto, Calif.

1. Introduction

Purpose

IN order to produce efficient, reliable designs and to avoid unexpected catastrophic failure of structures of which thin shells are important components, the engineer must understand the physics of shell buckling. The objective of this survey is to convey to the reader a "feel" for shell buckling, whether it be due to nonlinear collapse, bifurcation buckling, or a combination of these modes. This intuitive understanding of instability is communicated by a large number of examples involving practical shell structures which may be stiffened, segmented, or branched and which have complex wall constructions. With such intuitive knowledge the engineer will have an improved ability to foresee situations in which buckling might occur and to modify a design to avoid it. He will be able to set up more appropriate models for tests and analytical predictions. The emphasis here is not on the development of equations for the prediction of instability. For such material the reader is referred to the book by Brush and Almroth.[11]

Emphasis is given here to nonlinear behavior caused by a combination of large deflections and plasticity. Also illustrated are stress redistribution effects, stiffener and load-path eccentricity effects, local vs general instability, imperfection sensitivity, and modal interaction in optimized structures. Scattered throughout the text are tips on modeling for computerized analysis. The survey is divided into nine major sections describing: 1) several examples of catastrophic failure of expensive shell structures; 2) the basics of buckling behavior; 3) "classical" buckling and imperfection sensitivity; 4) nonlinear collapse and the appropriateness of linear bifurcation buckling analyses for general shells; 5) bifurcation buckling with significant nonlinear prebuckling behavior; 6) effects of boundary conditions, load eccentricity, transverse shear deformation, and stable postbuckling behavior; 7) optimization of buckling-critical structures with consequent modal interaction; 8) a suggested design method for axially compressed cylinders with stiffeners, internal pressure, or other special characteristics; and 9) two examples in which sophisticated buckling analyses are required in order to derive improved designs. The paper focuses on static buckling problems.

Some Catastrophic Failures

To the layman buckling is a mysterious, perhaps even awe-inspiring, phenomenon that transforms objects originally imbued with symmetrical beauty into junk (Fig. 1.1). Occasionally unaware of the possibility of buckling, engineers have designed structures with inadequate safety margins (Fig. 1.2). The large cylindrical tower on the left in Fig. 1.3 failed in 1956[1] because of buckling under internal hydrostatic pressure of a torispherical end closure at its lower end. A 38 m tall steel water tower, the tank portion of which is sketched in Fig. 1.4, collapsed in 1972[2,3] when it was being filled for the first time. The collapse of the entire tower was triggered by local instability in the conical portion of the tank at the deepest water level in a mode similar to that displayed for the Mylar laboratory model photographed in Fig. 1.5.[4] According to the prediction given in Fig. 1.6,[5] nonsymmetric bifurcation buckling occurs at a load factor $p_{nb}=0.943$, slightly below that corresponding to axisymmmetric collapse,

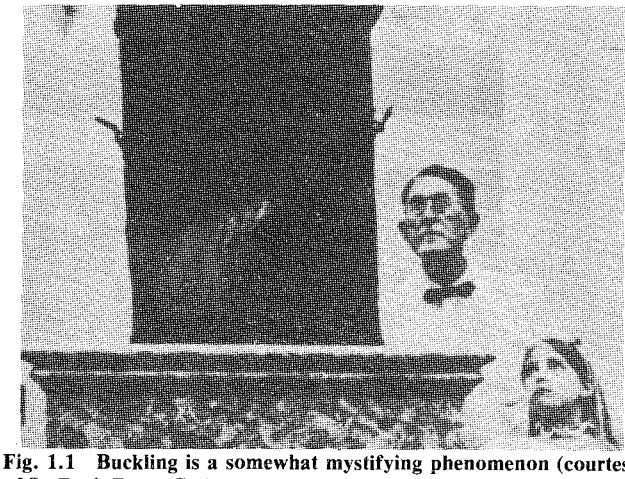

Fig. 1.1 Buckling is a somewhat mystifying phenomenon (courtesy of St. Regis Paper Co.).

David Bushnell joined Lockheed Missiles & Space Company, after receiving his B.S. and M.S. degrees in aerospace engineering from the Massachusetts Institute of Technology in 1961. In 1965, while at Lockheed, he earned his Ph.D. in Aeronautics and Astronautics at Stanford University. He then began extensive investigations of the stress, buckling, and vibration behavior of thin shell structures. That work has resulted in over 40 papers and ultimately in the development of the BOSOR4 and BOSOR5 computer programs, widely used codes for the stress, buckling, and vibration analysis of shells of revolution. Many of the examples in this survey article are based on applications of these computer programs to practical problems involving complex shell structures. In 1975 Dr. Bushnell received the ONR/AIAA Structural Mechanics Research Award, the topic of his investigation being "Stress, Buckling, and Vibration of Hybrid Bodies of Revolution." He served as Associate Editor of the *AIAA Journal* from 1977 to 1979 and was a member of the AIAA Structures Technical Committee 1978 to 1979. Dr. Bushnell was elected the Outstanding Engineer of the AIAA San Francisco Chapter for the year 1978, and is an Associate Fellow.

Presented as Paper 80-0665, the SDM Lecture, at the AIAA/ASME/ASCE/AHS 21st Structures, Structural Dynamics and Materials Conference, Seattle, Wash., May 12-14, 1980; submitted June 11, 1980; revision received April 17, 1981.

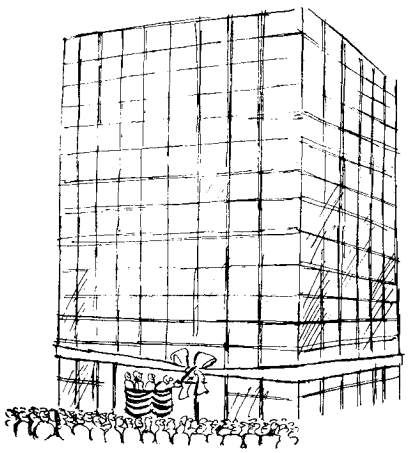

Fig. 1.2 Structures have been built with...

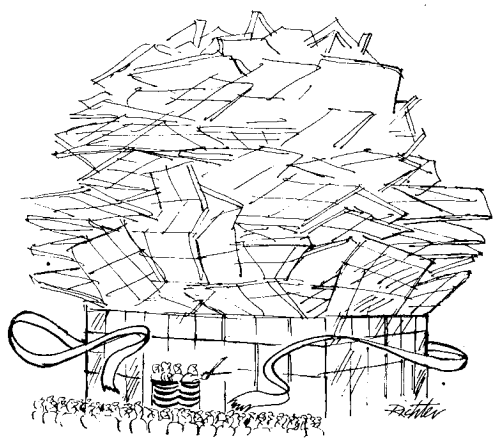

...insufficient margins of safety. (Drawing by Richter, © 1974 by The New Yorker Magazine, Inc.).

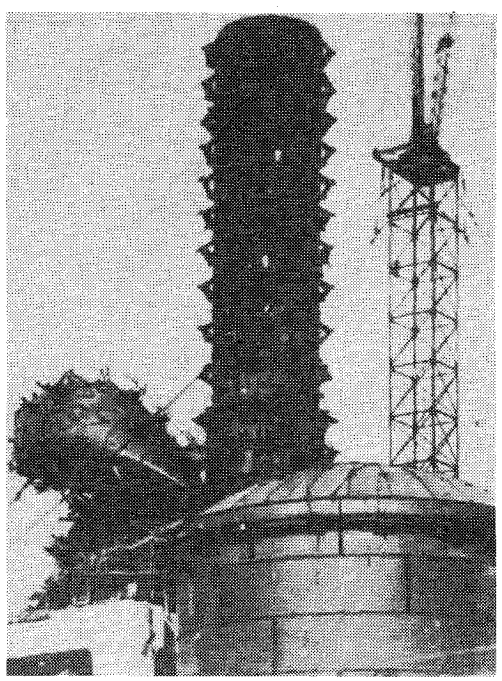

Fig. 1.3a Failure of a large (15 m diam) vessel due to buckling of the bottom torispherical end under internal pressure.

Fig. 1.3b Fragments of the bottom torispherical end (from Harding, A. G. and Ehmke, E. F., *Proceedings of the American Petroleum Institute*, Vol. 42, Sec. 3, 1962, p. 107).

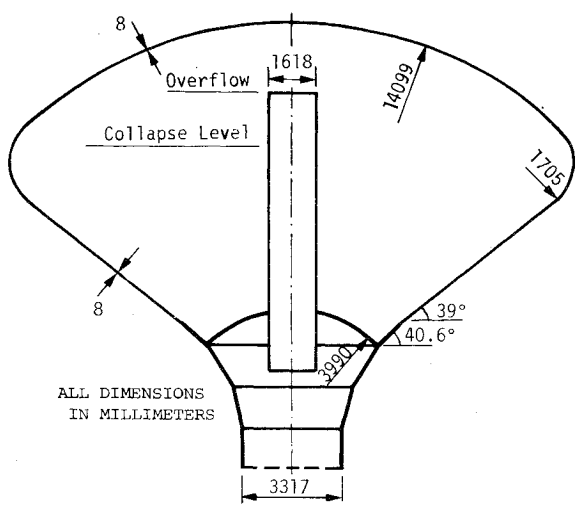

Fig. 1.4 Geometry of large steel water tank that failed in Belgium in 1972 (from Vandepitte[3]).

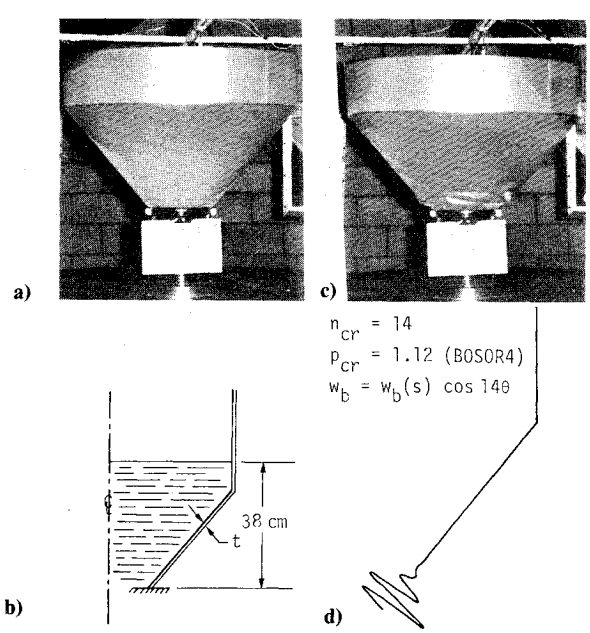

Fig. 1.5 Elastic buckling of conical water tank: a) specimen before buckling; b) tank geometry and water level; c) postbuckled specimen; and d) predicted bifurcation buckling load factor and mode from linear theory (photographs courtesy of Dr. G. Lagae, University of Ghent, Belgium).

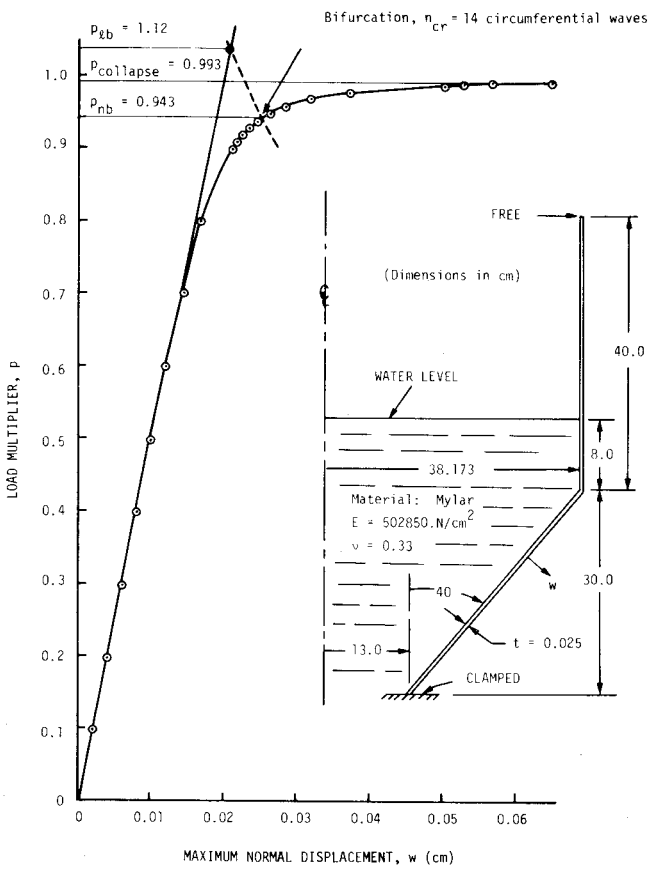

Fig. 1.6 Load-maximum-normal-deflection curve for conical water tank, with bifurcation points P_{lb} from linear and P_{nb} from nonlinear prebuckling theory and axisymmetric collapse load factor, $P_{collapse}$.

$p_{collapse} = 0.993$. A factor of unity corresponds to the water level at which the Mylar specimen failed in the test, a condition depicted in the sketch in Fig. 1.6.

On Jan. 24, 1980, over 100 stainless-steel wine storage tanks at the Wente Brothers winery in Livermore, Calif. buckled during an earthquake, a shown in Fig. 1.7. The tanks that failed were completely filled, so that fluid sloshing is not part of this problem. Buckling is due to the horizontal component of the ground motion. The inertial reaction of the wine creates a moment at the base of the tank which must be reacted to by a $\cos\theta$ axial membrane resultant. As the ground oscillates through several cycles in all directions, all locations around the circumference of the cylindrical shell at the base become axially compressed at some time during an earthquake. Thus, postbuckling damage is usually visible along the entire circumference. The problem is similar to that of the conical water tank shown in Figs. 1.5 and 1.6: buckling occurs under axial compression combined with circumferential tension, creating buckles that are circumferentially elongated. In many cases the wine tanks are perfectly axisymmetrically buckled at the base, as seen in Fig. 1.7a. The proximity of the nonsymmetric bifurcation failure and axisymmetric collapse demonstrated in Fig. 1.6 for the conical water tank is suggested in this case as well by the modes of failure of the wine tanks. Shih and Babcock[6] and Clough and Niwa[7] have studied this problem and the related problem of buckling during earthquakes of large water and oil storage tanks in which sloshing is important. The Nuclear Regulatory Commission is interested in the development of methods for the calculation of buckling loads of large steel reactor containment vessels under various dynamic loads, including those from an earthquake.[8] Figure 1.8 illustrates the predicted behavior of one such shell in which body forces from 1 g vertical and 1 g horizontal ground acceleration components are applied to the structure as if they were static, and a buckling load factor λ_{cr} is computed from the BOSOR4 computer program[9] as if the membrane stress distribution along the "worst" (most axially compressed) meridian were axisymmetric.

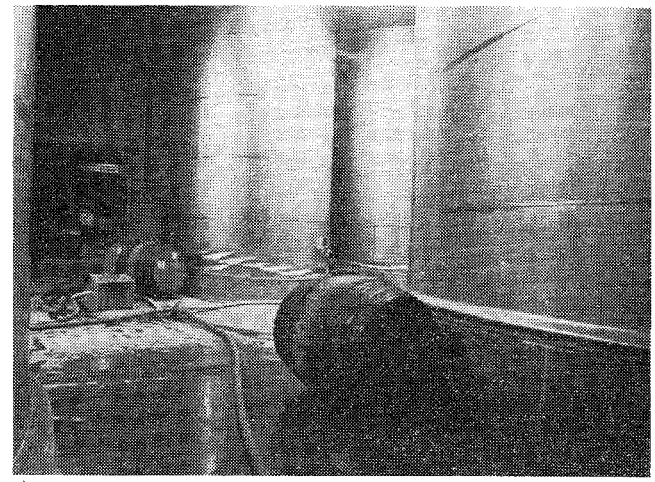

a)

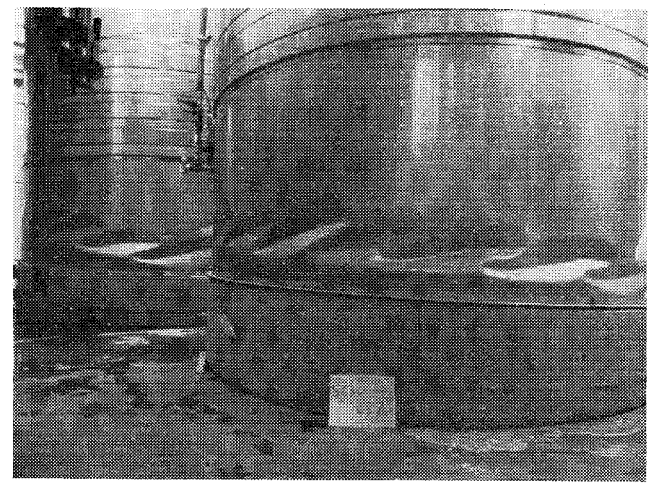

b)

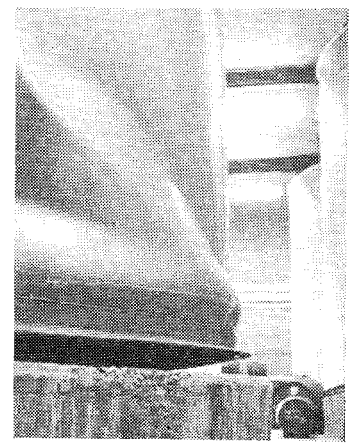

c)

Fig. 1.7 Stainless-steel wine tanks buckled at the Wente Brothers Winery in the Livermore, Calif., earthquake of Jan. 24, 1980; buckled tanks were all completely filled (photographs courtesy of J. Skogh). a) Nonsymmetric (left, background) and axisymmetric (right, foreground) buckling; b) nonsymmetrically buckled tanks; c) detail of local lifting at foundation.

In Fig. 1.9 is illustrated a local buckling failure of a large, expensive, semisandwich, corrugated ring-stiffened payload shroud (a and b) which was subjected to axial compression and bending. The shroud failed unexpectedly during proof testing because of local buckling near a field joint (c and d).[10] In short regions on either side of the field joint, where the external corrugations are cut away as shown in Fig. 1.9d, the axial load path is deflected inward from the neutral axis of the cross section of the combined corrugations and skin to the middle surface of the skin and doubler. This local inward deflection of the axial load path creates under axial compression the localized hoop compression that causes nonsymmetric bifurcation buckling in a mode shown in Fig. 1.9c. Because of the short axial length of the circumferentially compressed region, the critical mode has a rather large number of circumferential waves.

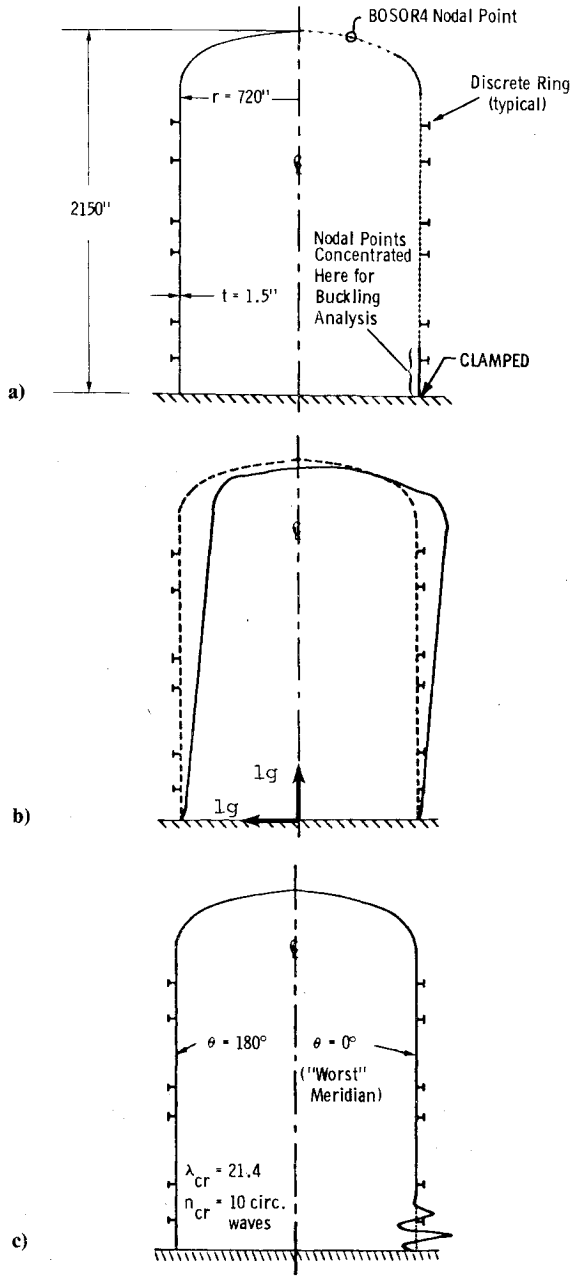

Fig. 1.8 Buckling of nuclear reactor steel containment vessel due to earthquake: 1) BOSOR4 discretized model; b) prebuckling deformations due to 1 *g* vertical and 1 *g* horizontal ground acceleration components; c) buckling mode and load factor λ_{cr}.

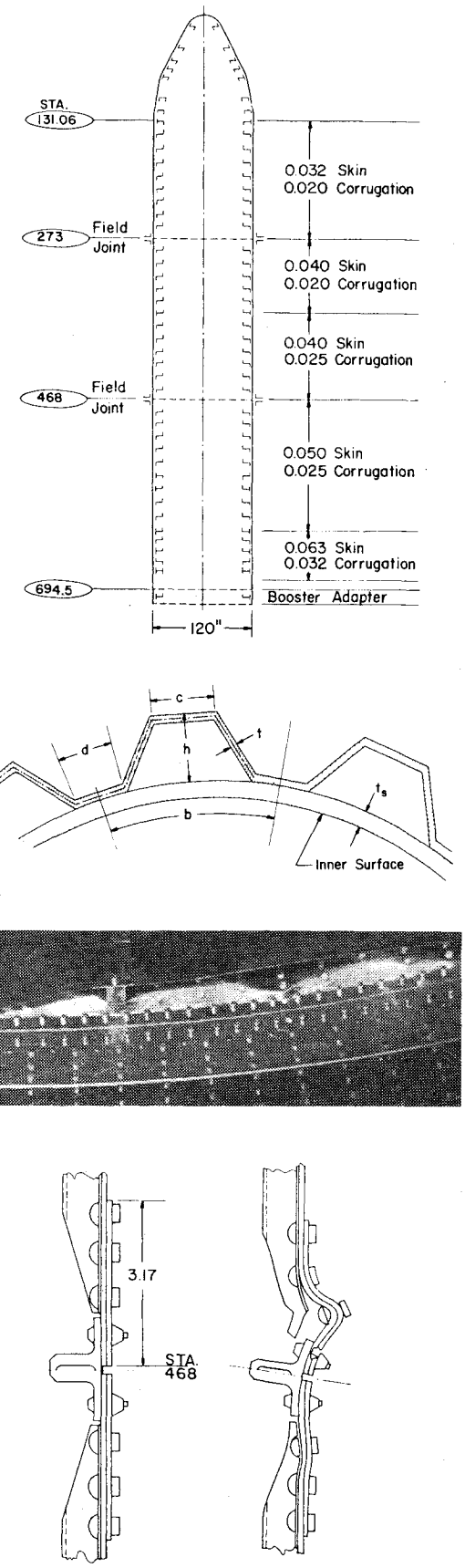

Fig. 1.9 Local failure of a large payload shroud under axial compression and bending. Buckling is caused by the narrow band of circumferential compression arising from the inward excursion of the axial load path near the field joint at station 468 (from Bushnell[10]). a) Typical ring-stiffened rocket payload shroud configuration; b) corrugated wall; c) interior view of portion of complete shroud buckled locally next to field joint at station 468 (see Fig. 1.9a), three waves are visible; d) field joint geometry and buckle configuration.

2. Some Buckling Basics

Why Do Shells Buckle?

The property of thinness of a shell wall has a consequence that is pointed out in Ref. 14: The membrane stiffness is in general several orders of magnitude greater than the bending stiffness. A thin shell can absorb a great deal of membrane strain energy without deforming too much. It must deform much more in order to absorb an equivalent amount of bending strain energy. If the shell is loaded in such a way that most of its strain energy is in the form of membrane compression, and if there is a way that this stored-up membrane energy can be converted into bending energy, the shell may fail rather dramatically in a process called "buckling" as it exchanges its membrane energy for bending energy. Very large deflections are generally required to convert a given amount of membrane energy into bending energy. The way in which buckling occurs depends on how the shell is loaded and on its geometrical and material properties. The prebuckling process is often nonlinear if there is a reasonably large percentage of bending energy being stored in the shell throughout the loading history.

What is Buckling?

To most laymen the word "buckling" evokes an image of failure of a structure which has been compressed in some way. Pictures and perhaps sounds come to mind of sudden, catastrophic collapse involving very large deformations. From a scientific and engineering point of view, however, the interesting phases of buckling phenomena generally occur before the deformations are very large when, to the unaided eye, the structure appears to be undeformed or only slightly deformed.

In the static analysis of perfect structures, the two phenomena loosely termed "buckling" are: 1) collapse at the maximum point in a load vs deflection curve, and 2) bifurcation buckling.

These two types of instability failure are illustrated in Figs. 2.1 and 2.2. The rather thick axially compressed cylinder shown in Fig. 2.1 deforms approximately axisymmetrically along the equilibrium path 0A until a maximum or collapse load λ_L is reached at point A. If the axial load λ is not sufficiently relieved by the reduction in axial stiffness, the perfect cylinder will fail at this collapse load, following either path ABC along which it continues to deform axisymmetrically or some other path ABD along which it first deforms axisymmetrically from A to B and then nonaxisymmetrically from B to D. Nonlinear buckling or "snap-through" occurs at point A and bifurcation buckling at point B. The equilibrium path 0ABC, corresponding to the symmetric mode of deformation is called the fundamental or primary or prebuckling path and the postbifurcation equilibrium path BD, corresponding to the nonaxisymmetric mode of deformation, is called the secondary or postbuckling path. Buckling of either the collapse or bifurcation type may occur at loads for which some or all of the structural material has been stressed beyond its proportional limit. The example in Fig. 2.1 is somewhat unusual in that the bifurcation point B is shown to occur after the collapse point has been reached. In this particular case, therefore, bifurcation buckling is of less engineering significance than axisymmetric collapse.

A perhaps more commonly occurring situation is illustrated in Fig. 2.2a. The bifurcation point B is between 0 and A. If the fundamental path 0AC corresponds to axisymmetric deformation and BD to nonaxisymmetric deformation, the initial failure of the structure would generally be characterized by rapidly growing nonaxisymmetric deformations. In this case the collapse load of the perfect structure λ_L is of less engineering significance than the bifurcation point λ_C.

In the case of real structures which contain unavoidable imperfections, there is no such thing as true bifurcation buckling. The actual structure will follow a fundamental path

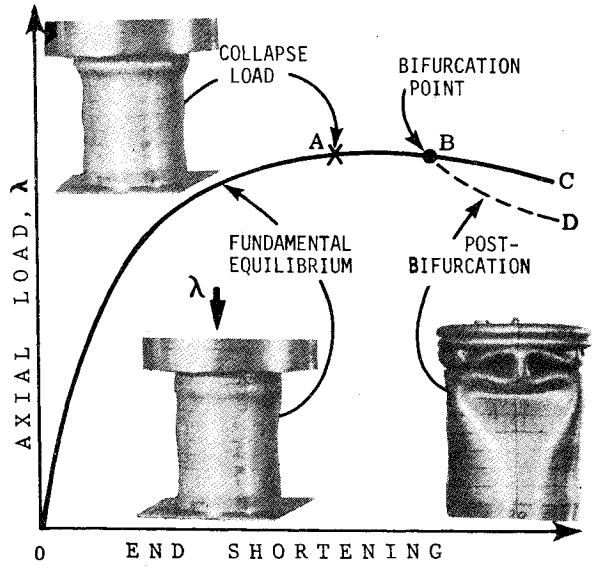

Fig. 2.1 Load/end-shortening curve with collapse load A, bifurcation point B, and postbifurcation equilibrium path BD (photographs courtesy of Sobel and Newman[87]).

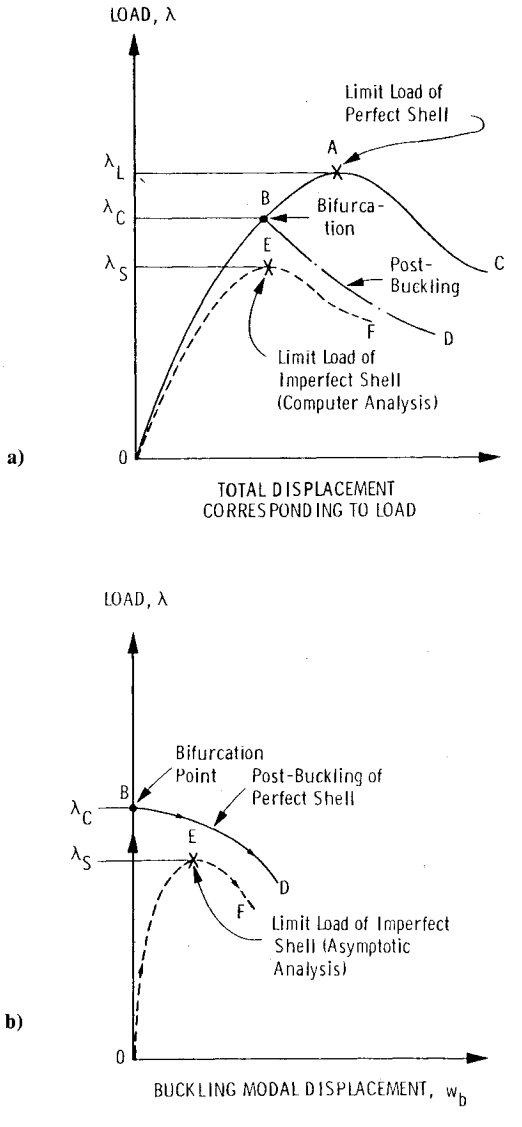

Fig. 2.2 Load-deflection curves showing limit and bifurcation points. a) General nonlinear analysis. b) Asymptotic analysis.

0EF, with the failure corresponding to the "snap-through" at point E at the collapse load λ_S. If point B in Fig. 2.2a corresponds to bifurcation into a nonsymmetric buckling mode, the collapse at E will involve significant nonsymmetric displacement components. Although true bifurcation buckling is fictitious, the bifurcation buckling analytical model is valid in that it is computationally convenient and economical and often leads to a good approximation of the actual failure load and mode.

Various Types of Bifurcation Buckling

In Fig. 2.2b the load is plotted as a function of amplitude of the bifurcation buckling mode. Since the bifurcation buckling mode is orthogonal to the prebuckling displacement pattern of the perfect shell, its amplitude remains zero until the bifurcation point B is reached. The curve BD in Fig. 2.2b implies that the postbuckling state is unstable: the load-carrying capability λ decreases with increasing amplitude of the bifurcation buckling mode.

All real structures are imperfect. The imperfection shape is, in general, not orthogonal to the bifurcation buckling mode. If one expressed the deformation of the imperfect structure as a sum of two components, the fundamental prebuckling equilibrium state of the perfect structure plus the bifurcation buckling mode of the perfect structure (presumed here to be unique), then one would obtain the curve 0EF in Fig. 2.2b if one plotted the amplitude of the bifurcation modal component vs the load for the imperfect structure. The amplitude of the bifurcation modal component would increase at an increasing rate until instability via nonlinear "snap-through"or collapse would occur at the reduced load λ_S. The difference between the critical bifurcation load λ_C of the perfect structure and the collapse load λ_S of the imperfect structure depends on the amplitude of the initial imperfection w_{b0}. A chart of λ_S/λ_C vs w_{b0} would characterize the sensitivity of the maximum load λ_S to initial geometrical imperfections. According to the jargon that has become accepted over the years, the structure to which the curves in Fig. 2.2b correspond is called "imperfection sensitive" because imperfections reduce its maximum load-carrying capability. (Of course, it is not the *structure* that is sensitive to imperfections, but the maximum *load* it can safely support!)

Not all structures nor mathematical models of them behave as shown in Fig. 2.2b. Figure 2.3 shows various types of postbuckling behavior. A linearized model of elastic stability, that is, an eigenvalue formulation of the buckling problem, implies a load-deflection behavior shown in Fig. 2.3a: The amplitude of the eigenvector, the bifurcation buckling mode, is indeterminate, which implies that the load λ remains constant $\lambda=\lambda_C$ with increasing modal deflections w_b. The equilibrium path for the slightly imperfect structure follows the rectangular hyperbolic path,

$$w_b = w_{b0}/(\lambda_C/\lambda - 1) \tag{1}$$

shown as a dotted line in Fig. 2.3a.

If nonlinear postbuckling effects are accounted for, equilibrium paths for most structures have the forms shown in Figs. 2.3b-d. The asymmetric nature of the curves in Fig. 2.3b indicates that the structure continues to carry loads above the bifurcation load λ_C if it is forced to buckle one way, but collapses if allowed to buckle the other. An example of this type of behavior is a structure with parts that move relative to each other as buckling proceeds in such a way that these parts come in contact and support each other for positive deflections but move away from each other and form gaps for similar negative deflections. Specifically, a built-up panel consisting of a flat sheet riveted to a corrugated sheet is such a structure. Roorda[15] has demonstrated this asymmetric postbuckling behavior for perfect and imperfect frames with eccentric loads. His results are summarized in Ref. 11. The symmetric stable postbuckling behavior displayed in Fig. 2.3c is typical of axially compressed columns and isotropic flat plates. The perfect column or plate loaded precisely in its neutral axis or surface buckles either way with equal ease and the postbuckled equilibrium state is stable. The symmetric unstable postbuckling behavior shown in Fig. 2.3d is typical of the early postbifurcation regimes of axially compressed thin cylindrical shells and externally pressurized thin spherical shells.

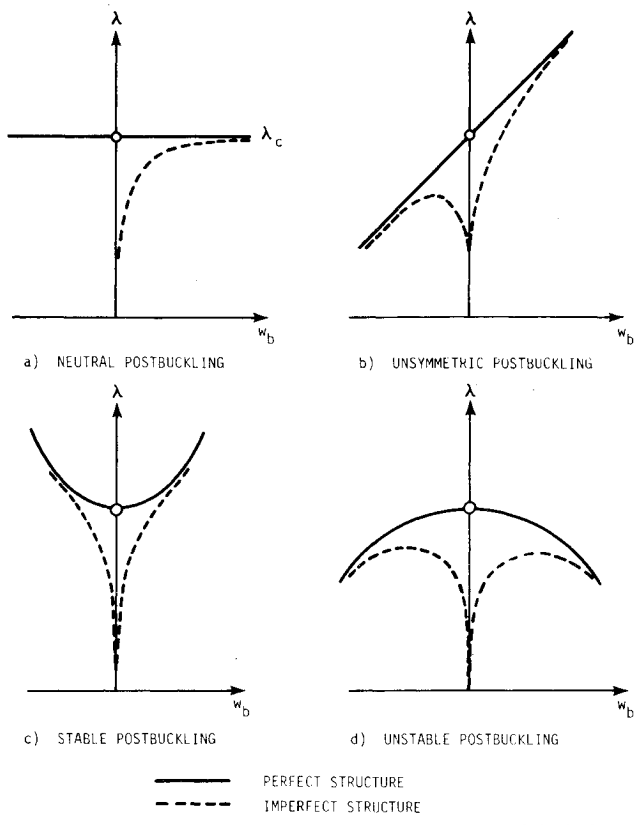

Fig. 2.3 Different types of load-displacement relations (λ is the load, w_b the buckling modal displacement).

Capsule of Recent Progress in Buckling Analysis

Recent progress in our capability to predict buckling failure can be categorized into three main areas:

1) Development of asymptotic postbuckling theories and applications of these theories to specific classes of structures, such as simple plates, shells, and panels.[16-18]

2) Development of general-purpose computer programs for calculation of static and dynamic behavior of structures, including large deflections, large strains, and nonlinear material effects.[19-21]

3) Development of special-purpose computer programs for limit-point axisymmetric buckling and nonaxisymmetric bifurcation buckling of axisymmetric structures.[9,22-24]

Asymptotic Analysis

The asymptotic analyses surveyed in Refs. 16-18 rest on theoretical foundations established by Koiter,[25] whose general elastic postbifurcation theory leads to an expansion for the load parameter λ in terms of the buckling modal amplitude w_b which is valid in the neighborhood of the critical bifurcation point in (λ, w_b) space. The primary aims of the asymptotic analyses are to calculate the maximum loads for perfect and imperfect structures. These analyses have contributed vital physical insights into the buckling process and the effect of structural or loading imperfections on this process.

General Nonlinear Analysis

The general-purpose computer programs in widespread use since the early 1970s and presently being written are based on principles of continuum mechanics established for the most

part by the late 1950s and set forth in several texts.[26-31] The structural continuum is discretized into finite elements as described in the texts[32-35] and various strategies are employed to solve the resulting nonlinear problem.[19] The nonlinearity is due to moderately large or very large deflections and nonlinear material behavior. Various plasticity models are described in texts, conference proceedings, and survey articles identified in Ref. 19. The primary aim of this vast body of work, most of which was done in the 1970s, has been to produce reliable analysis methods and computer programs for use by engineers and designers. Thus, the emphasis in the literature just cited is not primarily on the acquisition of new physical insight into buckling and postbifurcation phenomena, but on the creation of tools that can be used to determine the equilibrium path 0EF in Fig. 2.2a for an arbitrary structure and on proof that these tools work by use of demonstration problems, the solution of which is known. In most cases, no formal distinction is made between prebifurcation and postbifurcation regimes; in fact, simple structures are modeled with imperfections so that potential bifurcation points (such as B in Fig. 2.2a) are converted into maximum load points such as E. The buckling problem loses its special qualities as illuminated so skillfully in the asymptotic treatments and becomes just another nonlinear analysis, requiring perhaps special physical insight on the part of the computer program user because of potential numerical traps such as spurious or real bifurcation points and ill-conditioning due to maximum load points.

Figures 2.2a and 2.2b illustrate the two very different approaches to the buckling problem described in the last two paragraphs. In the general nonlinear approach, the computations involve essentially a "prebuckling" analysis or a determination of the unique equilibrium states along the fundamental path 0EF in Fig. 2.2a. In the asymptotic approach (Fig. 2.2b), the prebuckling state is often known a priori. The secondary path BD of the perfect structure and (in the elastic case) the maximum load point E on the fundamental path of the imperfect structure are determined by expansion of the solution in a power series of the bifurcation mode amplitude or amplitudes which is asymptotically exact at the bifurcation point B.

Axisymmetric Structures

The third approach to the buckling problem, development of special-purpose programs for the analysis of axisymmetric structures, forms a sort of middle ground between the asymptotic analysis and the general-purpose nonlinear analysis. The approach is similar to the asymptotic treatment because in applications it is restricted in practice to a special class of structures and the distinction between prebuckling equilibrium and bifurcation buckling is retained. It is similar to the general nonlinear approach in that the continuum is discretized and the nonlinear prebuckling equilibrium problem is solved by "brute force." The emphasis is on the calculation of the prebuckling fundamental path, 0B or 0A in Fig. 2.2a and determination of the bifurcation point B and its associated buckling mode, not on calculation of postbifurcation behavior BD or of the load-deflection path 0EF of the imperfect structure. The goals of this third approach are to create an analysis tool for use by engineers and designers and to use this tool in extensive comparisons with tests, both to verify it and to obtain physical insight into the buckling process.

3. "Classical" Buckling of Cylindrical and Spherical Shells and Asymptotic Imperfection Sensitivity Analysis

Cylindrical Shells

Monocoque Cylinders under Axial Compression

The problem of buckling of thin cylindrical shells under axial compression has received far more attention than most problems in structural mechanics because of the extraordinary discrepancy between test and theory which remained unexplained for so many years. Hoff[36] gives a meticulous and very readable survey of work done up to 1966. Brush and Almroth devote a major portion of a chapter of their book[11] to the subject.

The postbuckled state of an axially compressed cylinder is illustrated in Fig. 3.1. During a test of even a very carefully made cylinder an isolated buckle initially appears at an average stress considerably below the predicted bifurcation value of

$$\sigma_{cl} = [3(1-\nu^2)]^{-1/2} Eh/a \approx 0.6Eh/a \qquad (2)$$

This buckle is generally followed by a cluster of buckles in the same neighborhood which very rapidly deepen, change shape,

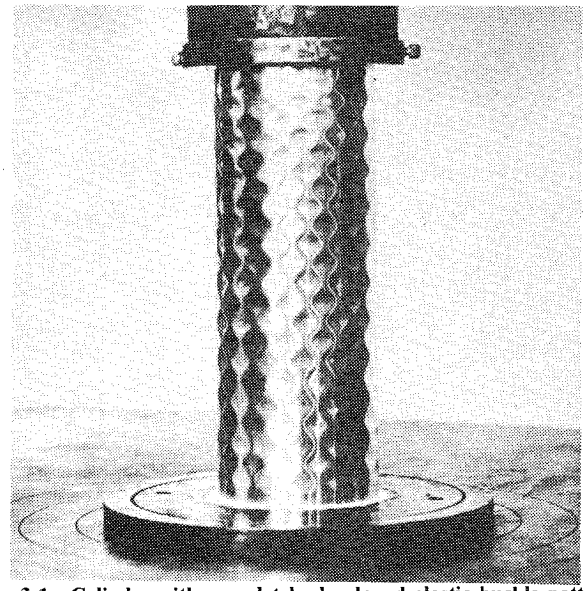

Fig. 3.1 Cylinder with completely developed elastic buckle pattern (from Horton et al.[44]).

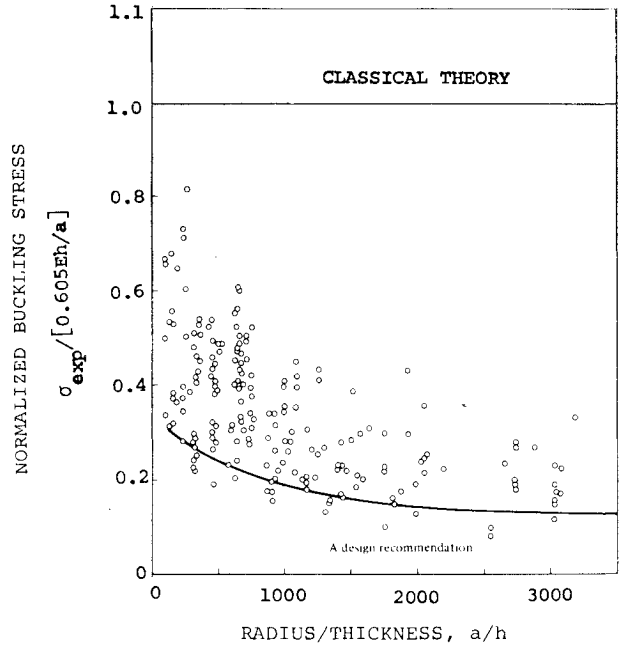

Fig. 3.2 Distribution of test data for cylinders subjected to axial compression. (From *Buckling of Bars, Plates and Shells* by D. O. Brush and B. O. Almroth.[11] Copyright © 1975 by McGraw-Hill, Inc. Used with permission of McGraw-Hill Book Co.)

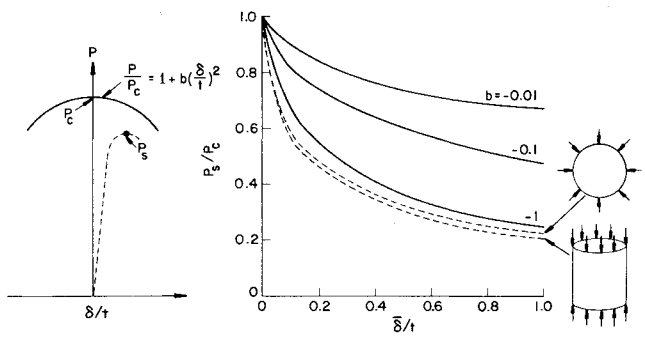

Fig. 3.3 Imperfection sensitivity as a function of parameter b for unique buckling mode and comparison with imperfection sensitivity of spherical shell under external pressure and cylindrical shell under axial compression; δ is the amplitude of the buckling mode and $\bar{\delta}$ is the amplitude of the imperfection (from Budiansky and Hutchinson[53]).

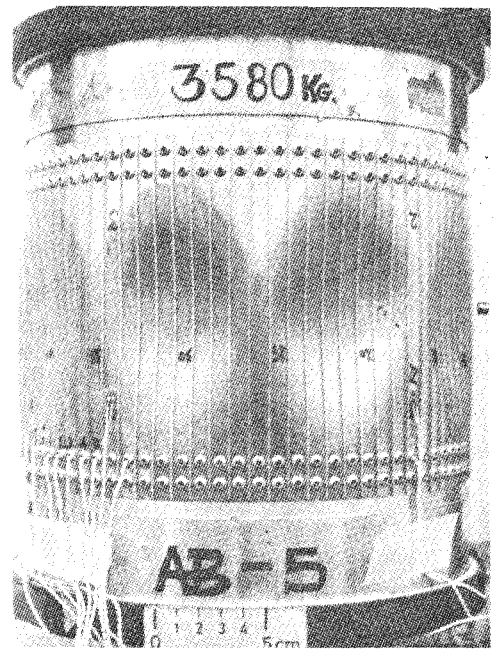

Fig. 3.4 Typical postbuckling pattern of axially compressed, stiffened cylindrical shell (from Singer and Abramovich[40]).

and spread over a considerable portion of the surface. The postbuckled pattern shown in Fig. 3.1 was obtained by axial compression of the cylinder with a close-fitting mandrel inside to prevent excessive growth of the buckles and consequent formation of plastic hinges at their boundaries. Thus the buckle pattern spread over the entire surface. Figure 3.2 demonstrates the dramatic discrepancy between test and theory over a wide range of radius-to-thickness ratios.

The most significant trend of these data is the increasing discrepancy between test and theory with increasing radius-to-thickness ratio a/h. It is this trend which provides the clue that the discrepancy arises from the extreme sensitivity of the critical load to initial imperfections: A reasonable measure of geometrical quality is the ratio of initial deviation $w_0(x,\theta)$ from the perfect cylindrical shape to thickness h. It is clear that for a given fabrication method, this ratio will increase with increasing radius-to-thickness ratio.

One of the first studies of the sensitivity of the critical load to initial geometric imperfections was carried out by Donnell and Wan.[37] They demonstrated qualitatively that the discrepancy between test and theory is caused by initial geometric imperfections. The Koiter theory,[25] which provides asymptotically exact formulas for the maximum load-carrying capability P_S of an imperfect structure, provides rigorous proof of the extreme sensitivity of the critical axial load of monocoque cylindrical shells to initial geometric imperfections (Fig. 3.3).

For many years several researchers attempted to obtain safe design loads for thin axially compressed cylinders by using numerical methods to calculate the postbuckling load deflection curve from nonlinear theory. It was thought that the minimum postbuckling load would provide a lower bound to the load-carrying capability of the shell. Those attempts are very carefully documented by Hoff.[36] Postbuckling load-deflection curves were calculated on the digital computer with the use of various trigonometric series expansions to express the postbuckling deflection pattern. A converged solution for the problem was never found. This approach was dropped because the extensive experimental evidence in Fig. 3.2 shows that the predicted postbuckling minimum load is unrealistically low to be useful as a guide to designers for all but the very thinnest shells. Hence, the current approach is to use the Koiter theory combined with empirical results to provide a confidence index, as will be described more fully later.

There was also an attempt to explain the discrepancy between test and theory by consideration of various boundary conditions. These studies are surveyed by Hoff.[36] The lowest critical load obtained for any set of edge conditions reported in Ref. 36 is $\sigma_{cr}/\sigma_{cl} = 0.38$. This load requires the tangential displacement v to be free at the boundaries. Several sets of edge conditions yield $\sigma_{cr}/\sigma_{cl} = 0.5$. However, they all require that either the normal deflection w or tangential displacement v be free at the edge. In view of measurements of deflections actually occurring during tests, it appears that sufficient friction is present to prevent significant displacements of v and w at the edges. The critical mode for the cases in which v is free corresponds to two circumferential waves, which does not resemble observed buckling modes.

The monocoque cylinder under axial compression is very sensitive to small initial imperfections because the critical buckling load corresponds to a mode the axial and circumferential wavelengths of which are quite small compared to the radius. Also the critical load is insensitive to wavelength. Note that the classical formula, originally derived for axisymmetric buckling by Lorenz in 1908[38] and for nonsymmetric buckling by Timoshenko in 1914,[39] does not contain any reference to n or m, the number of waves in the buckling pattern in the circumferential or axial directions, respectively. Thus, a great variety of small initial imperfections occurring anywhere on the entire shell surface would contain significant components of critical or almost critical bifurcation buckling mode shapes, modes of deformation that would grow as the load is increased, eventually causing snap-through at a load far below that predicted for bifurcation buckling of the perfect shell, as shown in Fig. 3.2.

A Caution for Novice Users of Computer Programs for Buckling

It is worth emphasizing that the problem of the axially compressed cylinder, which appears superficially to be an excellent, simple test case for a person learning to use a computer program that he has acquired elsewhere, is really quite demanding. The simplicity of the geometry tempts one to use a discretization with fewer degrees of freedom than are needed to obtain a converged solution corresponding to a buckling pattern with short axial waves. The result obtained from the computer program will probably be compared with the Timoshenko formula [Eq. (2)], which is based on the assumption of a uniform membrane prebuckling state. Depending on the edge conditions, the nonuniformity and nonlinearity of the prebuckling state near the edges lowers the predicted critical load by 8-20%. If nonlinear prebuckling analysis is used, the problem is further complicated by the fact that the nonsymmetric bifurcation buckling load is fairly close to the axisymmetric collapse load, a situation demonstrated in Fig. 1.6. A final difficulty is that several eigenvalues for the

bifurcation loads are clustered near the critical load, especially in models for which the edge effects in the prebuckling phase are not present or are ignored by the computer program. These difficulties are discussed in an example of an axially compressed monocoque cylinder presented in Ref. 9. The reader is urged to study that material before dismissing a computer program because it "can't even predict the classical buckling load for an axially compressed monocoque cylindrical shell."

Stiffened Cylinders under Axial Compression

The postbuckling state of an axially stiffened cylinder is shown in Fig. 3.4. Notice that the buckling mode has much longer characteristic wavelengths than does that for the monocoque cylinder pictured in Fig. 3.1. This is due to the increased axial bending stiffness and results in milder sensitivity of the buckling load to initial imperfections.

Cylinders under Uniform External Pressure or Torsion

Figures 3.5-3.8 show postbuckling states of cylinders subjected to hydrostatic pressure or torsion and comparisons between test and theory. As with the stringer-stiffened axially compressed cylinders, the buckling modes are characterized by long axial wavelengths and relatively few circumferential waves, which results in a milder sensitivity of buckling loads to initial geometric imperfections. The most sensitive systems are short cylinders ($10 \leq Z \leq 100$) under hydrostatic compression, cases for which the bifurcation buckling phenomenon resembles that for cylinders under axial compression (Fig. 3.6).

Spherical Shells under Uniform External Pressure

Kaplan[43] gives a thorough survey of buckling of spherical shells subjected to uniform external pressure. Early tests revealed that buckling initiates at some spot at which a small dimple forms. To the writer's knowledge the formation of multiple buckles in a complete spherical shell, as observed in axially compressed cylindrical shells, has not been observed for shells without an interior mandrel. Figure 3.9 shows a

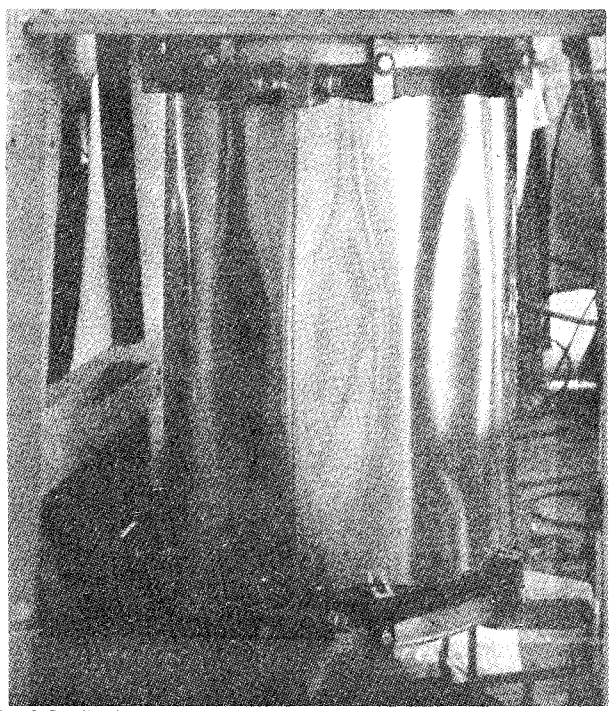

Fig. 3.5 Typical postbuckled pattern for medium-length cylindrical shell under external hydrostatic pressure (from Harris et al.[42]).

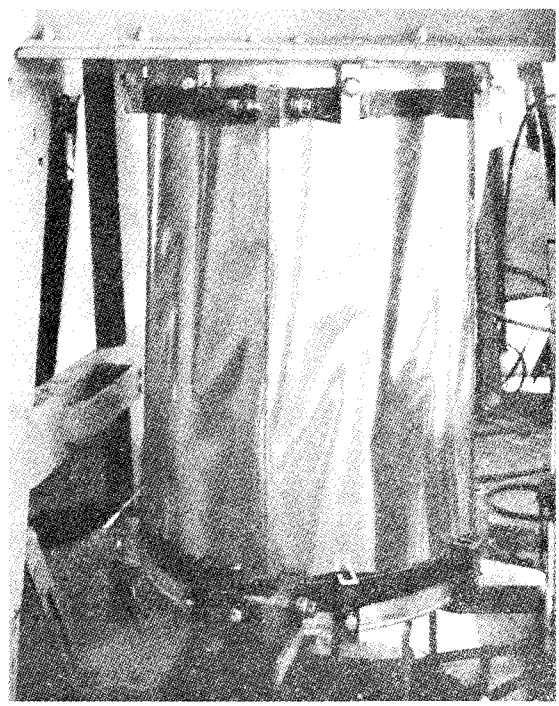

Fig. 3.7 Typical postbuckled pattern for unpressurized cylinder in torsion (from Harris et al.[42]).

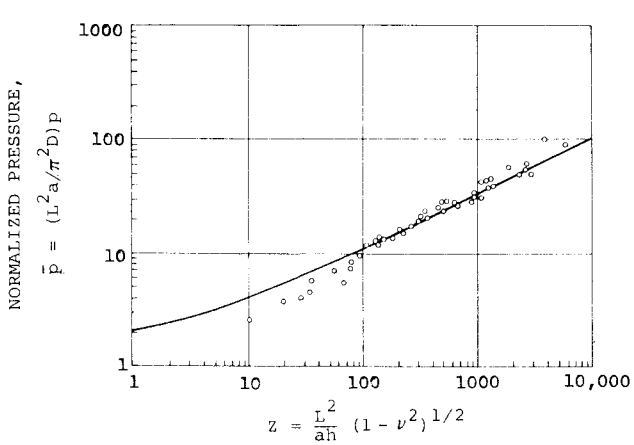

Fig. 3.6 Comparison of theoretical and experimental buckling pressures for cylinders subjected to external hydrostatic pressure (D = flexural rigidity). (From *Buckling of Bars, Plates, and Shells* by D. O. Brush and D. O. Almroth.[11] Copyright © 1975 by McGraw-Hill, Inc. Used with permission of McGraw-Hill Book Co.)

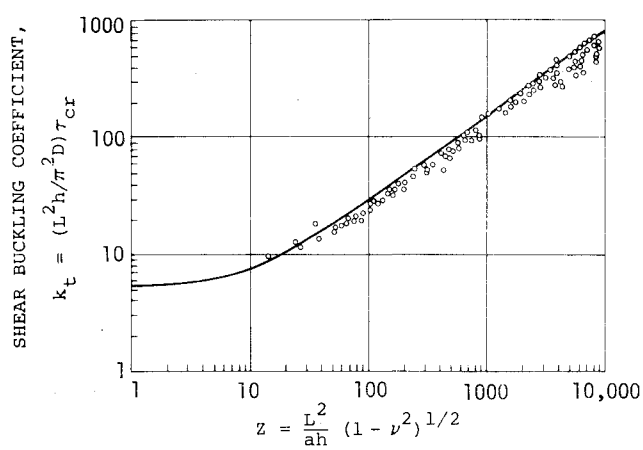

Fig. 3.8 Comparison of theoretical and experimental buckling loads for cylinders subjected to torsion. (From *Buckling of Bars, Plates, and Shells* by D. O. Brush and B. O. Almroth.[11] Copyright © 1975 by McGraw-Hill, Inc. Used with permission of McGraw-Hill Book Co.)

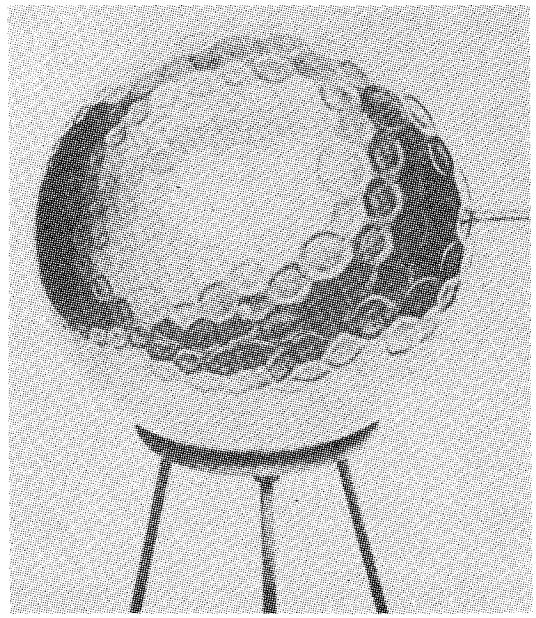

Fig. 3.9 Postbuckled state of a thin-walled spherical shell under uniform external pressure; buckling motion is restrained by an interior mandrel (from Carlson et al.[45]).

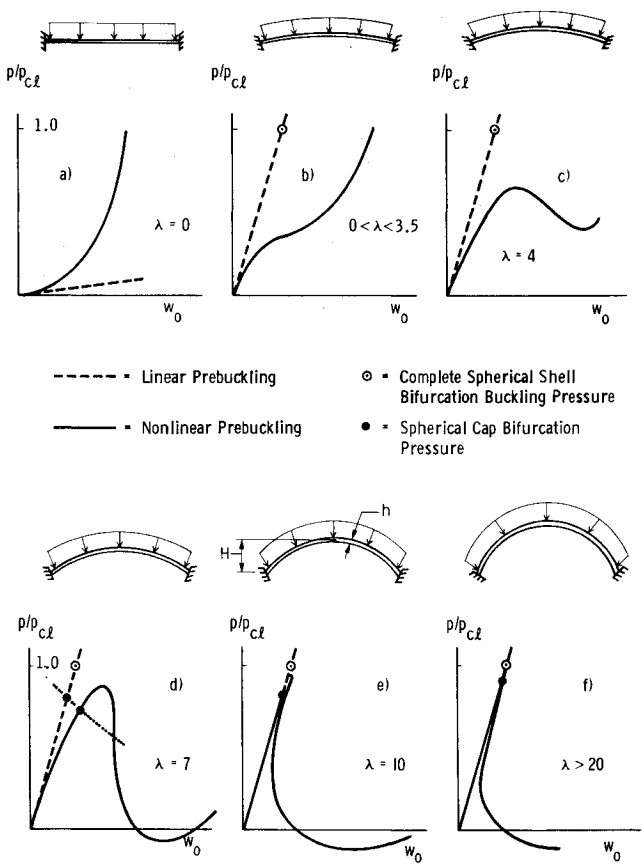

Fig. 3.10 Load-deflection curves and bifurcation buckling of spherical caps with various values of the shallowness parameter $\lambda = 2[3(1-\nu^2)]^{1/4}(H/h)^{1/2}$.

postbuckled state in a shell with a closely fitting interior mandrel. Each buckle subtends a small solid angle, just as in the case of an axially compressed monocoque cylinder in which each buckle covers a very small fraction of the surface. As might be expected from this behavior, the critical load of a spherical shell subjected to uniform external hydrostatic pressure is highly sensitive to initial geometric imperfections.

Spherical Caps

The fact that an initial buckle subtends a small solid angle stimulated those initially interested in complete spherical shells to model the problem of buckling of a complete spherical shell with use of a shallow spherical cap clamped at its edge. Over the years the shallow cap configuration evolved into a "classical" problem in its own right, studied with almost the same intensity and frequency as the axially compressed cylinder. However, as demonstrated in Fig. 3.10, the shallow cap problem has certain characteristics not present in the case of a complete spherical shell. These arise from the presence of the edge.

In Fig. 3.10 load-deflection curves are shown corresponding to linear and nonlinear theories for prebuckling axisymmetric deformations of caps clamped at the boundary. The open circles on the linear load-deflection lines indicate bifurcation buckling at the "classical" pressure for the complete spherical shell with the same radius-to-thickness ratio as the spherical cap. The quantity λ is a cap shallowness parameter given by

$$\lambda = 2[3(1-\nu^2)]^{1/4}(H/h)^{1/2} \tag{3}$$

where H is the rise of the cap above the plane in which the edge lies and h the shell thickness.

For λ less than about 7 or 8 the behavior of the shallow cap little resembles that of the complete spherical shell. With $\lambda = 0$ (flat circular plate) there is no similarity at all: The load-deflection curve exhibits a stiffening characteristic which results from the buildup of in-plane tension as the plate deforms (Fig. 3.10a). With λ less than about 3.5 the load-deflection curve has no horizontal tangent and no bifurcation point so that there is no loss of stability on the primary equilibrium path (Fig. 3.10b). For λ less than about 6 there is axisymmetric snap-through, but no bifurcation buckling (Fig. 3.10c). For $\lambda > 6$ bifurcation buckling into a nonsymmetric mode occurs at a lower load than either axisymmetric snap-through of the cap or classical buckling of a complete spherical shell (Figs. 3.10d-f). Notice that as λ increases above 7 the prebuckling behavior becomes more and more linear. Figure 3.10f corresponds to a configuration in which the cap is no longer "shallow," if that word may be used as a means of classifying shell behavior: The nonuniformity of prebuckling behavior occurs in a relatively narrow band or "boundary layer" near the edge. Any further increase in λ results in no further alteration in the curves or locations of the bifurcation points presented in Fig. 3.10f. No matter how high λ is, the behavior of the incomplete spherical shell clamped at its boundary will never be the same as that of the complete spherical shell because the presence of the boundary gives rise to edge buckling at a pressure 80-90% of the classical value p_{cl}.

For actual spherical shells and shallow caps, random imperfections play a major role in the loss of stability under uniform external pressure. Figure 3.11 demonstrates that the effect of initial imperfections is just as severe as in the case of cylindrical shells subjected to axial compression.

Asymptotic Postbuckling Theory

Koiter[25,46] was the first to develop a theory which provides the most rational explanation of the large discrepancy between test and theory for the buckling of axially compressed cylindrical shells and externally pressurized spherical shells: The early collapse is due to small, unavoidable geometrical imperfections. Excellent reviews of Koiter's theory and of the many applications of it to buckling of monocoque and stiffened elastic and elastic-plastic shells are given by Hutchinson and Koiter,[16] Tvergaard,[17] and Budiansky and Hutchinson.[47] The theory itself is reiterated in some detail by Budiansky,[48] Seide,[49] and Masur[50] and extended to dynamic buckling by Budiansky and Hutchinson[51] and Budiansky.[52] Many of the numerous applications of the theory to static buckling of shells of revolution reviewed in Refs. 16 and 53

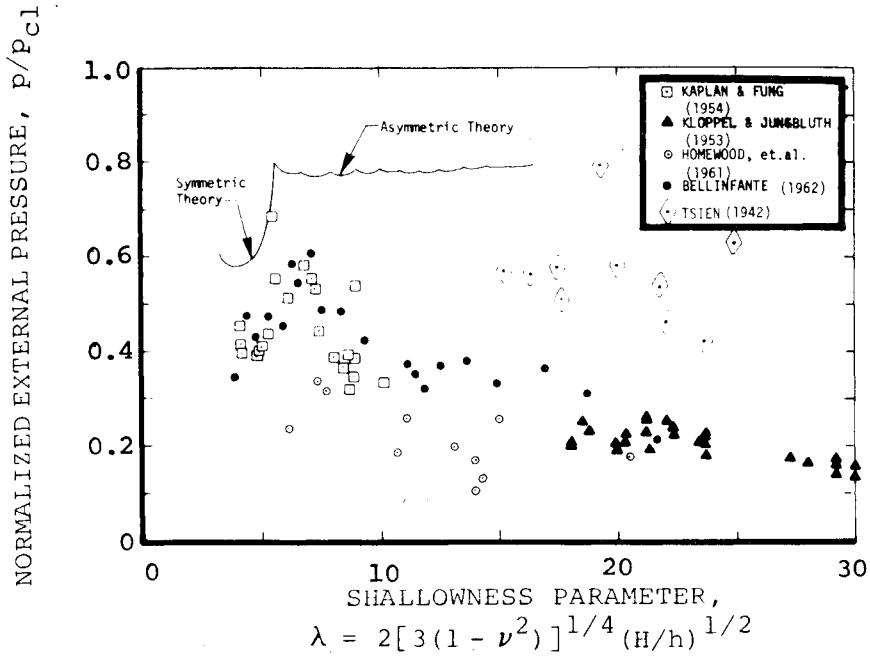

Fig. 3.11 Early experimental results for clamped spherical caps under external pressure (*H* is the rise of the apex of the cap above its base plane). [From Fung and Sechler, *Thin Shell Structures: Theory, Experiment and Design*, © 1974, p. 253. Reprinted by permission of Prentice-Hall, Inc., Englewood Cliffs, N.J. (Kaplan[43]).]

refer to the presentation of a simplified form of the Koiter theory for static analysis given in Refs. 51 and 52. Summaries of the main features of Koiter's theory appear in Refs. 11 and 17.

Essentially, the purposes of Koiter's theory are to:

1) Determine the stability of the equilibrium at the lowest bifurcation point on the equilibrium path.

2) Ascertain the sensitivity of the maximum load-carrying capacity of the structure to initial geometric imperfections.

A classical bifurcation buckling analysis represents a search for the load at which the equilibrium of a structure ceases to be stable and becomes neutral; it does not reveal information about the stability of the structure. Suppose that a structure is in equilibrium at some load smaller than the lowest bifurcation load (and furthermore suppose that we are concerned here with only *bifurcation* buckling, not nonlinear collapse). Any small additional displacement field which satisfies the requirements of continuity (compatibility) and geometric boundary conditions (kinematically admissible displacement field) will cause the energy of the system (structure plus potential energy of loads) to increase. Thus, the structure is in a state of stable equilibrium analogous to a ball at the lowest point on a wavy surface. At a higher load corresponding to the bifurcation point, the additional energy of the system due to the small disturbance does not change—the structure is in a state of neutral equilibrium analogous to the ball on a flat surface; the equilibrium state is not unique in a small neighborhood of the prebuckling state. At loads above the lowest bifurcation point, equilibrium on the fundamental (prebifurcation) load-deflection path is unstable, analogous to the ball on a peak.

In order to learn whether or not the structure is stable *at* the bifurcation point, it is necessary to determine the characteristics of the postbifurcation path in load-generalized-displacement space or in load-postbuckling-modal-deflection space in the neighborhood of the bifurcation point. Typical paths are displayed in Fig. 2.3. The stability of equilibrium *at* the bifurcation point is governed by third- and fourth-order terms in the energy function expressed as a series expansion of the incremental displacement represented by the difference of the displacement field corresponding to the fundamental state at the bifurcation point and that corresponding to a state on the postbifurcation equilibrium path close by. The first-order terms of the energy thus expressed cancel because the fundamental state at the bifurcation point is an equilibrium state; the second-order terms likewise cancel because the bifurcation point represents a state of neutral equilibrium. The shape of the postbifurcation load-deflection curve in the neighborhood of the bifurcation point is therefore governed by the third-order terms (Fig. 2.3b) or, if these vanish, by the fourth-order terms (Figs. 2.3c and 2.3d) in the expression for incremental energy.

Elastic Post-Bifurcation Analysis

At a bifurcation load λ_C where the buckling mode is unique, Koiter's general elastic postbuckling theory leads to an asymptotically exact expansion for the load parameter λ in terms of the normalized bifurcation buckling modal amplitude, w_b:

$$\lambda/\lambda_C = 1 + aw_b + bw_b^2 + \ldots \tag{4}$$

Four types of elastic initial postbuckling behavior are shown in Fig. 2.3. Solid curves show the behavior of perfect structures and dotted curves the behavior of imperfect structures with imperfections in the form of the unique critical bifurcation buckling mode. The ultimate load-carrying capabilities of the structures represented by Figs. 2.3b and 2.3d are sensitive to initial imperfections while those represented by Figs. 2.3a and 2.3c are not. For the case of Fig. 2.3b which is nonsymmetric with respect to the sign of the buckling modal amplitude w_b ($a \neq 0$), a negative normalized imperfection amplitude w_{imp} converts bifurcation buckling into limit-point or "snap" buckling at a reduced load λ_S given by Koiter's general theory as

$$\lambda_S/\lambda_C \simeq 1 - 2(-\rho a w_{imp})^{1/2} \tag{5}$$

in which ρ is a constant that depends on the imperfection shape. For the symmetric case (Fig. 2.3d), a in Eq. (4) is zero, $b<0$, and the limit load of the imperfect structure is approximately

$$\lambda_S/\lambda_C \simeq 1 - 3(-b/4)^{1/3}(\rho w_{imp})^{2/3} \tag{6}$$

Many applications of Eq. (5), and especially Eq. (6), appear in the literature. Figure 3.3 illustrates the relationship of the coefficient b in Eqs. (4) and (6) to the imperfection sensitivity for a system such as a shell of revolution, for which the lowest bifurcation buckling mode is unique and the initial postbuckling behavior is symmetric with respect to the sign of the postbuckling displacement field and unstable. The initial postbuckling load P of the perfect structure follows the solid curve shown in Fig. 3.3a. The quantity δ is the amplitude of the postbuckling displacement field, which is assumed to be in

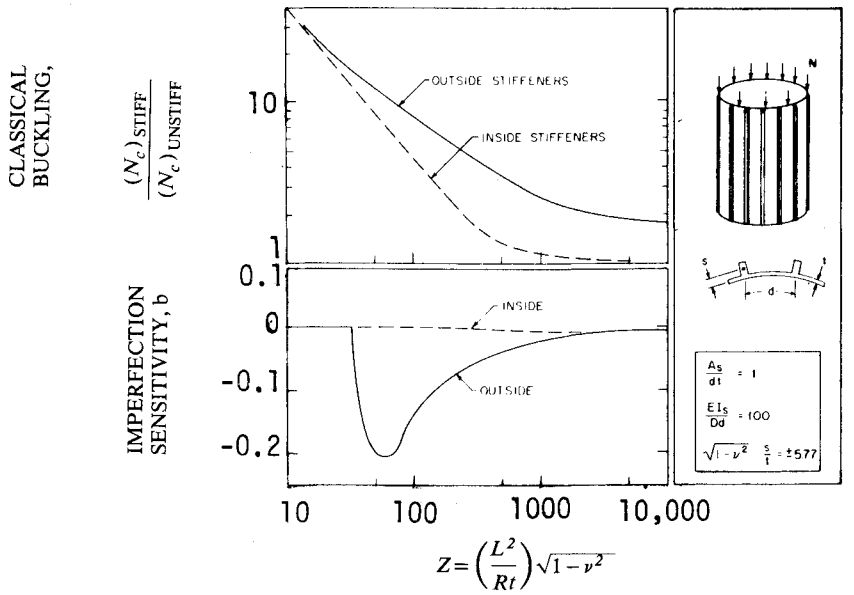

Fig. 3.12 Classical buckling and imperfection sensitivity of simply supported stiffened cylinders under axial compression (from Budiansky and Hutchinson[53]).

the form of the unique buckling mode. The quantity t is the shell thickness. The dashed curve pertains to an imperfect shell. The value of b depends on details of the geometry and loading. Buckling loads are sensitive to imperfections if b is negative and insensitive to imperfections if b is positive. As shown in Fig. 3.3b, more negative values of b are associated with greater sensitivity of the critical load P_S to initial geometric imperfections δ. Curves for the spherical shell under uniform external pressure and the cylindrical shell under uniform axial compression are shown in order to emphasize the extreme nature of imperfection sensitivity in these two cases. The curves are dashed because they are not derived from Eq. (6) as explained next.

There are important examples in which the lowest bifurcation point is associated with several buckling modes or in which there exists a cluster of bifurcation loads just above the critical load. The cylindrical shell under axial compression is an example of the former and the spherical shell under external pressure is an example of the latter. Structures optimized such that local and general instability occur at the same load provide another practical example. For cases in which there exist several simultaneous buckling modes, Eq. (4) is replaced by N asymptotic equations for the load parameter λ in terms of the buckling modal parameters w_{b1}, $w_{b2}, \ldots w_{bN}$ of the form

$$[(\lambda/\lambda_C) - I]w_{bi} = A_{ijk}w_{bj}w_{bk} + B_{ijkl}w_{bj}w_{bk}w_{bl} + \ldots \qquad (7)$$

in which the summation convention (from one to N) is implied for repeated indices. Koiter's general theory yields asymptotic estimates of the imperfection sensitivity λ_S/λ_C in the case of elastic buckling. Due to modal interaction the effect of initial geometric imperfections is usually severe, as will be demonstrated for built-up axially compressed columns and as is demonstrated by the dashed curves in Fig. 3.3b.

If the bifurcation buckling modes are *nearly* coincident, as they are for uniformly externally pressurized spherical shells, the imperfection sensitivity is also characterized by modal interaction, even though the initial postbuckling behavior of the perfect structure in the *immediate* neighborhood of the bifurcation point is governed by Eq. (4) for the single-mode case.[54]

The ultimate aim of all imperfection sensitivity analyses is to determine the maximum load-carrying capability (λ_S in Fig. 2.2, P_S in Fig. 3.3a). The search for λ_S or P_S has been accomplished in the following ways:

1) A general imperfection shape containing both axisymmetric and nonsymmetric components has been assumed and the nonlinear compatibility and equilibrium equations of the von Kármán-Donnell theory[55] have been used to trace the load-deflection curve up to and perhaps past its maximum. This is the approach taken, for example, by Donnell and Wan,[37] Hutchinson,[56] Arbocz and Babcock,[57] and Arbocz and Schler.[58]

2) An axisymmetric imperfection shape has been assumed and λ_S identified as the lowest load at which either axisymmetric collapse of nonsymmetric bifurcation occurs from the axisymmetrically deformed prebuckled state. This is the approach taken by Koiter in his classic paper published in 1963,[59] by Almroth et al.[12] in their extension of Koiter's "special theory"[59] for derivation of a design method for stiffened and internally pressurized cylindrical shells, and by Tennyson and Muggeridge[60] who investigated the effect of local axisymmetric imperfections.

3) Koiter's "general theory" is used to obtain the factor b in Eq. (4) (a is zero for shells of revolution because of the periodicity of the buckling mode in the circumferential direction) and Eq. (6) or its equivalent for the multimode case is used to obtain the peak load λ_S. This approach is used by Hutchinson and Amazigo[61] and Hutchinson and Frauenthal[62] in their studies of eccentrically stiffened and barreled cylindrical shells, and by Amazigo and Budiansky[63] in their asymptotic treatment of the buckling of axially compressed cylinders with localized or random axisymmetric imperfections.

4) A "brute-force" approach is used to obtain the peak load λ_S as discussed in the section on nonlinear collapse. For example, the STAGS computer program[64] has been used for the analysis of axially compressed cylinders with cutouts[11] and the BOSOR5 program[65] has been applied to determine axisymmetric collapse loads of elastic-plastic cylindrical shells.

Examples

Figures 3.12 and 3.13 demonstrate the kind of results that asymptotic imperfection-sensitivity theory generates. The top portion of Fig. 3.12 shows plots of normalized critical axial loads N_C (stiffened)/N_C (unstiffened) as functions of the Batdorf length parameter $Z = (L^2/Rt)\sqrt{1-\nu^2}$, and the bottom portion displays the imperfection-sensitivity parameter b. The load-carrying capability can easily be determined as a function of imperfection amplitude from Eq. (6). While classical bifurcation buckling theory yields a prediction that a design with outside stiffeners is more efficient than one with inside stiffeners, this advantage is counteracted by increased imperfection sensitivity over a wide range of Z. A common trend in shell buckling is here revealed: Design changes that raise the bifurcation buckling load of the

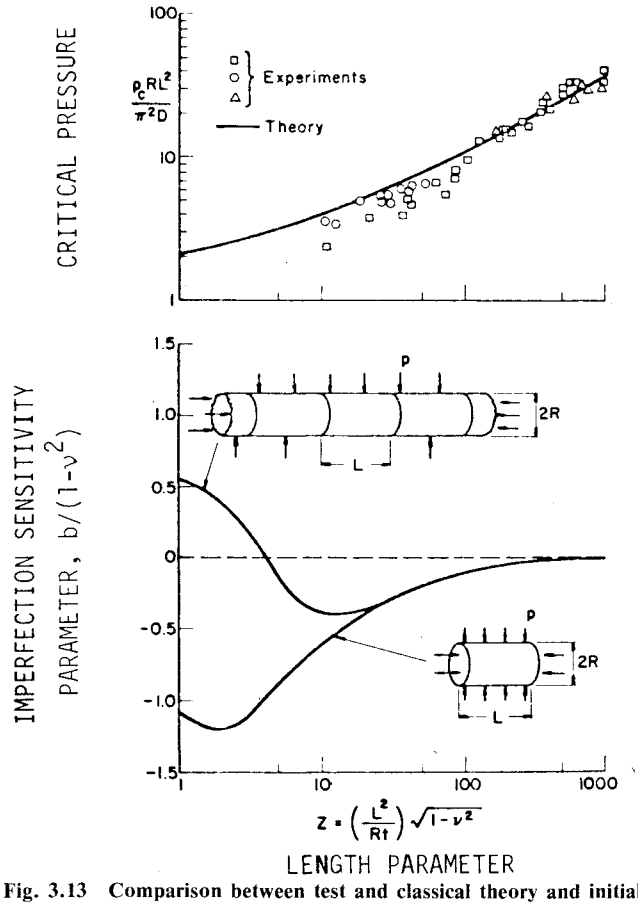

Fig. 3.13 Comparison between test and classical theory and initial postbuckling predictions for externally pressurized cylinders (from Hutchinson and Koiter[16]).

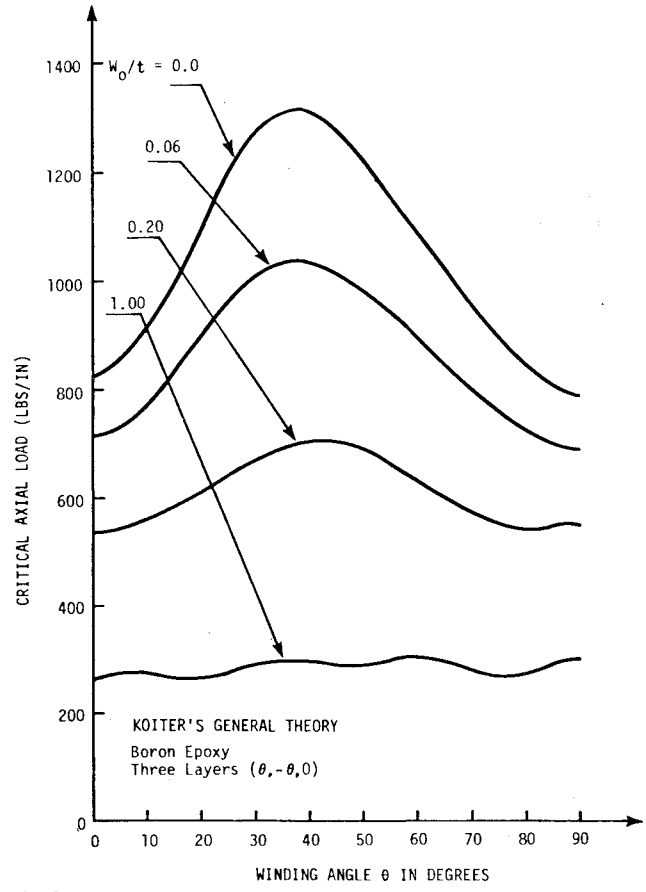

Fig. 3.14 Effect of initial imperfection amplitude w_0 on the buckling load of a composite cylinder; predictions are from Koiter's general theory, obtained by Khot and Venkayya.[67] (From Almroth[70].)

perfect shell without increasing the amount of material tend also to increase the sensitivity of the critical load to initial geometric imperfections. We shall see this phenomenon in a following section on buckling of axially compressed shells made of laminated composite materials and again later in the case of optimized buckling-critical structures.

The results of Hutchinson and Amazigo[61] shown in Fig. 3.12 are based on use of the membrane prebuckling state. Hutchinson and Frauenthal[62] extended the treatment of Ref. 61 to account for nonlinear prebuckling behavior and barreling of the cylinder generator. Inclusion of nonlinear prebuckling effects does not alter the conclusions demonstrated in Fig. 3.12 that location of the stringers on the outer surface of the shell enhances the resistance to buckling but simultaneously increases the sensitivity to initial geometric imperfections, at least over some of the range of Z.

Figure 3.13 demonstrates a qualitative agreement between test and asymptotic imperfection-sensitivity theory. In the range of Z in which experimental results fall below the classical critical bifurcation pressure, b is negative.

Laminated Cylindrical Shells Made of Composite Material

When composite materials as opposed to metals are used in plate and shell structures, the following questions arise:

1) Metal plates, stiffened shells, and shallow cylindrical panels with supported edges can sometimes carry loads considerably in excess of the lowest bifurcation buckling load. The skin may buckle locally, transferring its load to adjacent structural elements. Examples include axially compressed oval cylinders and stiffened panels with oversized stringers. In view of the brittleness of composite materials, will designs which permit local buckling remain feasible?

2) Are cylinders of composite material (with anisotropy and membrane-bending coupling) more or less imperfection sensitive than isotropic cylinders?

3) Will the actual size of typical geometric imperfections in practical applications be more or less severe than they are in metal cylinders?

4) Do other types of imperfections, such as voids and delaminations, affect the buckling load for structures made of composite material?

A number of publications attempt to answer the question of whether cylindrical shells of composite material are more or less sensitive to small geometric imperfections than are isotropic cylinders. Use of a nonlinear analysis,[66] Koiter's general theory,[67] and Koiter's special theory[68] indicate that in comparison to isotropic cylinders, composite cylinders may be somewhat less sensitive to geometric imperfections. Also, in keeping with the trend mentioned above, it is clear that cylinders with close to optimum fiber orientation are most sensitive. This is illustrated in Fig. 3.14.

The possibility remains that composite cylinders, while less sensitive to imperfections, as manufactured display more severe imperfections and therefore possibly more severe knockdown factors. Additional observations of experiments and measurements on practical structures are required before this question can be satisfactorily answered. The possibility must be faced that the composite-material plates and shells contain flaws of types other than those that affect isotropic cylinders. It does not seem likely that delaminations will pass undetected through any reasonable inspection if they are large enough to cause the type of separate buckling that is discussed in Ref. 69. However, smaller delaminations will still reduce the stiffness of the shell. Although the results of the bulk of the test data seem to be reassuring, the fear that repeated loading can cause a growth of such flaws is not completely dispelled.

A final evaluation of the state-of-the-art must, of course, be based on results from laboratory tests and from the experience acquired by use of composite material in structural

applications in the past. Many experimental results on the buckling of composite-material plates and shells have been presented over the last few years. In general, they tend to indicate that the theory for composites is approximately on a par with the theory for metal shells with respect to its reliability. It is prudent to assume, however, that quality control may be better for laboratory test specimens than for mass-produced structural components. The literature scanned during a recent evaluation of the state-of-the-art[70] contains little information about the performance of actual hardware.

In Ref. 12 a procedure is presented for calculation of a lower bound to the buckling load. This procedure, to be described in more detail later, is based on Koiter's special theory[59] and the assumption that cylinders with the same effective radius-to-thickness ratio $(R/t)_e$ have identical dimensionless amplitudes of axisymmetric imperfections when these imperfections are expressed as a percentage of the wall thickness of an equivalent isotropic shell with the same wall radius of gyration as that of the composite cylinder. Predictions with use of this method were compared in 1970 to the test results on composite cylinders available at that time. All the test specimens failed above the prediction by this lower-bound method. However, a comparison shows that the procedure is only slightly less conservative than direct application of the knockdown factor for the equivalent isotropic cylinder with the same $(R/t)_e$. A similar evaluation of results obtained in later experimental investigations would be of value. As of this writing there is little reason to recommend knockdown factors for cylinders of composite materials under axial compression different from those chosen from charts for the equivalent isotropic cylinder. For cylinders in torsion or external pressure, a knockdown factor of about 0.8 seems to be appropriate.[71] For fairly wide cylindrical panels (or local buckling between stiffeners of complete cylinders) the results in Ref. 72 indicate that knockdown factors similar to those for complete cylindrical shells must be used. Sufficiently narrow panels of isotropic material are able to carry loads above the critical load. However, due to brittleness, such use must be further tested before it can be recommended for the design of panels made of composite materials.

Elastic-Plastic Post-Bifurcation Analysis

Practically all of the development and application of asymptotic postbuckling theory including the effect of plasticity has been done in the last decade by Hutchinson, Tvergaard, Needleman, and their co-workers.[17-19,47,73-80] Hutchinson gives a summary in Ref. 18 and Tvergaard in Ref. 17. The theory represents extensions to the general theory of uniqueness and bifurcation in elastic-plastic solids derived by Hill in 1958-1959[81,82] and the general postbuckling theory developed by Koiter for elastic structures in 1945.[25,46]

Bifurcation in the plastic range occurs under increasing load, so that unlike the elastic cases, the maximum load-carrying capability of perfect structures is slightly above the bifurcation load λ_C and occurs at amplitudes w_b for which a finite amount of material has experienced strain reversal.

Perfect Elastic-Plastic Structures

For the plastic range an asymptotic theory of initial postbifurcation behavior of perfect structures was developed by Hutchinson.[18,73] An asymptotic expansion is obtained for the initial post-bifurcation load in terms of the bifurcation modal amplitude w_b, as in Koiter's elastic postbuckling theory. In the plastic range the treatment is complicated by the phenomenon of elastic unloading, which starts at bifurcation and spreads into the material as the buckling modal amplitude increases. When the buckling mode is unique the asymptotically exact expression for the load parameter λ in terms of the normalized buckling modal amplitude w_b is

$$\lambda/\lambda_C = 1 + \lambda_1 w_b + \lambda_2 w_b^{1+\beta} \tag{8}$$

with $0<\beta<1$. The value of β depends on the shape of the unloading regions.[18] The constant λ_1 is positive since bifurcation takes place under increasing load. Its value is determined by the requirement that plastic loading takes place. The coefficient λ_2 is negative, so that the truncated expansion [Eq. (8)] can be used to estimate the maximum support load of the perfect structure, which is slightly above the critical bifurcation load. An extension of the asymptotic expansion [Eq. (8)] to cases of several coincident buckling modes has not been carried out. The asymptotic theory for plastic post-bifurcation of perfect structures has been applied by Tvergaard and Needleman to study the behavior of structures with symmetric[74] and asymmetric post-bifurcation behavior.[75,83,84]

Imperfect Elastic-Plastic Structures

In 1972 Hutchinson[76] reported the results of a numerical axisymmetric plastic buckling analysis of perfect and imperfect spherical shells loaded by uniform external pressure. For very small imperfections the plastic buckling load is not as sensitive to imperfections as is the elastic buckling load. Also, as Hutchinson points out, imperfection sensitivity is not as severe a problem for plastic as it is for elastic shells because plastic buckling requires relatively high thickness-to-radius ratios for which it is much less difficult to manufacture "reasonably perfect" shells. This conclusion is borne out by the comparisons between test and theory for a great variety of axisymmetric shells shown in Ref. 65.

Hutchinson further discusses the effect of small imperfections on plastic buckling loads in Ref. 77. There he provides an asymptotic estimate of the load at which elastic unloading begins. For many unstable structures this load is only slightly below the maximum load. An asymptotic expression for the maximum load, such as given by Koiter's general theory for elastic shells [Eqs. (5) and (6)] is not yet available. The main problem is that the maximum load of the structure with an infinitesimal imperfection in the form of the critical bifurcation buckling mode is not infinitesimally close to the bifurcation point, as is true in the elastic range, but lies a finite distance away. Consequently, elastic unloading usually occurs before the maximum point is reached. An asymptotic expansion of the initial part of the equilibrium solution for the imperfect structure is valid only to the point at which elastic unloading begins. Representation of the remaining part requires a second asymptotic expansion that accounts for the growing elastic unloading region.

Hutchinson and Budiansky,[78] Needleman and Tvergaard,[79] and Tvergaard[80] have devised asymptotic theories for the plastic maximum loads λ_S of imperfect structures with use of hypoelastic theories (J_2 flow theory without elastic unloading). Even though these asymptotic analyses ignore elastic unloading, they yield accurate predictions of the maximum loads.

Qualitative Guidelines for Imperfection Sensitivity

The question so often asked by the analyst is: Given the idealized structure and loading and given the means by which to determine the collapse and bifurcation buckling loads, what "knockdown" factor should be applied to assure a reasonable factor of safety for the actual imperfect structure?

We shall see examples in which shells exhibit load-carrying capability considerably greater than that corresponding to the lowest eigenvalue. Postbuckling stability is also exhibited by simple columns and flat plates. On the other hand, it has been shown that the critical loads of axially compressed cylindrical shells and externally pressurized spherical shells are extremely sensitive to imperfections less than one wall thickness in magnitude. These highly symmetrical systems are very sensitive to imperfections because many different buckling modes are associated with the same eigenvalue or closely spaced eigenvalues, the structure is uniformly compressed in a membrane state, and the buckling modes have many small

waves. Very small local imperfections will tend to trigger premature failure. The buckling loads of most practical shell structures are somewhat sensitive to imperfections, but not this sensitive. How much so is a very important question.

Buckling loads associated with local failure due to some *known* peculiarity of the structure which can be modeled a priori are generally less sensitive to *unknown* imperfections than are loads associated with buckle patterns covering a large percentage of the surface area. Redistribution of the stresses occurs as the load is increased; a serious unknown imperfection is less likely to appear in the local area of the failure and considerable local prebuckling deformations to occur, tending to diminish the significance of the initial unknown imperfections. Failure loads of structures that are subjected to enforced displacements are likely to be less sensitive to initial imperfections than are those of structures subjected to enforced loads. In the former case the growth of an isolated buckle near the worst imperfection tends to cause a reduction of the stress in that area, shifting the load to the better parts of the structure. Buckling of cylinders with cutouts and locally loaded shells are examples of this. Thicker shells appear to be less sensitive to imperfections than thinner shells simply because it is easier during fabrication to control the quality of the shell. Imperfection amplitude expressed in terms of wall thickness is therefore likely to be smaller the thicker the shell. Cylinders subjected to external pressure are less sensitive to imperfections than are cylinders subjected to axial compression because the axial wavelengths of the buckles are longer in the former case and eigenvalues do not cluster above the critical value. Hence, very small local imperfections do not affect the critical pressure as much as they do the critical axial load.

4. Nonlinear Collapse

Three buckling phenomena will be discussed in this and the next two sections: nonlinear collapse (Fig. 3.10c), bifurcation buckling from a deformed prebuckling state in which nonlinear prebuckling effects are significant (Fig. 3.10d), and buckling which is critically affected by boundary conditions (Figs. 3.10e and 3.10f).

As has been emphasized already, loss of stability of a shell structure may be due to nonlinear collapse (snap-through) or to bifurcation buckling. The purpose of this section is to present examples in which the failure mode is nonlinear collapse. Examples discussed include axisymmetric collapse of elastic-plastic monocoque cylinders under axial compression and general collapse of a straight pipe under uniform bending, of cylindrical panels and shells with concentrated loads and cutouts, and of noncircular cylinders under axial compression. The section closes with an example of axisymmetric collapse of an axially compressed complex rocket interstage. The collapse is caused by a local load-path eccentricity that gives rise to concentrated bending and local plastic flow.

Elastic-Plastic Collapse of Axially Compressed Monocoque Cylinders

Tests have been conducted on fairly thick metal cylinders by Lee,[85] Batterman,[86] Sobel and Newman,[87] and others referenced in Sewell's survey.[88] Tests on truncated cylinder-like (steep) conical shells have recently been conducted by Ramsey.[89] In all of the tests, end displacement was controlled. Local end effects such as bulging due to Poisson's effect, so obvious in Fig. 2.1, were ignored in early analyses of plastic buckling of axially compressed cylinders. Batterman[86] used flow theory and Gerard[90] used deformation theory. Murphy and Lee[91] were the first to include the effect of radial end restraint on plastic buckling load predictions. End effects are also accounted for in the analyses of Bushnell[65] who used the BOSOR5 computer program, and Sobel and Newman,[87] who used STAGSC.[64] All of the studies in which end effects are included are based on incremental flow theory and all predict that the collapse load corresponding to axisymmetrical deformation occurs before bifurcation, as shown in Fig. 2.1. Comparisons between BOSOR5 predictions and Lee's and Batterman's tests are given in Ref. 65.

The inclusion of end radial restraint in theoretical models essentially eliminates the discrepancy between test and theory and reveals that, in the case of plastic buckling of axially compressed cylinders tested in the usual way, it is not necessary to resort to the use of a bifurcation buckling analysis with deformation theory or flow theory with a singularity in the loading surface in order to bring test and theory into agreement. Fairly thick metallic cylinders ($R/t<90$) are not very sensitive to initial random imperfections if they buckle at stresses above the material proportional limit. The axisymmetric bulge which develops near an end, so evident in Fig. 2.1, represents a predictable "imperfection" that grows with load and is much more significant than any unknown imperfections due to fabrication or handling errors.

Gellin[92] shows that collapse loads of axially compressed cylinders buckling in the plastic range are not as sensitive to initial axisymmetric imperfections as are collapse loads of elastic cylinders. Hutchinson[76] demonstrates the same result for externally pressurized elastic-plastic spherical shells. This fact, the fact that the tangent modulus of most metals decreases by more than an order of magnitude within a stress range of 20% of the 0.2% yield stress, the fact that high-quality cylinders with the relatively low radius-to-thickness ratios required for plastic buckling are easier to fabricate than those with high R/t, and the fact that significant predictable axisymmetric bulges due to radial end restraints grow as the load is increased combine to reduce dramatically the deleterious effect of random unknown imperfections. We can therefore make fairly accurate predictions of the collapse loads of axially compressed cylinders tested in the usual way. Note that this conclusion may not apply to cylinders in which the ends are locally tapered and in which other devices are introduced into a test to prevent failure due to end bulging as shown in Fig. 2.1.

Bending of Long Tubes and Elbows

The elastic-plastic collapse and bifurcation buckling analysis of straight and curved tubes subjected to bending is needed for the design and evaluation of nuclear powerplant piping components, offshore pipelines, and other structures involving tubular members. Most of the recent work on piping has been motivated by a desire to be able to predict stress, stiffness, and limit moments of piping systems in nuclear reactors. Since the most flexible and highly stressed piping components are elbows, a significant portion of the total effort has been focused on test and analysis of various elbows under in-plane and out-of-plane moments. In the offshore oil industry the laying of underwater oil pipelines involves the bending of rather large-diameter straight pipes in the presence of external hydrostatic pressure. The degree of ovalization of the pipe cross section under bending is very much affected by the external pressure.

One of the earliest efforts in nonlinear structural analysis was presented in 1926 by Brazier.[93] His paper is concerned with the problem of the stability of long cylindrical shells under bending. If a long tube is subjected to bending, its cross section flattens. Consequently, its bending stiffness deteriorates with increasing load. The primary path, a graph showing the bending moment as a function of applied curvature, exhibits a maximum. Brazier performed a somewhat approximate analysis and found that the limit of stability is given by

$$M=(2\sqrt{2}/9)\,(E\pi ah^2/\sqrt{1-\nu^2}) \tag{9}$$

in which a is the tube radius and h its thickness. If the maximum stress caused by this moment is computed with use of the undistorted cross-section properties it is found that

with $\nu = 0.3$

$$\sigma_{cr} = 0.33\,E(h/a) \tag{10}$$

The problem of the stability of circular cylindrical shells under bending was solved as a bifurcation buckling problem by Seide and Weingarten in 1961.[94] Assuming that the prebuckling behavior can be defined with sufficient accuracy by a linear membrane solution, they found that the critical buckling stress is only 1.5% higher than the critical uniform compression stress for a shell with $a/h = 100$. For thinner shells the difference is even smaller. Thus for all practical purposes, the critical stress corresponding to the Seide-Weingarten model with $\nu = 0.3$ is $\sigma_{cr} = 0.6E(h/a)$. This value is well above the critical stress found by Brazier for infinitely long cylinders.

Boundary conditions usually restrict deformations so that at the shell edges the cross section remains circular. This restrains the cross-section flattening at all axial stations. Finite-length shells therefore collapse at load levels that are higher than is predicted by Brazier's analysis, as shown in Fig. 4.1. For sufficiently short shells the prebuckling behavior is well approximated by the linear membrane solution. For longer shells there is a coupling between the flattening of the cross section and the formation of a short axial wavelength or wrinkling buckle pattern. The flattening of the cross section increases the local radius as well as the actual bending stress. Consequently, it reduces the load level at which the wrinkling pattern appears. For the infinitely long shell, one must consider the possibility that the critical load corresponds to bifurcation from a nonlinear prebuckling state. For a cylinder of finite length, the wrinkling pattern is not orthogonal to the smooth prebuckling flattening mode and therefore the situation is not one of pure bifurcation. However, the wrinkling mode as a component of the prebuckling displacement is extremely small until a load level is reached at which it begins to grow rapidly. The structural behavior is therefore approximately the same as if a bifurcation point did exist. More details are given in Refs. 5, 19, and 96, including a rather complete survey of elastic and elastic-plastic collapse analyses and tests of tubes and elbows under bending.

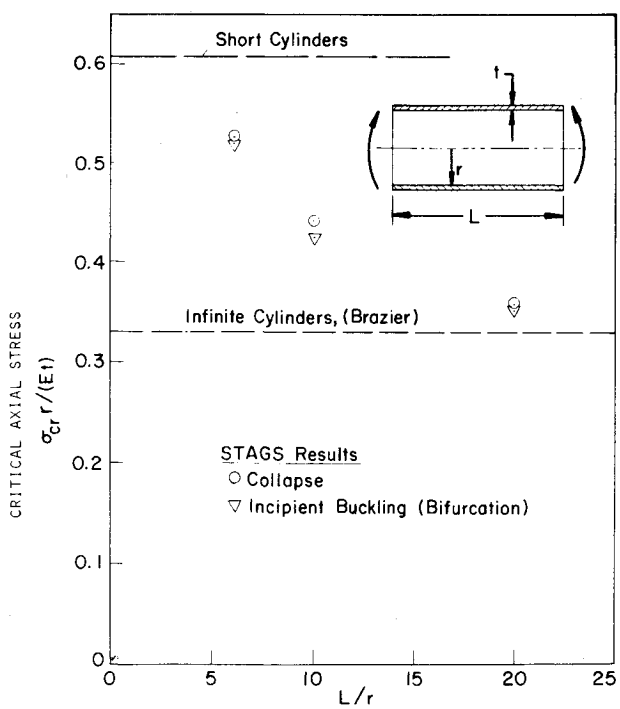

Fig. 4.1 Collapse due to cross-section ovalization and short-axial-wavelength bifurcation buckling of cylindrical shells subjected to bending—the ends are constrained to remain circular (from Stephens et al.[95]).

Numerical Strategies for Two-Dimensionally Discretized Problems

Most of the examples of nonlinear collapse shown so far can be analyzed with mathematical models in which the discretization is one-dimensional. An exception is the collapse of finite-length tubes in bending just described. The problems described in this section must also be treated with two-dimensional discretization. The distinction between one- and two-dimensional discretization is important because of the great difference in computer cost for cases with equivalent nodal-point density. With one-dimensionally discretized models, convergence with increasing nodal-point density is not too important because one can generally afford to provide more than enough nodes to be on the safe side. With two-dimensionally discretized models, however, limitations of budget for computer runs and limitations of computer core and auxiliary mass storage capacity often dictate the use of models with rather sparse nodal-point distributions. The quality of the solution is often questionable because the sparsely discretized models behave differently from the actual continuum and the size or even the sign of the error is rarely known.

Prediction of nonlinear collapse of structures that require two-dimensional discretization is expensive because large systems of equations must be set up and solved iteratively for many load increments. These systems of equations have fairly large bandwidths. The great expense of solving such systems has been a motivating factor in the search for efficient and accurate numerical strategies. Many of these are described in Ref. 19.

One of the strategies is to treat the two-dimensional problem as a *linear* bifurcation problem. This shortcut is cheaper than an incremental nonlinear analysis because it involves the solution of only one linear equilibrium problem plus one eigenvalue problem, which is usually equivalent to solution at about two-to-four load steps of a nonlinear equilibrium analysis. Several cases are outlined in this section, however, for which the linear bifurcation model is inadequate.

The question arises, of what use would a *nonlinear* bifurcation model be? There are two reasons why such a model is not usually advantageous. In the first place, bifurcation from the nonlinear fundamental state in perfect two-dimensional nonlinear shell problems is much rarer than for axisymmetric shells simply because there is less symmetry in the two-dimensional case. Therefore, bifurcation modes that are orthogonal to the prebuckled state (determined from nonlinear analysis) are less likely to exist. In the second place, it is generally just as expensive to calculate the nonlinear prebuckling state for the perfect system as it is to calculate the nonlinear precollapsed state for the same system in which a small general imperfection has been introduced in order to convert any bifurcation points (such as point B in Fig. 2.2a) into maximum load points (such as point E).

The only way in which a nonlinear bifurcation model might be used to advantage would be to provide intermittent estimates of the collapse load such that the total number of load increments required to find this critical load is reduced. Also, it may turn out that the collapse corresponds to the rapid development of a short-wave mode superposed on a smooth precollapsed state, as is seen in the example of the finite-length tube in bending.[95] In such cases one might set up two discretized models, a fairly crude one to capture the smooth nonlinear precritical deformation and a locally fine one in order to calculate accurately the short-wave bifurcation from the smooth precritical deformed state. The generally expensive prebifurcation nonlinear iterative solution would be carried out with the sparsely discretized model and the far less frequently performed eigenvalue analysis would be carried out with the more finely discretized model.

Cylindrical Panel with a Concentrated Normal Load

Figure 4.2 shows a panel with a normal load P applied at its

center. The panel has free longitudinal edges. The simply supported panel collapses because distortion (flattening) of the cylindrical cross section reduces the axial bending stiffness, an effect similar to the Brazier flattening of a long complete cylindrical shell due to bending. If the curved edges are restrained from axial motion (clamped), axial tension develops as the panel deflects, preventing collapse.

Note that the linear bifurcation buckling predictions for this case bear little relationship to the true behavior. In the simply supported case, the linear bifurcation load greatly overestimates the load at which the panel collapses because the bifurcation analysis does not account for the flattening of the cross section. In the clamped case, bifurcation is predicted when no collapse occurs because the linear analysis does not account for the stabilizing axial tension that develops in the panel as it deflects vertically.

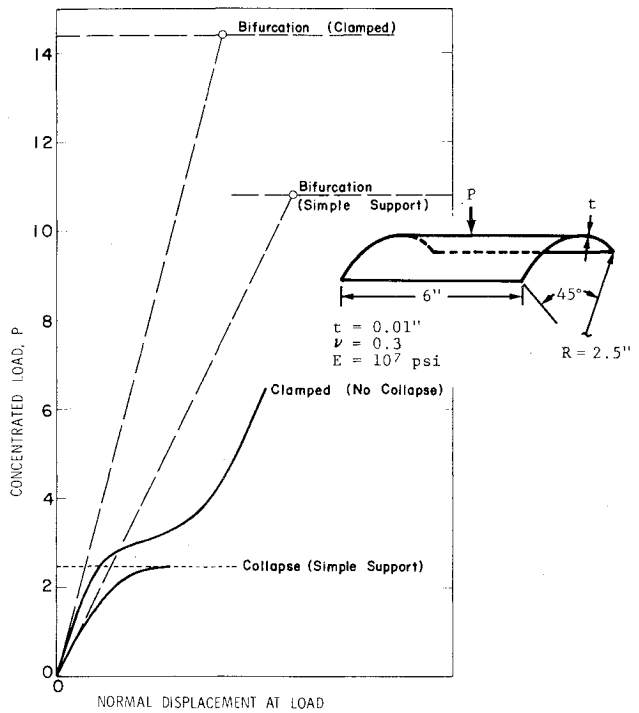

Fig. 4.2 Load-deflection curves for a cylindrical panel with bifurcation buckling loads predicted from linear theory—these results demonstrate the inadequacy of a linear bifurcation model (from Almroth and Brogan[97]).

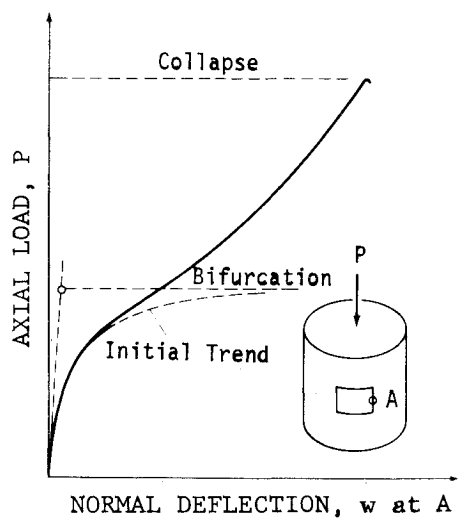

Fig. 4.3 Equilibrium paths for axially compressed cylindrical shell with two diametrically opposed cutouts. (From *Buckling of Bars, Plates, and Shells* by D. O. Brush and B. O. Almroth.[11] Copyright © 1975 by McGraw-Hill, Inc. Used with permisson of McGraw-Hill Book Co.)

Collapse of an Axially Compressed Cylindrical Shell with Diametrically Opposed Cutouts

A plot of load vs normal deflection at a point A on the edge of the cutout is displayed in Fig. 4.3, along with a prediction of failure from linear bifurcation buckling theory. In this case the bifurcation analysis underestimates collapse by more than a factor of two. The bifurcation model predicts the load at which the vertical edges of the cutout buckle. The linear bifurcation load does not correspond to failure of the structure. As bending occurs near the vertical edges of the cutouts the compressive stresses are redistributed away from these regions and the load is carried by the remaining portions of the shell. Thus, the shell shown in Fig. 4.3 collapses after significant stress redistribution has taken place. In the postbifurcation range the deformations in the neighborhoods of the cutouts have the effect of making these cutouts appear larger structurally than they do visually.

In general, one can assume that if the bifurcation buckling mode is fairly local and if alternate postbifurcation load paths are available, then a linear bifurcation buckling model will yield a conservative estimate of the collapse load. On the other hand, if the bifurcation buckling mode is global and if the precollapse deformation is significant, global, and of an unfavorable nature (e.g., curvatures decreasing) and if no alternative load paths are available in the postbuckled state, then the linear bifurcation buckling model will generally yield an unconservative estimate of the collapse load.

Collapse of Axially Compressed Noncircular Cylinders

Axially Compressed Elliptical Cylinder

Load vs end-shortening curves for perfect and imperfect elliptical cylinders are shown in Fig. 4.4. The cylinder has a length of 25.4 mm (1.0 in.), a thickness of 0.366 mm (0.0144 in.), and semiaxes of lengths 4.45 and 25.4 mm (1.75 and 1.0 in.). Young's modulus is 6.895×10^{10} Pa (10^7 psi) and Poisson's ratio is 0.3. It is subjected to a uniform end shortening with the edges free to rotate but restrained from moving in the radial and circumferential directions. The load/end-shortening curve for the perfect shell is that indicated by 0ABC. The other curves correspond to imperfect shells with the imperfection shape given by

$$\zeta = w_{\text{imp}}/t = -\xi\sin(\pi x/L)\cos(6\theta) \tag{11}$$

In a test on this shell, sudden changes in the deflection pattern (buckling) would be noticed at points A, B, and C. Notice that the shell may carry more load than the initial peak A indicates. While the primary buckling load A is rather sensitive to imperfections, it appears that the second maximum B is relatively insensitive to imperfections. Hence, it may be suitable as a design limit.

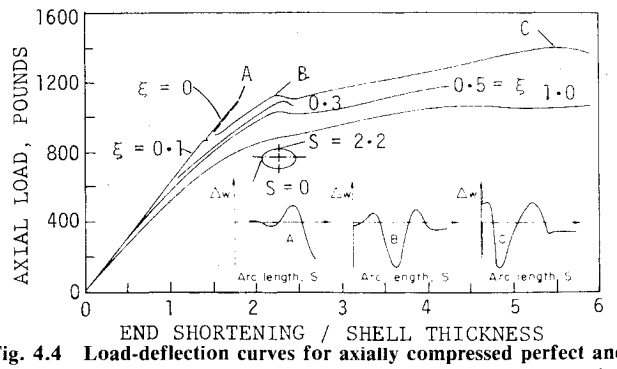

Fig. 4.4 Load-deflection curves for axially compressed perfect and imperfect cylinders with elliptical cross section, and fastest growing components of normal displacement at points A, B, and C (from Bushnell et al., *Computers & Structures*, Vol. 1, 1971, p. 380).

The curves Δw vs S at the bottom of Fig. 4.4 are buckling modes calculated by subtraction of the displacement vectors obtained in two sequential steps in end shortening and normalization of the result. Such a subtraction yields the shape of the fastest growing displacement component, which might be interpreted as a buckling mode. As one traces one's way along the load-deflection curve 0ABC, the axial stress in the shell is constantly being redistributed by the local growth of normal displacement. For example, early in the load history the most rapid growth of normal displacement occurs at the point labeled $S=2.2$, the area of minimum curvature. This growth relieves the axial stress there and permits loading above the initial peak A. At point B the most rapid growth of normal displacement is about halfway between the ends of the minor and major axes. This growth relieves the axial stress in the corresponding area and thus permits loading to an even higher peak C, where the rapid growth of normal displacement occurs near the end of the major axis in an area of relatively large curvature. The results shown in Fig. 4.4 were obtained with use of the STAGS computer program.[64]

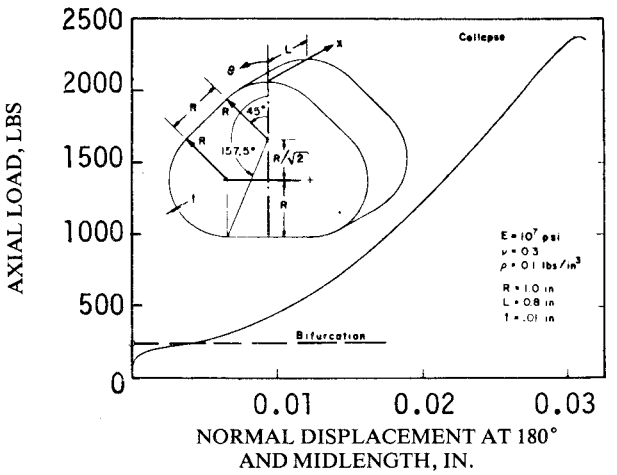

Fig. 4.5 Noncircular cylinder subjected to uniform end shortening (from Almroth and Brogan[97]).

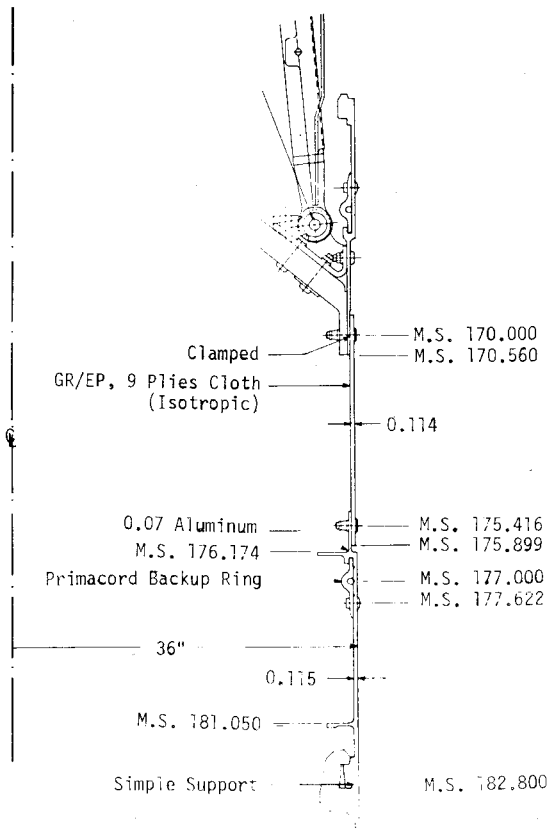

Fig. 4.6 Complex rocket interstage subjected to axial compression during launch (stability problems arise from the load path eccentricity at MS 175.9).

Axially Compressed "Pear-Shaped" Cylinder

A similar stress redistribution phenomenon occurs in the case of the noncircular cylinder depicted in Fig. 4.5. The behavior of this shell subjected to uniform end shortening was also investigated with the STAGS code.[64] The theoretical results are based on a two-dimensionally discretized model with 45 circumferential nodes and 9 axial nodes covering one-half of the circumference and one-half of the length.

The linear range in this case represents less than 1/30th of the total load history of the shell. The rapid change in slope of the load-deflection curve at about $P=444.8$ N (100 lb) corresponds to rapid growth in normal deflection (buckling) of the flat portions of the shell. Associated with this rapid growth in w is a redistribution of the axial stress so that the curved portions begin to take up a larger percentage of the total axial load P. As more and more of the axial load is borne by the curved portions, the slope of the load/end-shortening curve increases until just before collapse, at which load the entire structure fails. As in the case of the cylinder with the cutouts, a linear bifurcation model, which predicts buckling of the flat portions, is clearly too conservative an estimate of the load-carrying capability unless the material of the flat regions is so brittle that these sections fail due to excessive bending strain in their postbuckling states.

The rather complex behavior in this case indicates the need for a flexible strategy for calculation of collapse loads of shells. Small load steps and frequent refactoring of the equation system matrix are required in the load region between 444.8 and 889.6 N (100 and 200 lb), even though the displacements are relatively small in this range. Farther out on the load/end-shortening curve, where the displacements are larger, rather large load steps can be used and few refactorings are necessary. Just before collapse many small load steps and frequent refactorings of the stiffness matrix are

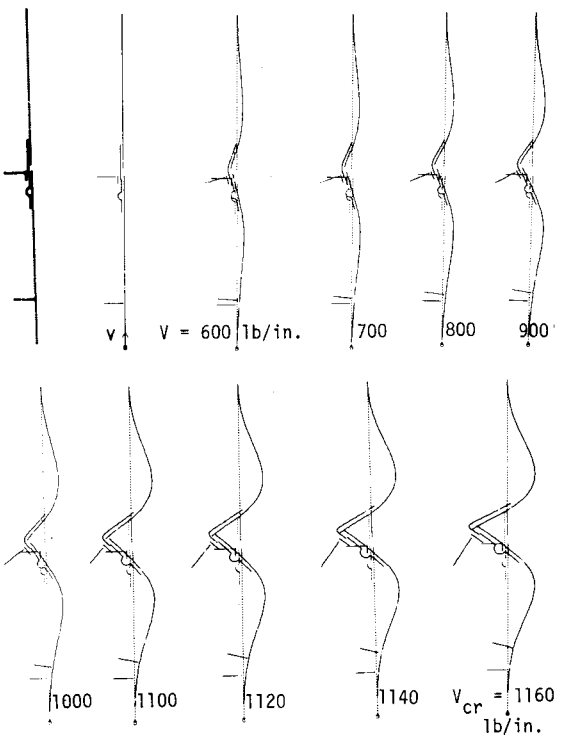

Fig. 4.7 Deformed profiles of the axially compressed rocket interstage with increasing axial compression V.

again required. Efficient use of the STAGS code, or any code for prediction of nonlinear behavior of shells, requires a sophisticated iteration strategy built into it and a well-trained user to take advantage of this strategy.

Axially Compressed Cylindrical Shell with Local Load-Path Eccentricity

Practical shell structures are often built up of several parts fabricated at different places. These parts must be assembled to create the finished product. The mating of the various parts often gives rise to instability problems which do not exist in the separate pieces, the design of which may not have included consideration of these "global" problems. Figure 4.6 represents such an assembled shell structure. It is a missile interstage with two sections, a forward adaptor made of composite material at missile stations (MS) 170.0-175.4, and an equipment section made of aluminum at MS 175.4-182.8. There is an aluminum primacord backup ring with a cavity for primacord at a notched separation joint at MS 177.0. This complex cylindrical shell structure must withstand axial compression during launch. The most severe problem of instability arises from inward excursion of the axial load path in the region between MS 175.4 and MS 177.6. This axisymmetric inward excursion causes axisymmetric deflections shown in Fig. 4.7, which was obtained with use of the BOSOR5 computer program.[65] Failure of the complex structure is due to elastic-plastic collapse in the short, thin [$t = 1.78$ mm (0.07 in.)] aluminum section located at MS 175.9. In a test of this structure failure occurred at a load within 1% of that predicted in the analysis.

5. Bifurcation Buckling in which Nonlinearity of the Prebuckling State is Important

Introduction

Whereas the emphasis in Sec. 4 was on nonlinear collapse rather than bifurcation buckling, the emphasis here is on bifurcation buckling with nontrivial prebuckling behavior. As was pointed out before, bifurcation from a nonlinear prebuckling state is of practical interest only in configurations with a great deal of symmetry. That is why the applications here all involve axisymmetrically loaded shells of revolution.

There are two principal kinds of influences that the prebuckling state has on the bifurcation buckling load:

1) The prebuckled loaded shell has a different shape from the unloaded shell; given a membrane prestress distribution, this new shape may be more likely or less likely to lose its stability than the original undeformed shape.

2) The prebuckling membrane stress distribution is an important factor; given a prebuckled shape of the shell, the membrane stress distributions calculated from linear or nonlinear analysis and membrane or bending shell theory may drastically affect the predicted bifurcation buckling load and mode shape.

In this section many examples will be given in which the combination of these two influences is present.

Particular emphasis is given here to elastic-plastic bifurcation buckling of internally pressurized torispherical shells, a complex problem for which both prebuckling shape change and nonlinear material properties greatly affect the prediction of the critical load. Comparisons from test and theory are then given for the hydrostatic buckling pressures of two ring-stiffened cylinders of nominally identical dimensions, one machined from a single billet and the other fabricated by first cold bending a flat sheet about a cylindrical die and then welding rings to it. Predicted residual deformation patterns due to welding are displayed for two cylindrical shells: one with rings welded to the inside surface and the other with rings welded to the outside surface.

Buckling of an Internally Pressurized Rocket Fuel Tank

Figures 5.1 and 5.2 pertain to this section. The geometry of the problem is shown in Fig. 5.1. The tank wall and skirt are

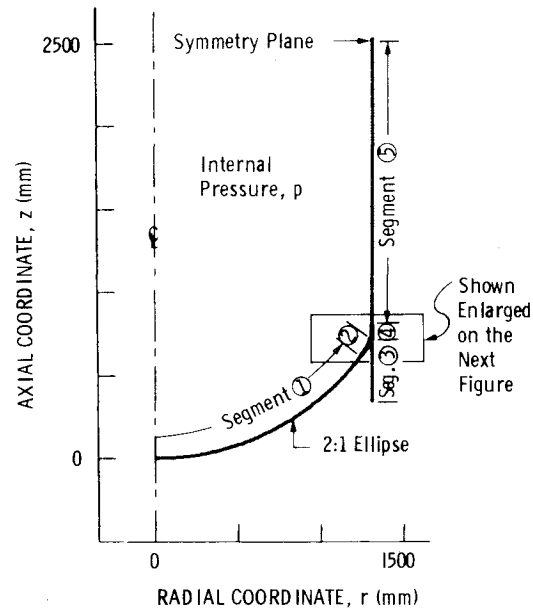

Fig. 5.1 Bottom part of rocket fuel tank as modeled for input to the BOSOR4 computer program.

divided into segments and analyzed with use of the BOSOR4 computer program.[9] Under small internal pressure the portion of the rocket fuel tank enclosed in the rectangle in Fig. 5.1 is drawn radially inward, resulting in development of a narrow band of hoop compression that might lead to bifurcation buckling. At the top of Fig. 5.2 is shown a bifurcation buckling mode predicted with use of linear theory. The modal normal displacement component $w_b(s,\theta)$ varies around the circumference as $w_b(s)\cos 90\theta$.

This is a problem for which the use of linear theory in the prebuckling phase of the analysis is inadequate. As the internal pressure is increased the ellipsoidal dome changes shape. The hoop stresses are redistributed and grow more slowly than linearly with pressure, as indicated in the bottom part of Fig. 5.2. As the internal pressure p is increased, the hoop resultant becomes tensile in the region where linear theory predicts bifurcation buckling to occur and the peak hoop compression initially increases more slowly than predicted by linear theory, eventually reaching a maximum value of about -800 N/mm at a pressure of 1.4 Pa, after which it decreases with further increases in internal pressure. Thus, the prediction with nonlinear prebuckling effects included is that bifurcation buckling will not occur at all.

Elastic-Plastic Buckling of Internally Pressurized Torispherical Vessel Heads

Introduction

The examples presented here fall into the same class as those with hoop compression. The problem is of special significance to designers of pressure vessels, many of which have torispherical or ellipsoidal heads. An example of a typical postbuckled pattern for an *elastic* shell is shown in Fig. 5.3.

This class of problems is particularly interesting because in the range of practical design parameters predicted behavior is found to be sensitive to prebuckling geometric nonlinearity as well as material nonlinearity, the former effect increasing the critical pressure and the latter decreasing it. Therefore, the problem serves as an excellent demonstration of the kinds of nonlinear phenomena an engineer should be aware of when he undertakes a stability analysis. The description here applies to both torispherical and ellipsoidal vessel heads.

Interest in buckling of internally pressurized torispherical heads was originally stimulated by the failure of a large fluid coker undergoing a hydrostatic proof test at Avon, Calif. in

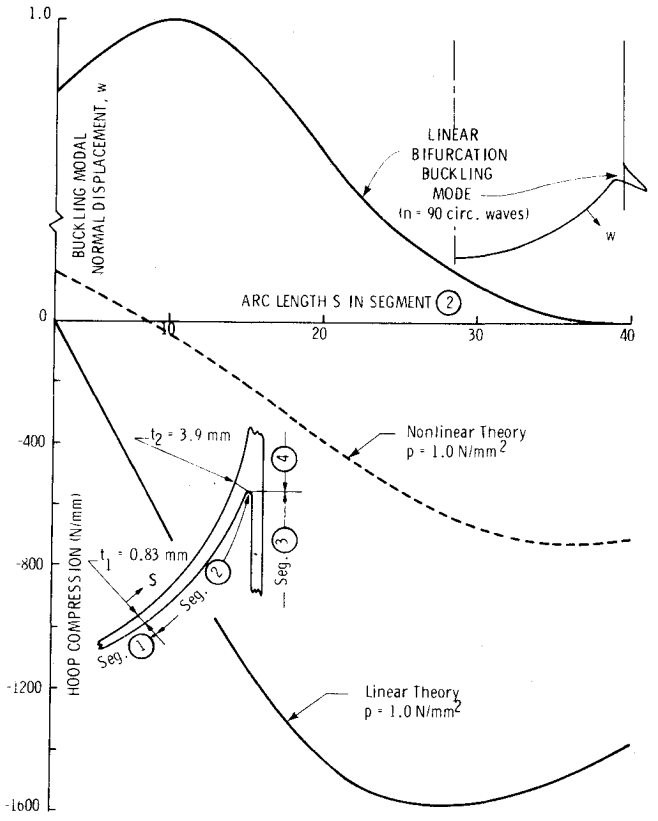

Fig. 5.2 Nonsymmetric buckling mode (top) and hoop resultants (bottom) for the part of the internally pressurized rocket motor indicated in Fig. 5.1.

1956. The failed vessel is shown in Fig. 1.3. The possibility of nonaxisymmetric buckling of such a system was first predicted by Galletly.[1] Mescall[98] was the first to present a solution of the nonaxisymmetric stability analysis. He used the small deflection theory. Adachi and Benicek[99] conducted a series of buckling tests on torispherical heads made of polyvinyl chloride (PVC), chosen primarily because of the high ratio of yield stress to Young's modulus, which insures that buckling occurs before large-scale yielding. The correlation of elastic analysis with these tests was much improved by inclusion of nonlinear geometric effects. Thurston and Holston[100] were the first to account for the moderately large axisymmetric prebuckling meridional rotations in the stability analysis of these heads. Since publication of Ref. 100 many computer programs have been written which calculate nonsymmetric buckling loads of arbitrary elastic shells of revolution, including geometric nonlinearity in the prebuckling analysis and prebuckling shape changes in the stability analysis.[9,22-24]

Recently, several papers have appeared on nonsymmetric buckling of elastic-plastic pressure vessel heads: Brown and Kraus[101] calculated critical pressures for internally pressurized ellipsoidal heads with the use of the small-deflection theory. Bushnell and Galletly[102] found buckling loads for externally pressurized torispherical heads pierced by nozzles and for conical heads with the use of large-deflection theory in the prebuckling analysis, and Bushnell and Galletly,[103] Lagae and Bushnell,[104] and Galletly[105,106] used the BOSOR5 computer program to compare theoretical predictions with tests by Kirk and Gill,[107] Patel and Gill,[108] and Galletly[105,106] for buckling of internally pressurized torispherical and ellipsoidal heads. Other work on stress and stability analysis of vessel heads is surveyed by Esztergar.[109]

Cause and Characteristics of Nonsymmetric Bifurcation Buckling

The development of visible buckles such as shown in Fig. 5.3 is a process and not the single event predicted by a

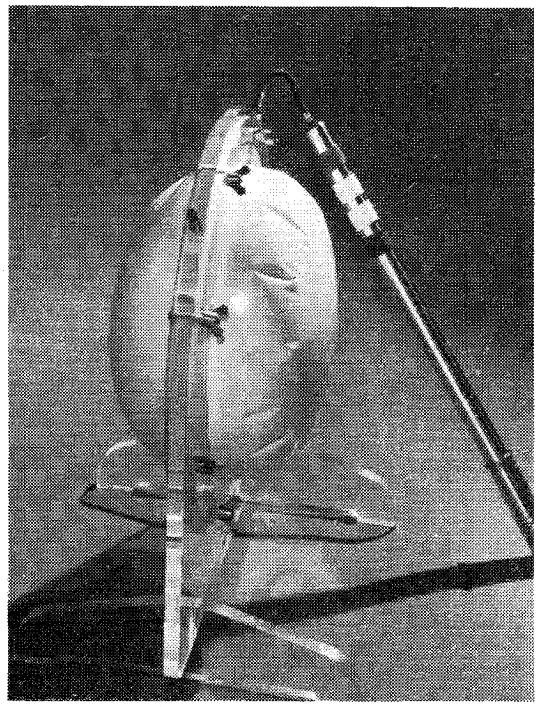

Fig. 5.3 Elastic buckling under internal pressure (from Galletly, *Proceedings of Institution of Civil Engineers*, Pt. 2, Vol. 67, Sept. 1979, p. 615).

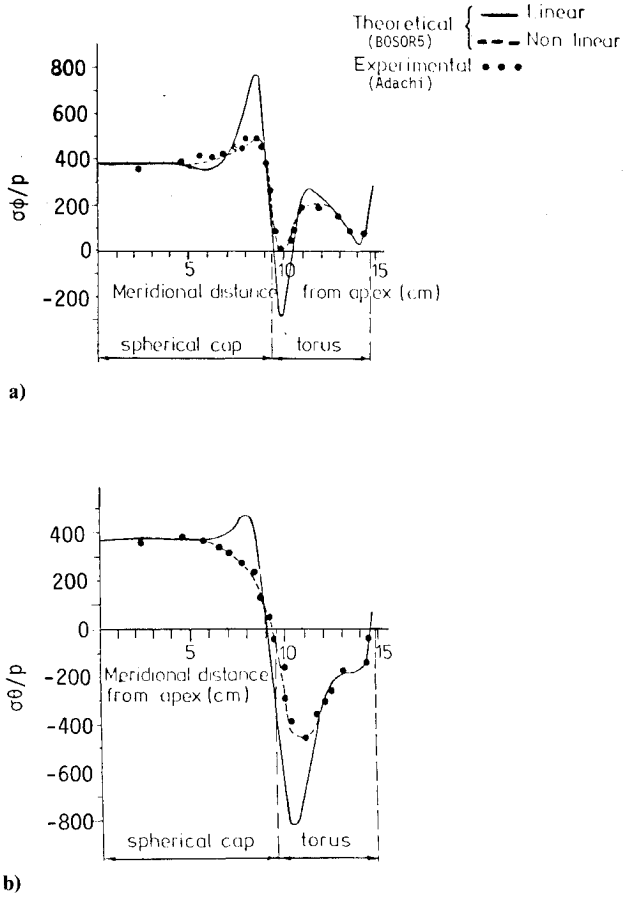

Fig. 5.4 Experimental and theoretical results for an elastic machined aluminum torispherical head subjected to internal pressure (from Galletly, *Proceedings of Institution of Civil Engineers*, Pt. 2, Vol. 67, Sept. 1979, p. 615). a) Meridional stresses on outside surface, $p = 414$ kPa; b) circumferential stresses on outside surface, $p = 414$ kPa.

bifurcation (eigenvalue) buckling analysis. As the pressure in a test specimen is increased above some critical value a very localized isolated incipient buckle forms in the knuckle region, invisible to the naked eye but detectable by a sensitive probe or a strain gage. The buckle grows slowly at first, then more rapidly, and suddenly becomes visible. This visible buckle generally covers most of the knuckle region in the meridional direction but has a very short circumferential wavelength. After formation of the first buckle the pressure can be further increased substantially, causing the formation of other visible buckles in the knuckle region, each isolated circumferentially from its neighbors, as shown in Fig. 5.3. An isolated buckle, generated by circumferential compression in the knuckle region, apparently causes the relief of this compression within a sector surrounding the buckle, thereby preventing the formation of the uniform buckle pattern typical of buckled axially compressed cylindrical or externally pressurized spherical shells.

The theoretical results shown here are derived from an analysis which is founded on the assumption that one is especially interested in the pressure at which the first incipient buckle forms. Therefore, buckling is treated as a single event predicted by means of an eigenvalue formulation which yields the bifurcation point B in Fig. 2.2a.

Geometric Nonlinear Effects

Given the assumption that the wall material remains elastic, the most significant determinant of the buckling pressure for a shell of given properties is the hoop stress resultant N_{20} in the area of the knuckle where buckling occurs. The bottom plot in Fig. 5.4 shows that in this region N_{20} does not grow linearly with pressure but quite a bit more slowly. The slower-than-linear growth of compressive N_{20} in the axisymmetric prebuckling regime is due to two factors: As the pressure is increased the torispherical shape "tries" to become more spherical. The second and smaller factor causing slower-than-linear growth of N_{20} is the pressure-rotation effect. The nonlinear growth of N_{20} explains why buckling pressures from nonlinear elastic theory are higher than those from linear theory.

There is another nonlinear geometric phenomenon which has the opposite effect on the buckling load: As the pressure is increased, the meridional curvature diminishes in the region where buckling occurs. This axisymmetric decrease in meridional curvature in the prebuckling regime has the effect of reducing the circumferential stress resultant required to cause buckling.

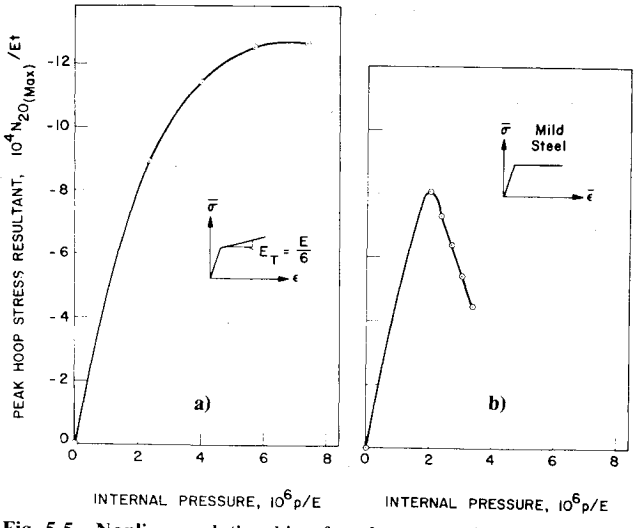

Fig. 5.5 Nonlinear relationship of peak compressive hoop resultant in torispherical head to internal pressure: a) material with considerable strain hardening, b) elastic-perfectly plastic material.

Nonlinear Material Effects

The two biggest effects of plastic flow on the predicted bifurcation buckling pressure are the following:

1) The rate of change of the compressive hoop stress resultant with increasing pressure is strongly dependent on the rate at which the material strain hardens.

2) The "tangent stiffness" (integrated constitutive coefficients) which govern at the bifurcation load are reduced from their elastic values. The values of these coefficients are sensitive to the postyield paths followed by the material points in the stress space and the postyield paths are sensitive to the rate at which the material strain hardens.

Figures 5.5 shows the peak hoop resultant as a function of internal pressure for two values of postyield hardening modulus E_T. A typical behavior of mild-steel torispherical shells is that they buckle nonsymmetrically at pressures for which the hoop compression is diminishing in the knuckle region, as shown in Fig. 5.5b.

Figure 5.6 demonstrates that the postyield path in the stress space of a typical material point in the knuckle region is strongly dependent on the hardening modulus E_T. Bifurcation buckling predictions for mild-steel torispherical heads are somewhat questionable because we do not yet understand metal plasticity well enough to be able to predict with certainty the state of a material that has undergone nonproportional biaxial loading.

Comparison of Test and Theory

Figures 5.7 and 5.8 pertain to aluminum torispherical specimens tested by Patel and Gill.[108] Figure 5.8 gives comparisons of predicted and measured incipient buckling pressures for the heads discretized for analysis with BOSOR5[65] as shown in Fig. 5.7. The ranges of pressures over which the buckling patterns were observed to develop are also indicated in Fig. 5.8. In Fig. 5.8:

P_{act} = pressure at which the first buckle was fully developed

P_{clear} = pressure at which the first buckle could be felt by touching the surface of the specimen

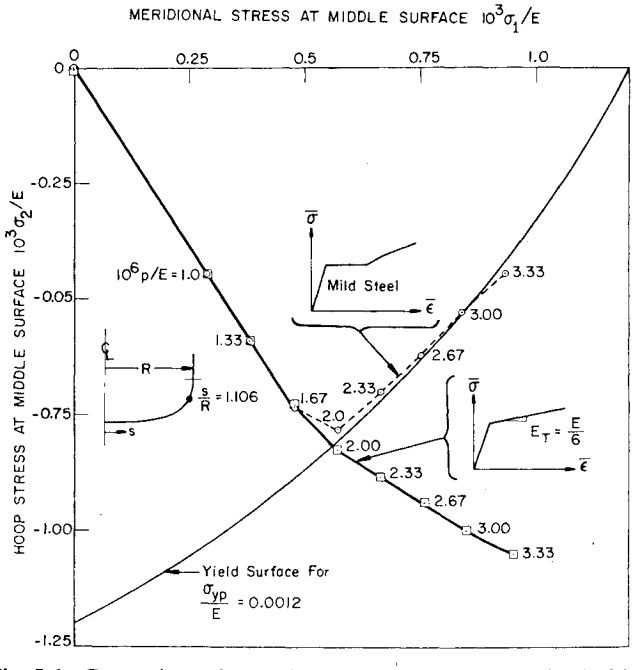

Fig. 5.6 Comparison of paths in stress space at station $s/R = 1.106$ with increasing internal pressure in ellipsoidal heads with two different hardening moduli (from Bushnell, *Transactions of ASME, Journal of Pressure Vessel Technology*, Vol. 99, Feb. 1977, p. 63).

$P_{incipient}$ = pressure at which the first buckle was detected by a sensitive probe revolved around the circumference at a station in the toroidal knuckle

It is seen in tests that what is being characterized in the analysis as a single event called "bifurcation buckling" is actually a process occurring over a finite range of internal pressure. The quality of the theoretical predictions of incipient buckling and the behavior of the test specimens as the pressure is increased above the incipient buckling pressure indicate that these types of vessels are not particularly sensitive to initial imperfections.

Effect of Fabrication Residual Stresses and Deformations on Plastic Buckling of Ring-Stiffened Cylinders under External Hydrostatic Pressure

In 1958 Ketter[110] identified four sources of residual stresses and deformations of fabricated metal structures: differential cooling during and after rolling sheet metal, cold bending, various erection procedures, and welding. He considered the effect of differential cooling in the fabrication process on buckling loads of axially compressed I-beams.

Cold Bending

Several authors have investigated residual stresses due to cold bending. Almen and Black[111] give the residual stress pattern through the thickness of a bar which has been bent about a circular die. Queener and De Angelis[112] derive approximate formulas for residual stresses and the ratio of the die radius R_0 to the final radius after springback R_f for materials with stress strain curves of the form $\sigma = K\epsilon^n$. Lunchick[113] determines the effect of cold bending on buckling loads of cylindrical pressure vessels. He calculates effective stress-strain curves for the prestressed material by averaging effective stresses and strains at 12 stations through the thickness of the shell wall. Such curves depend on the service loads. Lunchick's model is based on elastic-perfectly-plastic material and deformation theory. It is determined in Ref. 113 that bending residual stresses have the greatest weakening effect for cylindrical shells in which the effective stress in the wall is near the material proportional limit at the buckling pressure calculated with neglect of these residual stresses. For such structures, the reduction in buckling pressure due to cold bending can be as much as 30%. Tacey[114] has written a computer program for the calculation of the residual stress distribution and the effective stress-strain curve of cold-bent beams for a wide range of practical cross-section geometries. The Bauschinger effect and possible inelastic behavior on springback are accounted for. The hardening rule used in Tacey's program is a combination of isotropic and kinematic rules.

Welding

During the 1970s much work was done on the numerical modeling of mutlipass welding. The ASME volume, *Numerical Modeling of Manufacturing Processes*,[115] contains several papers on this subject. Masubuchi[116] wrote a survey of the field in 1975. Three frequently referenced papers are by Hibbitt and Marcal,[117] Nickel and Hibbitt,[118] and Friedman.[119] The results presented in these papers are generally obtained from sophisticated computer programs for multidimensional analysis. Although the heat conduction and the thermal stress problems are uncoupled, the models include nonlinear boundary conditions for solid and liquid regions, temperature-dependent material effects, latent-heat effects, and convective and radiative heat-transfer boundary conditions.

It is impractical to incorporate such elaborate models of the welding process into an analysis of buckling of a ring-stiffened shell with many welds. A simple, computationally efficient model is introduced in Ref. 65 in which buckling pressures are calculated for a welded ring-stiffened ellipsoidal shell. The shell and rings are assumed to be machined and stress relieved separately and then welded together. The effects of weld shrinkage are simulated in Ref. 65 by means of the assumption that a certain amount of material in the local neighborhoods of each weld is cooled below ambient temperature to a difference approximately equal to the annealing temperature. The residual stress distribution thus generated is characterized by local tensile circumferential yielding near the welds and elastic circumferential compression over the rest of the cross sections of the shell wall and ring stiffeners. The structure prestressed in this way remains axisymmetric, of course, but the radial shrinkage varies in the meridional direction, introducing an axisymmetric imperfection with a characteristic wavelength equal to the ring spacing. The weld effect thus modeled reduces the predicted buckling pressure by about 10%.

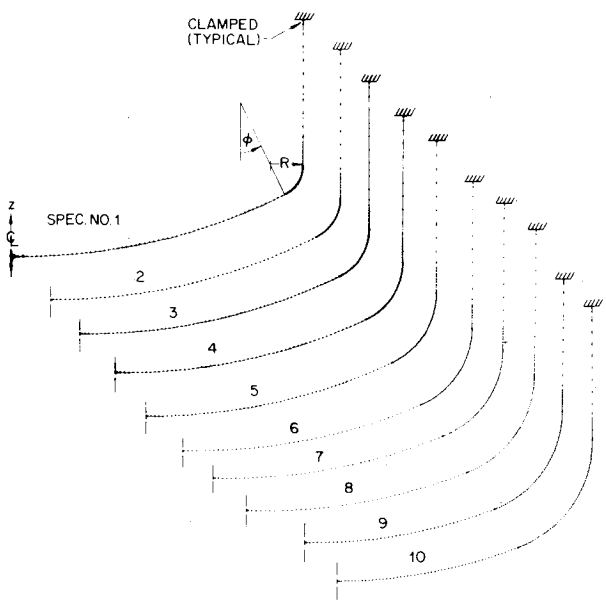

Fig. 5.7 Discretized models of torispherical heads under internal pressure tested by Patel and Gill[108] (from Lagae and Bushnell[104]).

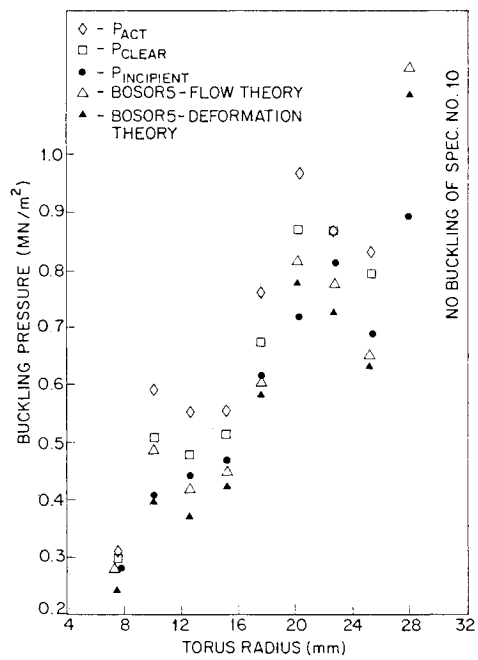

Fig. 5.8 Variation in buckling pressure with radius of toroidal knuckle: comparisons of test results of Ref. 108 with BOSOR5 predictions for incipient buckling (from Lagae and Bushnell[104]).

Bending and Welding

Few papers exist in which residual stresses are calculated for more than one fabrication process. Chen and Ross[120] calculate residual stresses from cold bending a flat sheet into a cylindrical shape and then welding the longitudinal seam. They suggest that these residual stresses will cause early column buckling of long cylinders under axial compression. Faulkner[121] gives a survey of work done on calculation of residual stresses due to welding ring stiffeners to cylindrical shells and cold bending sheets into cylindrical shells and beams into rings. He states that when ring stiffeners are welded to a cylindrical shell of thickness t there is a tensile yielding over a length of shell equal to $2\eta t$ and over a length of the ring web equal to ηt. These tensile regions are balanced by compressive residual stresses distributed over the remainder of the shell and ring cross sections. Typical values of η obtained from measurements are in the range of $1.5 \leq \eta \leq 4.5$. The measured radial shrinkage at the welds is approximately 10% of the shell thickness t.

Residual Deformations from Welding Internal vs External Rings

In 1957 Krenzke[122] investigated experimentally the effect of welding residual stresses and deformations on plastic buckling of ring-stiffened cylinders under external hydrostatic pressure. Two of his specimens, designated "M1" and "M2" were nominally identical except that the rings of specimen M1 were internal and those of M2 external. Krenzke measured average welding distortions for specimen M1 approximately equal to those exhibited in Fig. 5.9b, which are predicted by BOSOR5[65] to result from the imposed nonuniform temperature distribution shown in detail AA. An analogous temperature distribution corresponding to externally welded rings yields a predicted residual deformation shown in Fig. 5.9c. These displacements have the distribution measured by Krenzke for specimen M2 but the amplitude of the predicted waves is about twice that measured. It seem that, in this case at least, about half as much "cooldown" is required to simulate the welding process with external rings as is required for the simulation of welding internal rings.

In the tests the externally stiffened specimen M2 collapsed at a pressure about 5% higher when corrected for different material yield strengths than that for the internally stiffened specimen. The same difference is predicted by BOSOR5. The collapse mode is characterized by formation of an axisymmetric inward dimple. The "hungry horse" residual welding deformation pattern displayed in Fig. 5.9b represents an initial imperfection that is more harmful than the "caterpillar" mode exhibited in Fig. 5.9c because the former resembles the collapse mode whereas the latter has a shape opposite to that of the collapse mode.

Effect of Cold Bending and Welding on Buckling of Ring-Stiffened Cylinders

The BOSOR5 computer program can be used for calculation of bifurcation buckling on cold-bent and welded ring-stiffened cylinders under external pressure. Residual stresses and deformations from cold bending and welding can be included in the model for buckling under service loads by introduction of these manufacturing processes as functions of a time-like parameter, "time," which insures that the material in the analytical model experiences the proper sequence of loading prior to and during application of the service loads. The cold-bending process is first simulated by a thermal loading cycle in which the temperature varies linearly through the shell wall thickness, initially increasing in "time" to simulate cold bending around a die of radius R_0 and then decreasing in "time" to simulate springback to a final somewhat larger design radius R. The welding process is subsequently simulated by the assumption that the material in the immediate neighborhoods of the welds is cooled below the ambient temperature by an amount that leads to weld shrinkage amplitudes typical of those observed in tests. In Ref. 123 buckling loads are calculated for a configuration including and neglecting the cold-bending and welding processes. These predictions are compared to values obtained from tests by Kirstein and Slankard[124] and Slankard[125] on two nominally identical specimens, shown in Fig. 5.10. The specimen designated BR-4 was fabricated by cold bending the shell and then welding machined ring stiffeners to it, and the specimen designated BR-4A was carefully machined. Figure 5.11 illustrates the loading sequence followed in an analysis with use of BOSOR5.

In the analysis the machined specimen is predicted to fail at 3.723 MPa (540 psi), precisely in agreement with the test on specimen BR-4A. Simulation of only the cold-bending process leads to a prediction of $p_{cr} = 3.172$ MPa (460 psi) and simulation of both cold bending and welding does not change this result. The predicted radial shrinkage due to welding is maximum at the ring stiffeners (equal to about 8% of the shell thickness) and minimum midway between rings, a mode similar to that shown in Fig. 5.9c. The welding process apparently has little influence on the buckling pressure because of two counteracting effects: the residual welding stresses

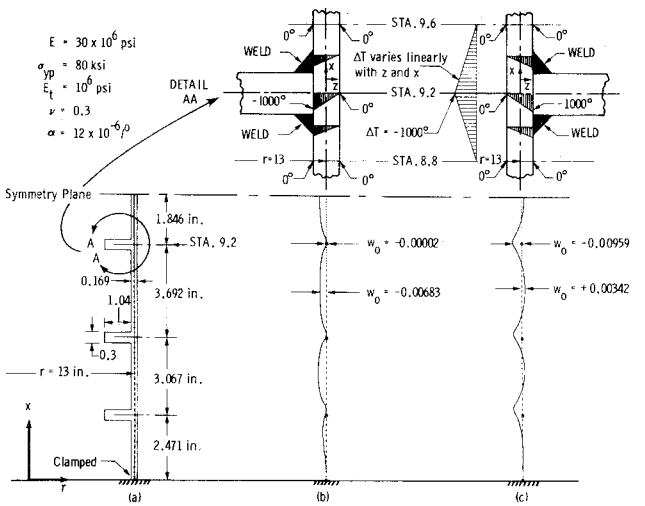

Fig. 5.9 Cylinder with welded internal and external rings: a) dimensions and BOSOR5 discretized reference surface; b) predicted residual deformations after welding and before loading of specimen with internal rings; c) predicted residual deformations after welding and before loading of specimen with external rings.

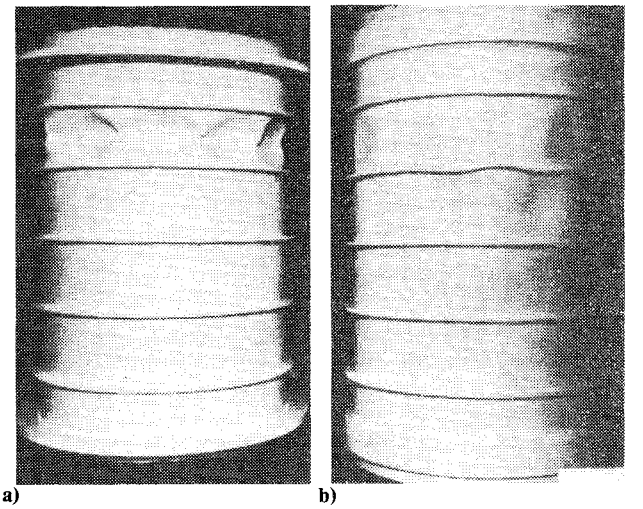

Fig. 5.10 Buckling patterns in ring-stiffened cylindrical shells: a) the cold-bent and welded specimen BR-4, ($p_{cr} = 390$ psi); b) the machined specimen BR-4A, ($p_{cr} = 540$ psi) (from Wenk, E., Jr., "Pressure Vessel Analysis of Submarine Hulls," *Welding Research Supplement*, June 1961, p. 277).

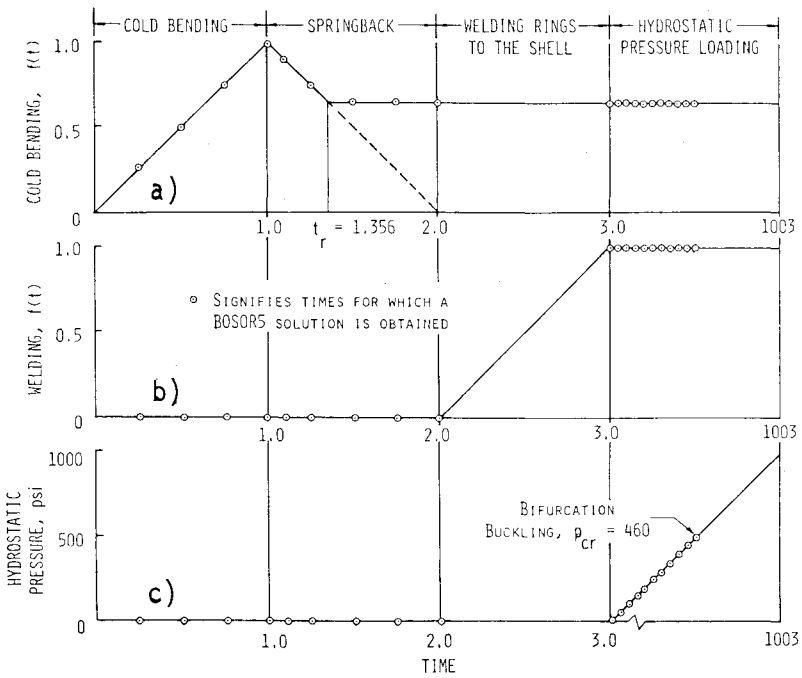

Fig. 5.11 Loading functions of "time" for BOSOR5 analysis of the fabricated ring-stiffened cylinder BR-4: a) cold-bending process; b) welding the rings to the cylinder; c) application of the external hydrostatic pressure.

weaken the shell but the "caterpillar" type residual deformations strengthen it.

The BOSOR5 simulation of the fabrication process explains a little more than half of the experimental difference between the buckling pressures of the machined model BR-4A and the cold-bent, welded model BR-4. The remaining discrepancy is probably caused by some combination of the following effects not included in the BOSOR5 model:

1) There exist nonaxisymmetric initial imperfections which are greater for fabricated models than for machined models. These include nonuniformity in shell thickness. Measurements of the steel plate from which specimen BR-4 was fabricated indicate that the thickness varied by as much as 10%.[125]

2) The stress-strain curve of the "Alan Wood steel" from which specimen BR-4 was made is unknown. The material proportional limit may have been less than the yield stress quoted in Ref. 125. If so, inclusion of the Bauschinger effect in the BOSOR5 model would have generated yielding in compression at lower pressures than those calculated with the present model, which is based on an isotropic hardening law. Presumably, the critical pressure would then also have been lower.

3) The welding simulation is a heuristic model which is in qualitative agreement with measurements on other specimens made of other materials.[65,121,122] A rigorous treatment including welding sequence and nonaxisymmetric effects might lead to a lower critical pressure.

4) The sheet from which specimen BR-4 was fabricated may have contained initial residual stresses due to differential cooling during and after it was rolled into its flat form of thickness 3.35 mm (0.132 in.).

6. Boundary Conditions, Transverse Shear Deformation, and Stable Postbuckling Behavior

Introduction

This section contains a potpourri of buckling phenomena and modeling tips for the solution of buckling problems. First, boundary conditions are discussed. They influence buckling loads in two ways: through the prebuckling membrane stress field and through the admissible buckling mode. An important effect is load eccentricity, which is particularly significant for axially compressed, axially stiffened cylindrical shells. An example is given in which the boundary constraint has an unexpectedly large influence on the critical load of a test panel, forcing it to buckle in a higher crippling mode not likely to occur in the actual flight environment the test was supposed to simulate. The section closes with a discussion of results from buckling analyses of two rather large discretized models, one in which collapse loads calculated with and without transverse shear deformation are compared and the other in which the far postbuckled state is stable.

Effects of Boundary Conditions and Load Eccentricity

Practical shell structures are very often built in parts with different organizations or even companies being responsible for the design of "their" part. Very often buckling loads for each part are calculated with the sometimes unjustified assumption of simple support or clamping at the boundaries of that part. The main purpose of this discussion is to sound a note of warning not to take these factors for granted, especially when one is designing test specimens and performing final detailed analyses.

Figure 4.6 is an example in which a short region of particular interest, the rocket interstage between stations MS 170.0 and 182.8, is isolated and analyzed separately from the remaining structure through the assumptions of clamping at MS 170.0 and simple support (with additional support provided by a rather large edge ring) at MS 182.8. The thicknesses of the adjacent structural parts to which the interstage is attached seem to justify these assumptions. However, usually it is best to include portions of the adjoining segments in the discretized model, possibly with a cruder nodal point density. This is especially true if the structure is axisymmetric and a one-dimensionally discretized model is sufficient. A good general rule in such a case is to include in the model all parts of the structure that are defined, or all parts between stations at which there is no doubt as to what boundary conditions and loading should be assumed.

If little is known about the adjoining structures, sensitivity studies should be performed in which both upper and lower bounds on the degree of boundary constraint are assumed. Before expensive test specimens are fabricated, analytical simulations of the test should be performed, with proper representation of the boundary conditions to be applied in the test and account taken of the possibility of local buckling. The effort in building and testing the expensive shroud shown in Fig. 1.9a, for example, was largely wasted because of

unexpected local crippling near the field joint, a failure which could have been predicted before the test if the joint had not been treated merely as a simple support for the surrounding structure but instead had been modeled more rigorously.

Because of limitations in computer budgets or lack of definition of the adjacent structural parts, it is often necessary to establish boundaries at which there is some doubt as to what the support conditions are and where the load path is. For example, if one assumes that the end of the model of the rocket interstage depicted in Fig. 4.6 is at MS 182.8, one must then decide which of the displacement and rotation components u, v, w, and β are to be restrained and at what radius the axial load is to be applied. The purpose of this section is to provide some examples which reveal the sensitivity of predicted bifurcation buckling loads to assumptions such as these.

A linear bifurcation buckling problem has the following form

$$[\boldsymbol{K}_1 + \lambda \boldsymbol{K}_2]q = 0 \tag{12}$$

in which $\boldsymbol{K}_1$ is the stability stiffness matrix, λ the load factor (eigenvalue), $\boldsymbol{K}_2$ the load-geometric matrix, and q the eigenvector. Boundary conditions and eccentric loading influence the stability, in particular the bifurcation buckling load λ, in two ways:

1) The prebuckling membrane stress resultants at a given load depend on these factors; therefore the load-geometric matrix, $\boldsymbol{K}_2$ in Eq. (12) depends on them.

2) The prebuckling deformations and the structural stiffness at the boundary depend on these factors; therefore the stiffness matrix, $\boldsymbol{K}_1$ in Eq. (12), depends on them.

It is often true that the boundary conditions affect the bifurcation buckling load and mode most strongly through their influence on the stability stiffness matrix $\boldsymbol{K}_1$, whereas the load eccentricity affects the bifurcation buckling load and mode most strongly through its influence on the prebuckling state and hence on the load-geometric matrix $\boldsymbol{K}_2$. This statement is probably more valid when applied to cylindrical shells than to shells of other geometries. (Note that in relating boundary conditions to the stability stiffness matrix $\boldsymbol{K}_1$, we tacitly assume that the Lagrange multiplier or penalty function method is being used or that certain rows and columns of $\boldsymbol{K}_1$ have been modified to account for the boundary constraint conditions.)

The prebuckling state of a uniformly axially compressed, fairly long, thin monocoque cylindrical shell loaded at its middle surface depends on the boundary conditions only within a "boundary layer" or a distance of approximately two or three times $(Rt)^{1/2}$ of the edge. The prebuckling conditions at the edge have only a mild influence on the predicted bifurcation buckling load, as seen from Table 6.1. However, there are several different sets of boundary conditions for which the prebuckling behavior and hence the load-geometric matrix $\boldsymbol{K}_2$ is the same but the bifurcation buckling load and mode shape change radically. For instance, any change in the boundary condition having to do with the circumferential tangential displacement v, which does not appear in the prebuckling problem at all, drastically affects the bifurcation buckling load and mode through changes in the stability stiffness matrix $\boldsymbol{K}_1$ only. A dramatic example is an axially compressed cylindrical shell with free edges. The axisymmetric prebuckling solution is characterized essentially by the uniform compressive axial resultant $N_{10} = -P/2\pi R$, but the bifurcation buckling load P_{cr} is several orders of magnitude smaller than the classical value because the possibility of inextensional buckling modal deformation exists.

On the other hand, the major effect of load eccentricity on cylindrical shells under axial compression is to produce bands of prebuckling hoop compression or tension as well as meridional curvature change. The load eccentricity effect is especially significant in cylinders with axial stiffening because the stiffeners provide an eccentric surface to push against and the boundary layers near the supported edges are longer than they are in the case of monocoque cylinders. Therefore, the circumferential tension or compression generated in these boundary layers has an important effect on the load-geometric matrix $\boldsymbol{K}_2$ and hence on the buckling load.

Boundary Conditions

Much of the early work on the effect of boundary conditions on the buckling of cylindrical shells is reviewed by Hoff.[36] Von Mises,[126] Nash,[127] Galletly and Bart,[128] Singer,[129] and Sobel[130] studied cylindrical shells under uniform hydrostatic external pressure. Nachbar and Hoff,[131] Stein,[132] Fischer,[133] and Almroth[134] and others identified in Ref. 36 treated cylindrical shells under uniform axial compression. Detailed investigations were carried out by Sobel[130] and Almroth.[134] They assumed that buckling would be symmetrical about the midlength of the cylinder generator, and they calculated buckling loads for the eight boundary conditions listed in Table 6.1.

The most significant result of Sobel's analysis is the revelation of the important effect of axial restraint $u = 0$ on buckling pressures, even for moderately long cylinders. The most significant results obtained by Almroth are those corresponding to edge conditions S3 and S4, for which the circumferential tangential displacement v is free ($N_{xy} = 0$). This result, first calculated by Stein,[132] is similar to that obtained by Nachbar and Hoff[131] for axisymmetric buckling of an axially compressed cylinder with a completely free edge. However, neither type of free-edge buckling is likely to occur in practice because friction at the ends of the axially compressed cylindrical shell is sufficient to prevent the buckling modes from developing.

Inextensional Modes

Even lower buckling loads for axially compressed cylindrical shells than those calculated by Almroth[134] are possible

Table 6.1 Influence of boundary conditions and prebuckling behavior on the buckling load (from Ref. 57)

Sobel[130] nomenclature	Singer[140] nomenclature	Actual boundary conditions	λ_{crit} Hoff and Soong[135] (membrane prebuckling)	λ_{crit} Almroth[134] (rigorous prebuckling)
S4		$w = w_{,xx} = \sigma_x = \tau_{xy} = 0$	0.5	0.502
S3		$w = w_{,xx} = u = \tau_{xy} = 0$	0.5	0.503
S2	SS3	$w = w_{,xx} = \sigma_x = v = 0$	1.0	0.844
S1	SS4	$w = w_{,xx} = u = v = 0$	1.0	0.867
C4		$w = w_{,x} = \sigma_x = \tau_{xy} = 0$	1.0	0.908
C3		$w = w_{,x} = u = \tau_{xy} = 0$	1.0	0.926
C2		$w = w_{,x} = \sigma_x = v = 0$	1.0	0.910
C1		$w = w_{,x} = u = v = 0$	1.0	0.926

if one assumes that the edges are completely free. Cohen[136] was the first to point this out. The critical buckling stress is several orders of magnitude lower than the classical value, $0.6Et/R$, and the mode is antisymmetric about the midlength of the cylinder, and it involves no change in curvature of the generators. This mode is prevented if the buckling modal displacement pattern is assumed to be symmetrical at the symmetry plane at the cylinder midlength. The buckling mode is inextensional, that is, the middle surface undergoes no stretching. This mode is unlikely to occur in tests of axially compressed cylindrical shells because of friction.

A physical appreciation of the flimsiness of a thin cylindrical shell with free ends can be gained by rolling a sheet of paper into a cylindrical shell and taping the seam. The two lowest-energy modes of deformation are uniform ovalization (cylinder acting like a thin ring with $n_{cr}=2$ circumferential waves) and nonuniform ovalization in which opposite ends ovalize with a circumferential shift of 90 deg in the phase angle of the normal displacement field. Again, $n_{cr}=2$. A gentle squeeze at one end of the paper cylindrical shell will reveal the latter mode. Since the axial load does no work as the shell deforms in the uniform ovalization or ring mode, only the antisymmetric $n=2$ mode is critical.

A physical appreciation of inextensional behavior of spherical shells can be gained by cutting a ping-pong ball in half and squeezing one of the halves between your fingers. Large deflections occur with a very small applied force. A coffee cup dispensed from a vending machine is made with a reinforcing ring at the top to limit the amplitude of inextensional deformations caused by the squeezing pressure of your fingers required to keep the full cup from dropping to the floor. The shallow conical Viking aero shell[137] used for deceleration during entry into the Martian atmosphere was designed on a similar principle: Potentially large inextensional deformations caused by nonsymmetric re-entry pressures and $n=2$ type buckling are prevented by a large edge ring. Rocket nozzles are similarly designed.

Because of the small amount of energy required to deform shells inextensionally, designers should avoid configurations in which inextensional deformations of the wall are free to occur in systems subjected to destabilizing loads. Analysts investigating buckling of shells should avoid the use of boundary conditions that might permit inextensional buckling unless these conditions represent the actual support. It is the writer's experience that users of BOSOR4 have had difficulty when leaving some branch of the structure free at the end because "it's not the part I'm interested in." Often the lowest eigenvalue corresponds to large buckling modal displacements at the end left dangling. The program user is not able to obtain buckling in the region he is concerned about unless he restrains this troublesome end, either through an edge ring or by direct application of displacement constraints.

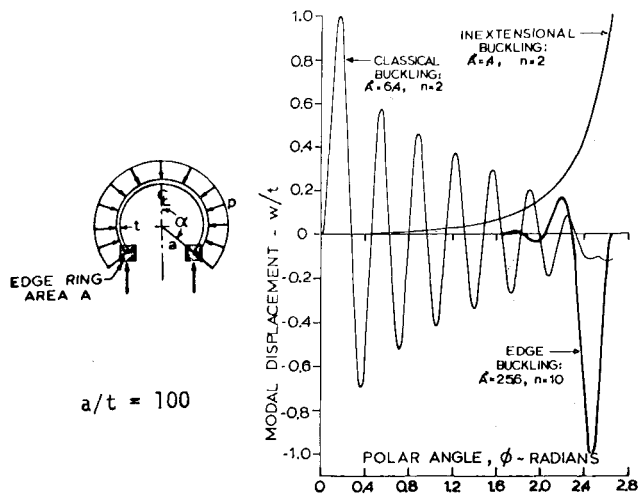

Fig. 6.1 Buckling modes for an externally pressurized spherical shell with an edge ring of dimensionless area $A^*=(A/at)(a/t)^{1/2}=0.4$, 6.4, and 25.6 (from Bushnell, *AIAA Journal*, Vol. 5, 1967, p. 2046).

Change in Buckling Behavior with Change in Boundary Stiffness

Figure 6.1 shows predicted buckling modes for an externally pressurized spherical shell with an edge ring of square cross section. With a very small edge ring, the buckling mode is almost inextensional with maximum normal buckling modal displacement at the edge and a low critical pressure $p_{cr}=0.03\,p_{CL}$ (p_{CL} = classical buckling pressure of the complete spherical shell). With a ring of such an area as to permit a perfectly membrane prebuckled state, the classical mode is critical with $p_{cr}=p_{CL}$. With a very large ring, the buckling modal displacements are confined to a "boundary layer" near the edge and the critical pressure is $p_{cr}=0.84\,p_{CL}$.

"Long" Boundary Effect for Axially Stiffened Cylinders

Boundary conditions can have an unexpectedly strong effect on critical loads, even though our intuition may contradict this. Figures 6.2-6.4 illustrate this point. Figure 6.2 shows nonsymmetric pressure loading on the ring-stiffened, corrugated rocket payload shroud depicted in Figs. 1.9a and 1.9b. The pressure distribution (Fig. 6.2a), measured in a wind tunnel, corresponds to a small angle of attack. The payload shroud, attached to a heavy motor stage at its aft end, bends as a beam and the side under maximum axial compression, the leeward side (Fig. 6.2b), buckles between discrete rings (Fig. 6.2c). (Buckling does not occur at the root of the beam because the shell wall is made of thicker gage material there, as indicated in Fig. 1.9a.) A decision was made to test cylindrical panels clamped at the curved edges with the same wall construction as the shroud. The question naturally arose, how wide and long should the panels be so that the test is representative of the situation depicted in Fig. 6.2? At the time it seemed reasonable to assume that a panel large enough to permit about two to three half waves of the buckling pattern around the circumference and along an interior length at least one bay removed from the clamped edges would be adequate. However, when tested such panels failed at loads considerably above those predicted for the full shroud. The failure mode, an example of which is photographed in Fig.

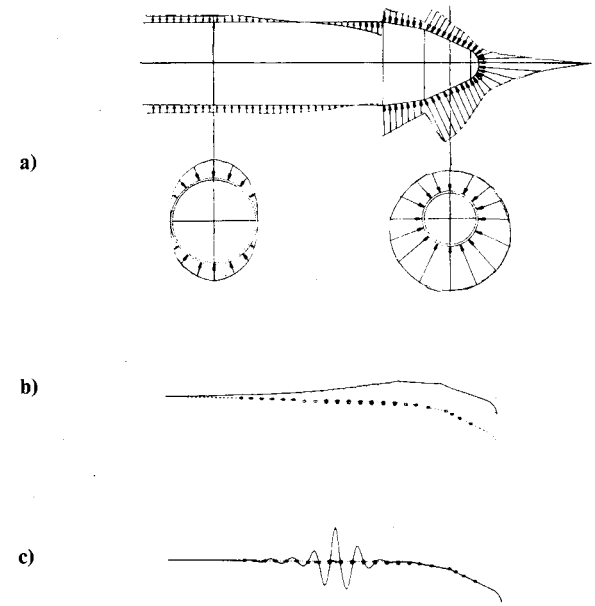

Fig. 6.2 Nonsymmetric pressure loading on the payload shroud shown in Figs. 1.9a and 1.9b (from Bushnell[9]). a) Pressure distribution. b) Prebuckling beam-type deflection. c) Nonsymmetric buckling mode. $n_{cr}=13$ circumferential waves.

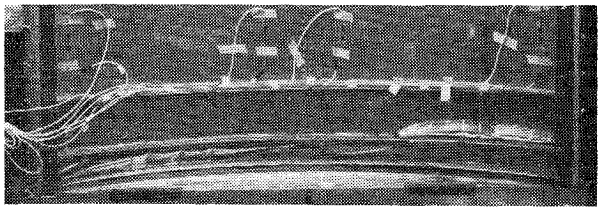

Fig. 6.3 Crippled corrugated semisandwich panel which was supposed to fail in a mode similar to that shown in Fig. 6.2c, but was prevented from doing so by clamped boundaries.

6.3, was crippling near one of the clamped boundaries rather than inter-ring buckling as displayed in Fig. 6.2c. An explanation is provided in Fig. 6.4: Many bays along the length are required for the critical load of a clamped panel to closely approach that of a simply supported panel, even though the critical buckling mode has the inter-ring characteristic displayed in the inset sketch in Fig. 6.4. As a result, the test corresponding to Fig. 6.3 was unconservative. A longer panel might have failed well below the theoretical asymptote indicated in Fig. 6.4 because of random imperfections in the panel, fabrication residual stresses, or other causes not included in the computerized model that generated the results in Fig. 6.4.

Ignorance of the length effect demonstrated in Fig. 6.4 might result in designs which are not optimum with respect to weight. For example, the dimensions of the corrugated semisandwich wall construction shown in Fig. 1.9b may be arrived at by an assumption that local crippling is to occur at the same axial load as inter-ring buckling, such as shown in Fig. 6.4. If the critical load level for inter-ring buckling is calculated with the assumption that the panel is of length equal to the ring spacing and is simply supported at its ends, then the local dimensions of the wall cross section will be established based on a critical load equal to that indicated by the asymptote in Fig. 6.4. However, actual panels used in a practical structure contain a finite number of bays and may be effectively clamped at certain bolted connections. Because of the significant length effect displayed in Fig. 6.4, these structures will cripple in a mode such as that photographed in Fig. 6.3 before buckling in the inter-ring mode depicted in Fig. 6.2 or 6.4.

Load Eccentricity

One of the first studies of the effect of eccentricity of axial load on the buckling of axially compressed cylinders is reported in Ref. 138. Singer and his colleagues have published several papers on this topic.[139-141]

An interesting although somewhat indirect example of the sensitivity of a buckling load to load eccentricity is represented in Fig. 6.5. The problem is buckling under uniform external pressure of a shallow spherical cap with an edge ring. Nonsymmetric bifurcation buckling is due to the narrow band of circumferential compression that develops near the edge. Plotted in Fig. 6.5 are prebuckling distributions of circumferential compression at the critical pressures for two analytical models, cases 1 and 2. In both cases there is, in addition to the uniform external pressure, an edge moment $M_{10} = 3.56$ N·m/m (0.8 in.·lb/in.). The test result was obtained by Wang.[142] The test most resembled case 1. In case 2, the shell is considered to penetrate the ring and terminate at the ring centroid. In each configuration, the external pressure is assumed to be reacted by an axial load acting through the ring centroid. Buckling occurs at the pressures p_{cr} indicated. The predicted buckling modal displacements have 18 circumferential waves in both cases and are maximum near the edge where the hoop stress resultants are maximum compressive.

The predicted buckling pressure is most sensitive to the axial component e_2 of the ring eccentricity. This eccentricity

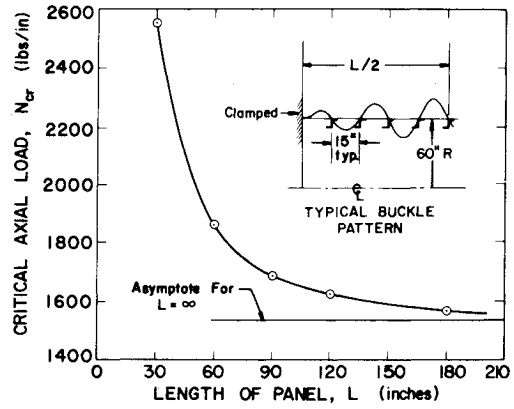

Fig. 6.4 Theoretical axial buckling loads for clamped corrugated cylinders of various lengths with discrete rings on 15 in. centers. Even though buckling is inter-ring, as shown, clamping raises the critical load significantly above the asymptote corresponding to simple support for cylinders with many bays (from Bushnell[10]).

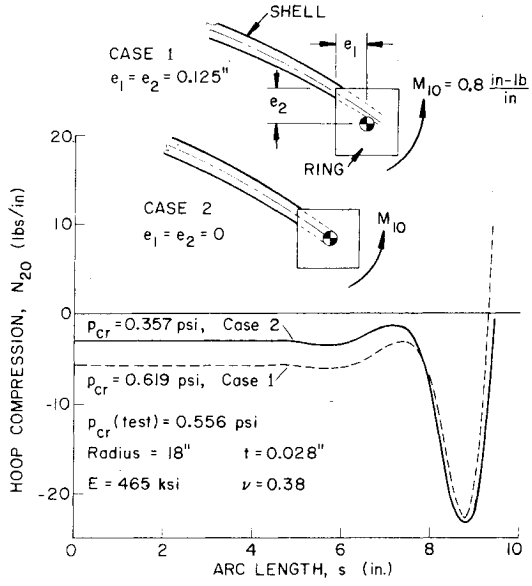

Fig. 6.5 Effect of edge ring eccentricity on predicted buckling pressures of shallow spherical cap (from Bushnell[143]).

has essentially the same effect as eccentric application of a radial load equal to that produced by the ring. In case 1 the meridional prebuckling stress resultant N_{10} produces a clockwise moment about the ring centroid, which acts to reduce the destabilizing hoop compression near the edge of the cap and thus raise the critical pressure. Notice that the hoop compression distributions near the edge corresponding to the two very different values of critical pressure, p_{cr} (case 1) = 0.619, p_{cr} (case 2) = 0.357, are very similar, providing a clue that it is this quantity that has the greatest influence on the bifurcation buckling load and not the meridional compression or the prebuckling shape change of the spherical cap.

General Comments about Modeling

For configurations such as just shown, in which bifurcation buckling is due to a localized effect, the predicted buckling load is often very sensitive to seemingly insignificant changes in the structure or in the analytical model of it. If the analyst perceives that a local buckling phenomenon may occur, for instance, if he performs a stress analysis and notices local regions of destabilizing compressive membrane forces, he should take great care with the modeling. Local load-path eccentricities, meridional discontinuities, prebuckling shape change effects, and prebuckling geometric and material

nonlinear behavior should be faithfully modeled and included in the stability analysis. If a stress analysis reveals a local band of circumferential or meridional compression, then a bifurcation buckling analysis should be performed. The minimum buckling load will generally correspond to a rather high number of circumferential waves. A reasonably accurate estimate, at least to within an order of magnitude, of the critical circumferential wave number can be calculated from the assumption that the axial and circumferential wavelengths of the buckles will be of approximately the same lengths. If the analytical model of the structure is reasonably good, the predicted buckling load should be fairly close to the test loads. Sensitivity to imperfections is much less important in such cases because the structure has a built-in, known, local imperfection that is generally large compared to any random manufacturing errors.

Transverse Shear Deformation Effects

Plate and shell theories represent means to simplify the general analysis of structures by the introduction of assumptions that make the displacement functions of two rather than three spatial coordinates. Usually this reduction is achieved by use of the assumptions:

1) Normals to the reference surface remain straight during deformation.

2) Normals to the reference surface remain normal after deformation.

3) The transverse normal stress is negligibly small.

The assumption that the normals remain normal to the deformed surface means that transverse shear deformation has been neglected. This assumption is certainly acceptable if the shell is sufficiently thin compared to its smallest surface dimension. Such theories are referred to as first-order theories. A second-order theory may, for example, be obtained if the first of the three assumptions is retained but the second discarded. Such theories have been presented by Reissner[144] and Mindlin.[145] Higher order theories can be obtained if the first assumption is also discarded, but it is questionable whether uses of such theories have any advantages in comparison to a complete three-dimensional analysis.

Laminated Composite Materials

The argument for retention of the effect of transverse shear deformations in analytical models of plate and shell structures made of laminated composite materials is much stronger for geometries typical of practical designs than it is for isotropic metals because the transverse shear moduli G_{13} and G_{23} are usually one to two orders of magnitude smaller than the longitudinal modulus E_1. (In keeping with generally accepted nomenclature, we will refer to longitudinal and transverse elastic moduli, E_1 and E_2, as the moduli in the plane of the lamina parallel and normal to the fiber direction. The in-plane shear modulus G_{12} is distinguished from the two transverse shear moduli, G_{13} and G_{23}.) Typical values for a lamina may be of the order $E_1/E_2 = 20$, $G_{13} = 0.6\ E_2$, and $G_{23} = 0.4\ E_2$. Since the transverse shear moduli for a lamina are small in comparison to the longitudinal elastic modulus, the transverse shear deformations must have a bigger effect on the buckling load of composites than it has on metallic plates or shells. That is, the composite shells must be thinner relative to in-plane dimensions or wavelengths before the transverse shear effect can be omitted.

Since most generally available computer programs presently do not include the effects of transverse shear deformation, it is important for the designer to know the limits of the first-order theory. For a simply supported isotropic plate, first-order theory yields buckling loads in error by 5% at most if the width-to-thickness ratio b/h is greater than 10. In order to obtain similar accuracy for composite material, the reliable use of first-order theory is restricted to even thinner plates. For a material with $E_1/E_2 = 30$, transverse shear deformation should be included if the width-to-thickness ratio is less than about 20.[146,147] It should be noted that this result applies to plates with simply supported edges. With respect to buckling of plates, the effect of clamping the edges is essentially equivalent to reduction of the in-plane dimensions by a factor of two. It might be surmised therefore that for clamped plates the transverse shear deformation effect should be accounted for if $b/h < 40$. Similarly, it appears that the opposite argument applies for a flange with one free edge: the transverse shear effect can probably be omitted if $b/h > 10$. More numerical comparisons are needed for guidance in design. In particular, if composites are used at elevated hygrothermal conditions, E_1/E_2, E_1/G_{13}, and E_1/G_{23} may be very large, and the transverse shear deformation effect therefore increased.

Sandwich wall construction may be thought of as a class of laminated composite shell wall which is weaker in transverse shear stiffness than ordinary isotropic or orthotropic construction. Figure 6.6 shows a predicted collapse mode of an actual part of a space vehicle. The cone is a ring-stiffened sandwich structure supported by a monocoque cylindrical skirt. The sandwich construction is made of aluminum honeycomb core with composite face sheets. The nonlinear

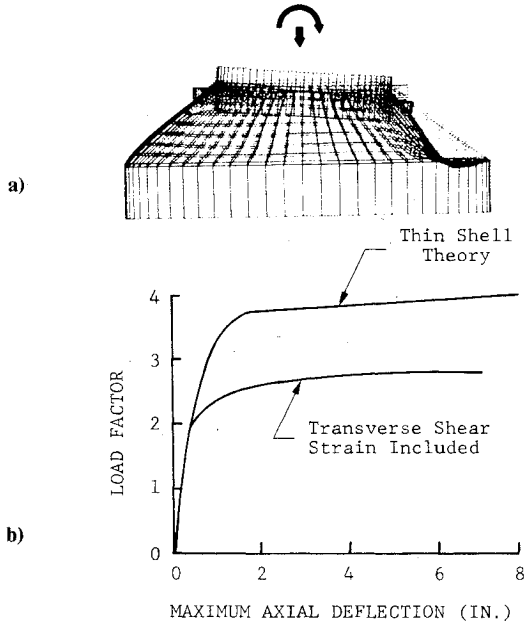

Fig. 6.6 Collapse of stiffened conical shell with sandwich wall construction (from Sharifi[48]). a) Deformation at collapse. b) Collapse load factors with and without transverse shear deformation effects.

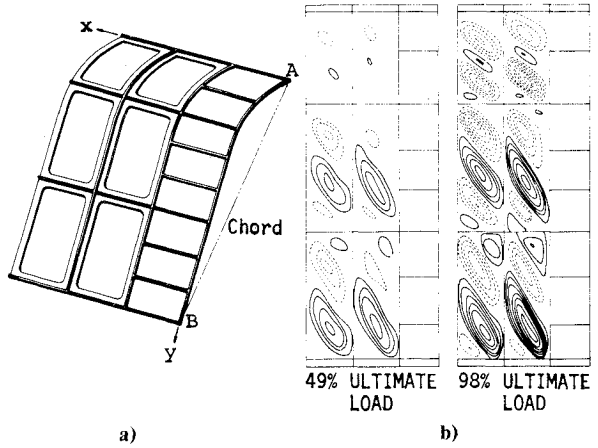

Fig. 6.7 Computer analysis of shear panel (from Skogh and Stern[151]). a) Complex stiffened shear panel. b) Postbuckling behavior predicted with the STAGS computer program.

collapse load of this structure was investigated with the use of two finite-element models and the NEPSAP computer program.[148,149] In the thin-shell theory model the sandwich core and facings are represented as multilayered composite elements with the effect of the transverse shear deformation of the honeycomb core neglected. In the other analysis the sandwich construction was modeled "exactly" with use of three-dimensional orthotropic solid elements for the core and composite shell elements for the facings. Figure 6.6a shows the collapse mode, and Fig. 6.6b gives the load-deflection characteristics of the two models. A 30% drop in the predicted value of collapse as a result of shear deformation in the core is indicated.

Bifurcation Buckling with Stable Postbuckling Behavior

The effective stiffness of buckled shear panels has traditionally been estimated semiempirically.[150] With advanced computer programs it is now possible to calculate the postbuckling behavior of such panels rigorously. Figure 6.7 shows a curved, stiffened panel which was analyzed with the STAGS computer program.[151] The panel was subjected to imposed displacements at corners A and B. As the imposed displacements are increased, the six subpanels buckle but continue to carry load. Contour plots of normal displacement are shown in Fig. 6.7, with solid lines indicating outward and dashed lines inward buckles. The modified Newton method was used, with 198 displacement increments and 35 refactorings of the stiffness matrix being required to reach a displacement slightly in excess of the ultimate imposed displacement, which was provided as a given value. According to this numerical analysis, the effective shear moduli of the buckled subpanels ranges 36-48% of that of the unbuckled sheet. The discrete model contained 21 rows and 58 columns, corresponding to a total of 4230 degrees of freedom and a stiffness matrix bandwidth of 478.

7. Optimum Design and Modal Interaction of Built-Up Thin Panels and Shells

Perfect Structures

Lightweight structures are often composed of curved or flat thin sheets reinforced by fairly deep stiffeners which are welded or riveted to the sheets. Weight limitations dictate that the stiffeners be thin compared to their height. The problem of designing such built-up shell structures is complicated by the existence of many different failure modes and by the fact that the shell wall distorts locally as loads are applied and during buckling and vibration.

Three Types of Buckling

Three distinct types of buckling are often investigated, usually in separate analyses. Long-wavelength "general" instability is treated by smearing the stiffeners[152] over the sheet surface. Intermediate-wavelength or panel instability is explored with the assumption of certain boundary conditions at the stiffener locations or by inclusion of the stiffeners as discrete elastic structures the cross sections of which are not permitted to deform. Short-wavelength crippling is usually predicted by analysis of flat or cylindrical panels under axial compression.

Simple Design Procedure

Such structures are often designed through the use of an optimality criterion: Dimensions of the shell wall and stiffener spacing are determined such that buckling in a general instability mode, such as shown in Fig. 7.1a, occurs at the same load as buckling of the skin between adjacent stiffeners, such as shown in Fig. 7.1b. The heights and thicknesses of the stiffener segments are established such that the local crippling of each of these parts, as shown in Figs. 7.1c and 7.1d, occurs at the same critical compressive strain as that in the shell wall corresponding to general and local instability (Figs. 7.1a and 7.1b). The design is arrived at by calculation of buckling strains with the assumption that each part can be analyzed separately and can buckle independently of the rest of the structure. Simple support edge conditions are imposed at the boundaries of each part in order to permit the use of simple expressions for the assumed buckling mode, such as $\sin(\pi x/L) \times \sin n\theta$.

"Rolling" Buckling Modes

Figures 7.1e-g show another type of stiffener buckling, called "rolling." Three kinds of stiffener rolling are depicted, one in which the panel skin participates (Fig. 7.1e) and two in which it does not (Figs. 7.1f and 7.1g). In the former the stiffener cross section does not deform but simply rotates about its line of attachment to the skin. In the latter two rolling modes the stiffener web deforms and the portion of the cross section attached to this web translates and rotates. Buckling of the type shown in Fig. 7.1f occurs because of compression perpendicular to the plane of the paper. Buckling of type in Fig. 7.1g occurs in the cases with internal rings on externally pressurized cylindrical shells of external rings on internally pressurized cylindrical shells. It is due to compression in the web in the plane of the paper, a compression generated because the portion of the ring attached to the end of the web resists radial displacement. The resulting radial compression in the web can lead to axisymmetric "wide-column" buckling of the web.

Complicating Factors

One might think at first that the design method just summarized should be conservative if the effect of geometrical imperfections is ignored. It is clear that local buckling of the skin between two adjacent stiffeners cannot occur as drawn in Fig. 7.1b without forcing the stiffeners to rotate. Similarly, local buckling of each stiffener cross-section segment cannot occur as exhibited in Figs. 7.1c and 7.1d independently of the other segments, because these segments are not hinged at their junctions. The model with many hinges

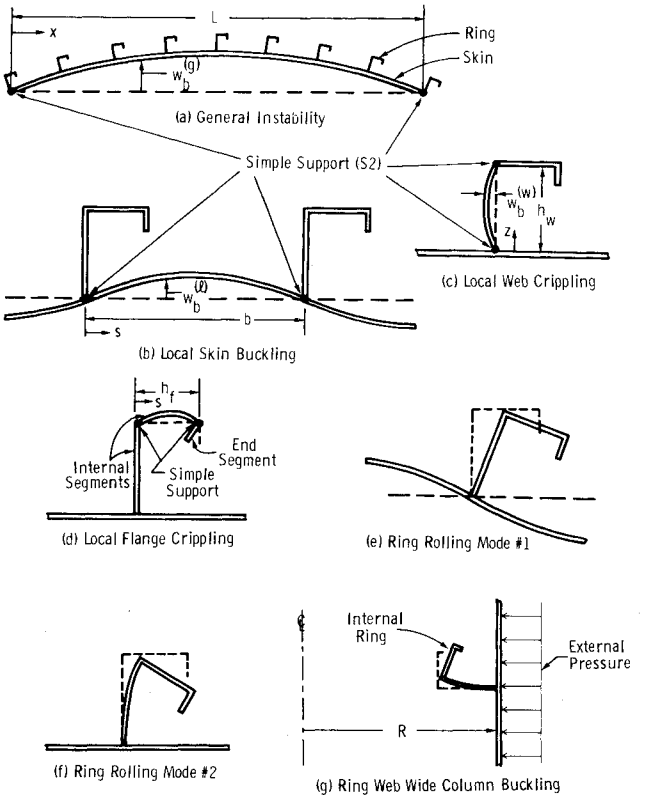

Fig. 7.1 General and local bifurcation buckling modes for a stiffened panel.

between its parts should yield lower bound estimates of buckling loads and therefore thicker parts than required for the actual (perfect) structure, a designer might well reason.

However, because of the interaction of local and general instability modes and the interaction of various local instability modes, critical buckling loads calculated for an assembled perfect structure are often lower than are those calculated separately for the parts of this structure treated as if they were hinged at their boundaries. In other words, there are many cases for which the various types of instability described above are not distinct. Local distortions of rings and stringers may affect to a significant degree general and panel instability predictions, and fairly long-wavelength disturbances may significantly affect crippling predictions. Figure 7.2 shows some examples. The T-ring and the cylinder in Fig. 7.2a deform in such a way that neither component is fully effective. Treatment of the T-ring as discrete with a nondeformable cross section leads to nonconservative estimates of prestress and buckling loads. Under axisymmetric lateral pressure the cross-section area of the T-ring is not fully effective because the flange does not move inward uniformly. Similarily, the out-of-plane bending stiffness and torsional stiffness of the T-ring are not fully effective in preventing buckling. On the other hand, neglect of these stiffness components entirely may lead to results that are overly conservative.

If the ring has a faying flange (flange next to the shell wall), it is often important to consider in detail the means by which this flange is fastened to the cylinder. Treatment of the flange as part of the ring, with the ring considered to be attached at a single point to the cylinder, may lead to underestimation of the buckling load since this model neglects the contribution of the faying flange to the axial bending stiffness of the cylinder. However, if the faying flange is considered to be an integral part of the cylinder wall, the resulting overestimation of the axial bending stiffness leads to nonconservative estimates of the buckling load. These effects are explored in Ref. 153.

Figures 7.2b and 7.2c show parts of a semisandwich corrugated panel undeformed, buckled (b) and crippled (c) under an axial load (normal to the plane of the paper). Classical analysis of buckling of such a panel treats it as an equivalent orthotropic sheet with the wall cross section, of course, not permitted to deform locally. The presence of such local deformations makes it very difficult to assign a priori a torsional stiffness per length. This J factor is particularly important in this case because of the enclosed trapezoidal areas. Local distortions also affect the axial bending stiffness, another significant determinant of the predicted buckling load. The degree of local distortion is largely governed by the way in which the corrugated sheet is fastened to the flat sheet. Figures 7.2b and 7.2c correspond to cases in which the centers of the troughs of the corrugations are riveted to the sheet. Bonding along the entire widths of the troughs markedly reduces the amount of distortion with a corresponding increase in the stiffness and buckling load. This difference between bonding and riveting would not be reflected in a classical orthotropic plate analysis, except through the empirical introduction of appropriate knockdown factors applied to the constitutive law to bring test and theory into agreement. A significant example of the effect of the interaction of local and general instability is displayed in Fig. 7.3c, which shows nonsymmetric buckling of a shallow, externally pressurized, ring-stiffened conical shell of the type used to decelerate the Viking payload upon entry into the Martian atmosphere.[137] Figure 7.3b demonstrates the dramatic difference between the predictions with use of discrete ring theory and branched shell theory and Fig. 7.3c illustrates the significant amount of local ring cross-section deformation in the general instability mode.

The simplifications of the various classical analyses lead to errors of unknown magnitude. The errors frequently cancel, leading to fortuitous agreement between test and theory or between predictions with crude and refined models. This is the case with internally ring-stiffened cylinders under hydrostatic compression. A discrete ring model should lead to overestimation of the buckling load because the ring cross section is not permitted to deform. However, errors in the discrete ring model, such as the assumption that the shear center and centroid coincide, lead to a more than counteracting underestimation of the ring stiffness. For this and

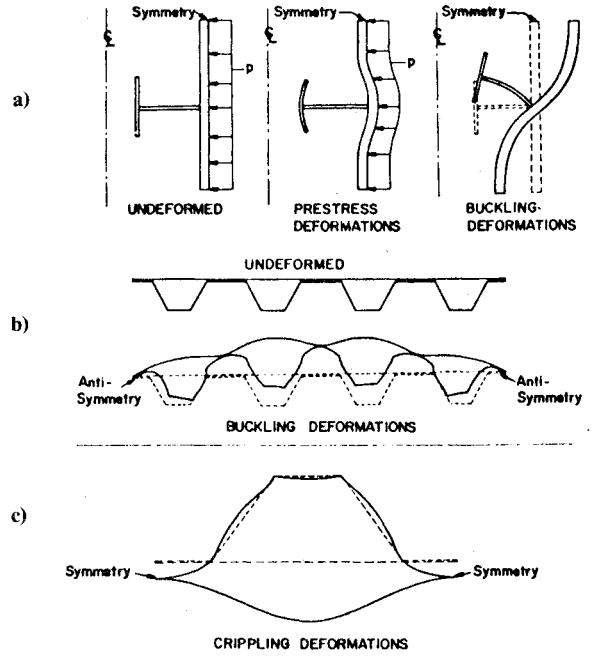

Fig. 7.2 Some structures built up of thin sections which deform locally during loading and buckling (from Bushnell, *AIAA Journal*, Vol. 11, Sept. 1973, p. 1283).

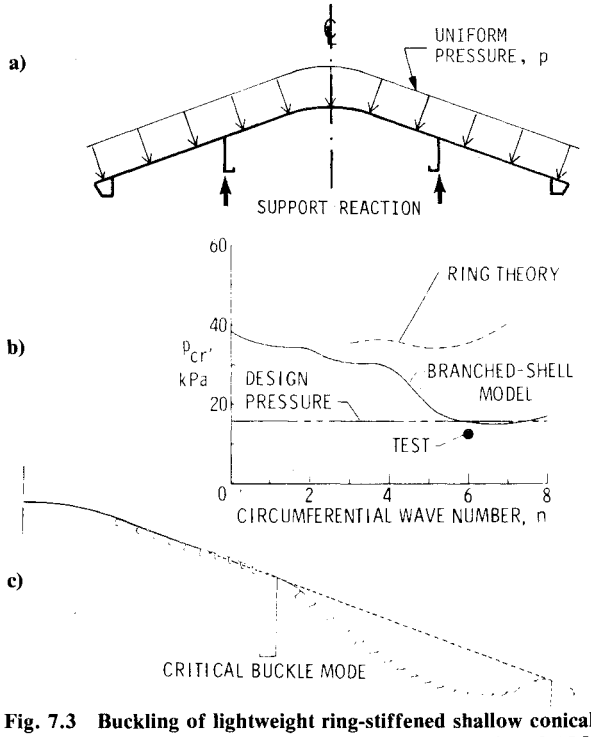

Fig. 7.3 Buckling of lightweight ring-stiffened shallow conical shell designed by NASA for decelerating a payload entering the Martian atmosphere (from Leonard et al.[137]). a) Loading; b) comparison of buckling test and predictions from two analytical models; c) critical buckling mode, showing interaction of general buckling and local deformation of rings.

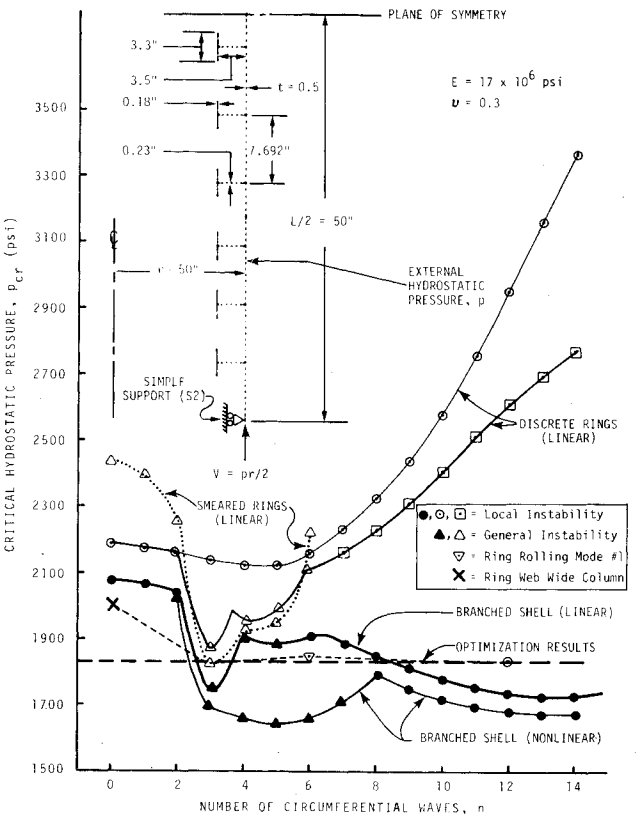

Fig. 7.4 Predicted buckling pressures from various discretized models of ring-stiffened cylinder which had been previously optimized with use of simple formulas.

other reasons it is often very difficult intuitively to construct an accurate, simple model.

Brief Survey of Work Done

Until about 10 years ago axially stiffened panels were analyzed as equivalent orthotropic plates. A great deal of work of this type was done by Becker, Tsai, Block, Card, Mikulas, Anderson, Jones, Peterson, and others at NASA in the 1950s and 1960s. References to their work are given in Ref. 154. In 1968 Wittrick[155] published an analysis of prismatic structures composed of flat plates. Since 1971 a series of papers[154,156-164] has appeared on the treatment of buckling and vibration of prismatic shell structures. In most of the papers the buckling and vibration modes are assumed to be sinusoidal in the axial direction, with the wavelength of deformation the same in all of the segments of the complex structure. This assumption, which limits the analysis to simply supported panels, permits the separation of variables with consequent reduction of the problem from two-dimensional to one-dimensional. Wittrick's analysis[155] predicts, in a unified approach, all three types of instability identified in the second paragraph of this section—general, panel, and crippling; the treatment of Viswanathan et al.[154] extends that of Wittrick to allow orthotropic wall properties and intermittent elastic beam-type supports; Williams[158] extends Wittrick's analysis to include vibration and to incorporate substructuring techniques; Wittrick and Williams[162] formalized their treatment in a computer program called VIPASA; and Anderson and Stroud combined VIPASA with an optimization routine by Vanderplatts and Moses[165] to produce a computer program called PASCO for the optimization of layered, stiffened composite panels.[164] van der Neut[166] presents an accurate and simplified method for determining critical axial loads of panels stiffened by Z-shaped stringers. He finds that sideways flange bending dominates the Euler component of the general instability

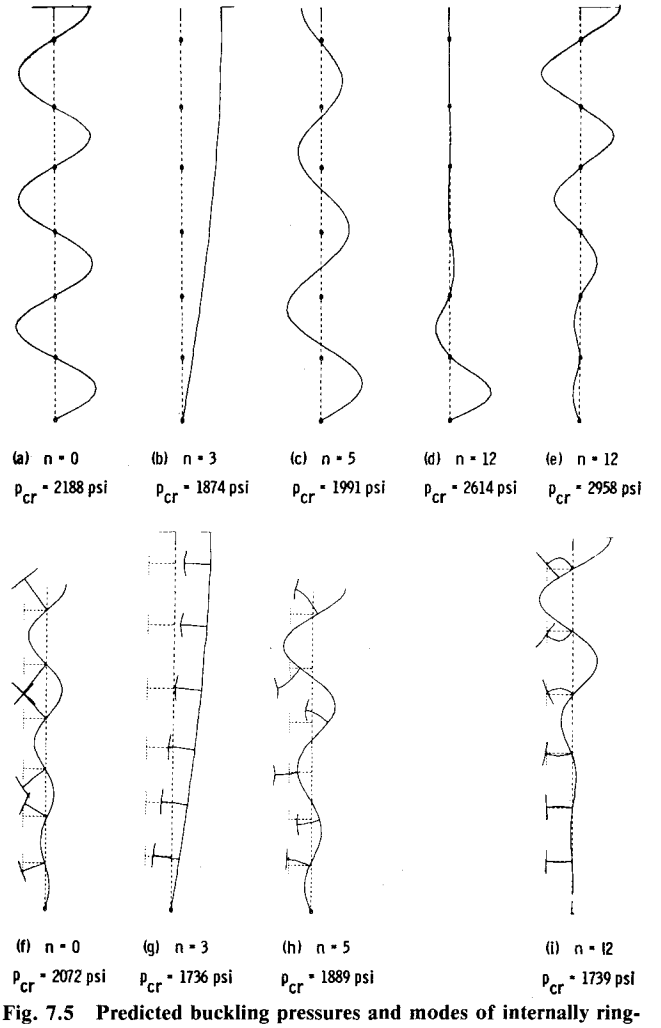

Fig. 7.5 Predicted buckling pressures and modes of internally ring-stiffened cylindrical shell. (a-e) T-shaped rings treated as discrete (cross sections cannot deform). (f-i) T-shaped rings treated as flexible shell segments (cross sections deformable).

buckling mode more and more with decreasing restraint of the web root.

Buckling of an Optimized Ring-Stiffened Cylinder

Figures 7.4-7.6 demonstrate the complex buckling behavior of an optimally designed internally ring-stiffened cylindrical shell subjected to uniform external hydrostatic pressure. Half of the cylinder length is shown in Fig. 7.4 with symmetry conditions imposed at the plane of symmetry and simple support conditions (S2 in Table 6.1) imposed at the edge. The insert in Fig. 7.4 depicts the discretized branched shell model provided as input to BOSOR4.[9]

The configuration with the dimensions identified in Fig. 7.4 was arrived at in the following way: Given that the structure must be an internally ring-stiffened cylinder with Young's modulus $E = 11.7 \times 10^{10}$ Pa (17×10^6 psi), radius $r = 1.27$ m (50 in.), and length $L = 2.54$ m (100 in.), we are asked to find the configuration corresponding to minimum weight subject to the constraint condition that the perfect shell will not buckle under a uniform external hydrostatic pressure of 12.55 MPa (1820 psi). Application of the optimization programs described in Ref. 167 leads to a minimum weight configuration with very closely spaced rings. If one is willing to accept a rather small penalty in weight (about 3%), one can impose a lower bound on the ring spacing so that the final design is more amenable to analytical treatment as a branched shell. (Actually, the ring stiffeners in submarine pressure hulls, for example, are farther apart than a simple op-

timization scheme would dictate because of the expense and practical spatial problems encountered in welding the rings to the shell.) The dimensions called out in Fig. 7.4 correspond closely to the optimum design with the lower bound on ring spacing set equal to 19.5 cm (7.692 in.). This optimum design is generated from the simplified buckling models described in connection with Fig. 7.1.

The dashed line near the bottom of Fig. 7.4 shows buckling pressures predicted from simplified theory corresponding to ring web-wide column buckling ($n=0$, Fig. 7.1g), general instability ($n=3$, Fig. 7.1a), ring rolling mode 1 ($n=6$, Fig. 7.1e), and local skin buckling ($n=12$, Fig. 7.1b), all of which are active buckling constraint conditions at the optimum design point.

The other curves in Fig. 7.4 were all obtained with the BOSOR4 computer program.[9] If the shell were perfect and if the material remained elastic, buckling would occur with five circumferential waves at a pressure of 11.35 MPa (1646 psi), as indicated by the minimum load on the curve labeled "branched shell (nonlinear)." This curve represents results of the most accurate analysis of the shell. The discrete ring model yields erroneous results for high n because the ring web is not permitted to deform in that model, with the result that far too much strain energy is predicted to be stored in the flange during buckling. Replacement of the ring by a simple support restraint, as is done in the crude optimization analysis, leads to a far better estimate of the actual buckling pressure corresponding to $n=12$ circumferential waves, as seen from the location of the open circle on the dashed line at $n=12$.

Predicted buckling modes corresponding to bifurcation with linear prebuckling analysis are exhibited in Fig. 7.5. Local instability, identified by circles or squares in Fig. 7.4, corresponds to modes in which the attachment lines of the ring webs to the cylindrical shell do not move radially or circumferentially, as illustrated by curves a, d-f, and i of Fig. 7.5. General instability, identified by triangles in Fig. 7.4, corresponds to modes in which at least one of these attachment lines moves radially, as illustrated by curves b, c, g, and h of Fig. 7.5. Note that for $n \geq 6$ the two curves in Fig. 7.4 labeled "discrete rings" correspond to modes of the types in Figs. 7.5d and 7.5e. From the branched shell model it is clear from Figs. 7.5f-i that the degree of bending in the ring webs increases with increasing n. This is because the strain energy stored in the flange increases with n^4 for a given amplitude of flange neutral axis modal displacement in the axial direction. For $n=12$ circumferential waves there is a great deal less modal axial flange displacement in the branched shell model than exists for $n=5$, and for $n=5$ there is less than for $n=0$.

Figure 7.6 shows the prebuckled state and buckling modes corresponding to the lowest curve in Fig. 7.4. The critical buckling mode for $n=5$ circumferential waves is very different from that corresponding to the linear treatment.

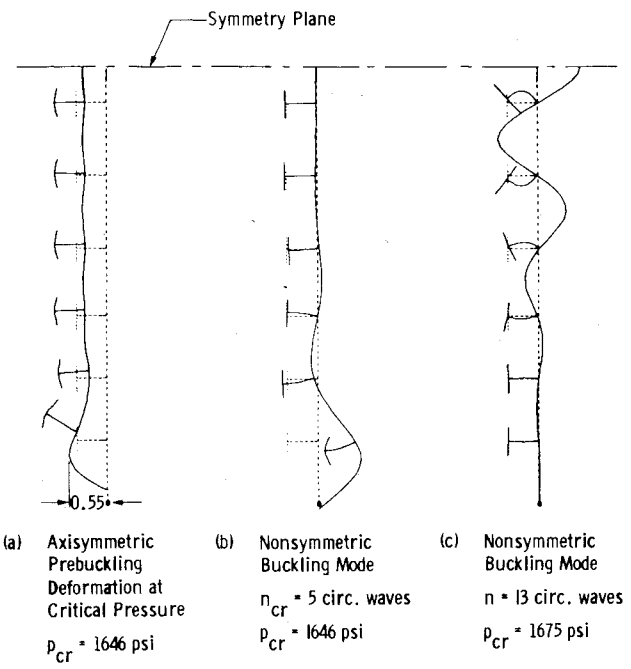

Fig. 7.6 Bifurcation buckling of internally ring-stiffened cylindrical shell shown in Fig. 7.4, with nonlinear prebuckling effects included.

Imperfect Structures

Two Types of Modal Interaction

We have already seen several examples of one type of buckling modal interaction: Bifurcation buckling in which the critical mode contains characteristics of more than one kind of buckling, such as general and local instability. The modal interaction effect to be discussed in this section is fundamentally different from the examples just described. It is related primarily to local imperfections in the structure which have the effect of decreasing the stiffness of it in such a way as to decrease the critical load corresponding to general instability. As shall be seen, the modal interaction effect to be described here, that is, the reduction in load-carrying capability due to small imperfections, is especially severe at the design point corresponding to simultaneous general and local instability.

Survey of Work Done

Tvergaard[168] presents an excellent survey of the work done on modal interaction. Bijlaard and Fisher[169] established that local buckling of the plate elements in a column reduces the critical load corresponding to Euler-type buckling of the column. In 1962 Koiter and Skaloud[170] emphasized that the load-carrying capability of structures with simultaneous local plate buckling and Euler-type column buckling may be especially sensitive to initial imperfections. van der Neut[171] proved Koiter's conjecture correct in a very thorough analysis of a two-flange column with idealized webs. Although the axially compressed simply supported plates from which the column shown in Fig. 7.7 is constructed exhibit stable postbuckling behavior by themselves, van der Neut proved that a column built up of such plates will experience the sudden collapse usually associated with highly imperfection-sensitive shell structures if the local plate buckling and general column instability loads are close. Figure 7.7 demonstrates that the degree of imperfection sensitivity is greatest in the neighborhood of the design for which local and general in-

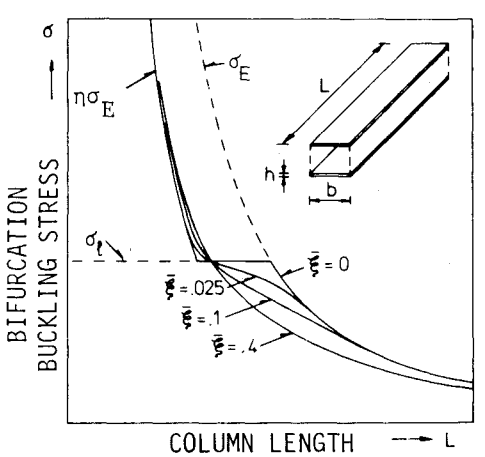

Fig. 7.7 Column buckling load for two-flange model of given cross section as function of column length and flange imperfection amplitude. This configuration was studied by van der Neut[171] and Thompson and Lewis[172] (from Tvergaard[168]).

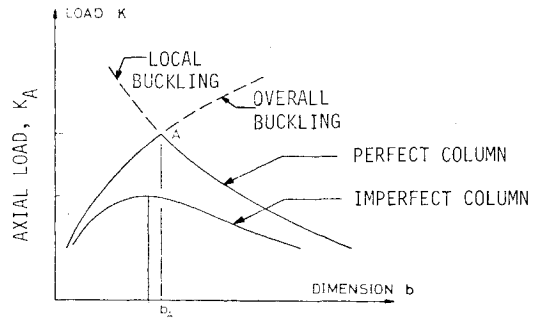

Fig. 7.8 Degeneration of an optimum design because of imperfections (from Thompson and Lewis[172]).

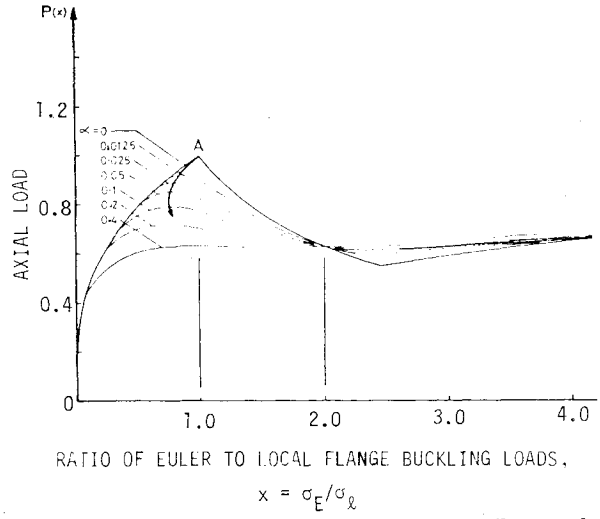

Fig. 7.9 Erosion of the optimum load of the two-flange column shown in Fig. 7.7 by initial flange imperfections α (from Thompson and Lewis[172]).

stability of the perfect column occur at the same stress.

Thompson and Lewis[172] determined optimum designs for van der Neut's two-flange model, taking into account initial imperfections of the flanges but assuming that the column axis remains straight. They found that with growing imperfections the optimum load-carrying capacity decreases steeply from the value corresponding to simultaneous local and general instability of the perfect column, and that for very small imperfections the optimum design shifts away from that obtained from imposition of the simultaneous buckling criterion to a design in which Euler-type buckling of the column occurs at a lower load than local buckling of the flanges, as shown in Fig. 7.8. Crawford and Hedgepeth[173] calculated optimum designs for lattice columns and truss-core sandwich panels with initially locally wavy members. They determined that both structures are imperfection sensitive, the lattice column more so than the truss-core panel, and that the effect on optimum design obtained with the assumption of small imperfections is opposite to that obtained with the assumption of larger imperfections, a finding in agreement with that of Thompson and Lewis (Fig. 7.9). Their major conclusion is that in neither case is the penalty great for using the conventional practice of arriving at an optimum design by equating local and general instability of a perfect structure. (However, it is obvious that a load margin has to be provided to account for initial unknown imperfections.) Maquoi and Massonnet[174] discuss the optimum design of a square-box column obtained from an analysis in which the effective width concept is used and collapse is assumed to occur if the maximum stress reaches the yield stress. Graves-Smith[175] calculates collapse loads of box columns including the effects of welding residual stresses, "cylindrical" imperfections due to welding of the plates at the corners of the box column, and initial local waviness.

Plates reinforced by axial stiffeners on one side are common in civil, marine, and aerospace structural designs. Tvergaard[176,177] has used Koiter's general theory of elastic stability[25] to obtain asymptotic estimates of the imperfection-sensitivity of such structures. The panels are assumed to be infinitely wide with constant spacing b between the stiffeners, are simply supported at the two edges on which the compressive load acts, and are free on the unloaded edges. The eccentric stiffeners are represented as simple beams. A panel designed so that local buckling coincides with buckling as a wide Euler column displays a high sensitivity to initial imperfections due to modal interaction.

For the analysis of panels for which the local and general bifurcation buckling loads are not coincident, Tvergaard uses the Galerkin method. The strong sensitivity to small imperfections is revealed in a continuous manner for simultaneous and nearly simultaneous buckling. However, as the model deflections increase, the postbuckling equilibrium curves tend to flatten out so that the sensitivity to larger imperfections is far less severe than that predicted by the asymptotic equations derived from Koiter's theory. The solutions are used to study the optimum design of panels with various combinations of column mode imperfections and local mode imperfections. For certain prescribed stiffener spacings the local maxima near the design point corresponding to simultaneous buckling vanishes for rather small imperfection amplitudes. The maximum carrying capacity of the panel is attained above the critical stress for local buckling. However, from the point of view of retaining high axial stiffness at the highest possible load level, the optimum usually corresponds to a design with the Euler load lower than the critical load associated with local buckling of the skin between the stringers.

A similar panel configuration has been considered by Koiter and Pignataro,[178] who found a panel with a single axial bay to be very sensitive to small initial imperfections at a design corresponding to simultaneous wide column and skin buckling but relatively less sensitive to larger imperfections, a result in agreement with those of Refs. 176 and 177. In addition to the single-bay panel, Koiter and Pignataro treat the important case of a panel continuous over several bays in the longitudinal direction. For this multibay panel, the imperfection sensitivity is found to be further decreased because of the elimination of the load eccentricity effect induced by the shift of the neutral axis due to the crippling of the skin.

van der Neut[179] analyzed modal interaction for a hat-stiffened panel with use of a two-flange model similar to that used for the box column in Ref. 171. The sensitivity of the critical load to the initial local waviness of the plate and of the top of the hat stiffeners is greatest for designs for which local and wide column bifurcation buckling loads coincide.

Thompson, Tulk, and Walker[180] performed experiments on pin-ended eccentrically stiffened panels made of epoxy plastic. Local imperfections of the skin between the stringers were "fabricated" by heating the plastic, loading it, and then cooling it, thus "freezing" in an initial deformation pattern with relatively low residual stresses. Imperfections in the form of the Euler wide column mode were simulated by eccentric application of the end load. The sensitivity of the critical load to initial imperfections in the form of the local as well as the wide column buckling modes is observed to be maximum at designs for which local and general buckling of perfect panels coincide.

Tvergaard and Needleman[83,84] have investigated modal interaction of elastic-plastic panels. They used J_2 flow theory with isotropic strain hardening. The panels are infinitely wide and the stringers are modeled as simple beams. The effect of local and global imperfections for single-bay and multibay panels (multiple bays in the axial direction) are investigated. They found that modal interaction leads to imperfection

sensitivity in a single-bay panel with column mode deflections such that the skin is being further compressed by bending. For column mode deflections in which the skin is being stretched, the considerable imperfection sensitivity found by Tvergaard and Needleman is entirely due to the material nonlinearity. This effect of material nonlinearity explains why the multibay panel is not less imperfection sensitive than the single-bay panel, as is the case in the elastic range.[178]

Byskov and Hutchinson[181] solve the problem with use of an asymptotic method similar to Koiter's[25] that provides uniformly valid results whether the modes are simultaneous, nearly simultaneous, or well separated. For the perfect shell, the optimum design has simultaneous overall and local buckling loads. Overall buckling loads and mode shapes are calculated from a theory in which the stringers are smeared out and the torsional rigidity of the stringers is neglected. Local buckling is also calculated on the basis of neglect of the torsional stiffness of the stringers. The stringers are considered to be stocky enough that they do not cripple. Initial imperfections have the form of a sum of i bifurcation buckling modes corresponding to the lowest i eigenvalues of the perfect structure.

Modal Interaction in an Axially Compressed Two-Flange Column

van der Neut[171] was the first to study in detail the behavior of the axially compressed two-flange column shown in Fig. 7.7. The model consists of two load-carrying flanges of width b and thickness h, connected at a distance $2c$ by webs which are rigid in shear and laterally but which have no longitudinal stiffness. The webs offer simple support to the flanges. In this way the flanges have boundary conditions that are easy to take into account analytically.

Figure 7.7 gives a review of the buckling behavior of such a model. Long perfect columns buckle in an Euler mode ($\sigma_{cr}=\sigma_E$). The behavior of short columns is more complicated: Initially the simply supported flanges buckle locally at a stress $\sigma_{cr}=\sigma_\ell$. However, the postbuckling behavior of long rectangular plates is stable, so that the column with crippled flanges continues to carry additional axial load until it buckles in an Euler mode at a flange stress $\sigma_{cr}=\eta\sigma_E$, in which η is a factor (η equals approximately 0.4083 for simply supported long plates) that accounts for the reduced incremental axial stiffness of the crippled flanges. Perfect columns of such an intermediate length that $\eta\sigma_E \le \sigma_{cr} \le \sigma_E$ fail at $\sigma_{cr}=\sigma_\ell$ because of modal interaction: The crippling of the flanges causes a "sudden" reduction in their axial stiffness with consequent reduction of the Euler stress from σ_E to $\eta\sigma_E$.

It is reasonable to suspect that the critical loads of columns in the intermediate range of lengths corresponding to the neighborhood of $\sigma_E=\sigma_\ell$ would be sensitive to small initial imperfections, that is waviness, in the flanges. The amplitude of the waves would grow as the axial load is increased, with the result that the axial stiffness of the wavy flanges would decrease, precipitously approaching the limiting value $\eta=0.4083$ times the stiffness of the perfectly straight flanges at a load well below σ_E or σ_ℓ and leading to Euler buckling of the beam in the range $\eta\sigma_E<\sigma<\sigma_E$.† Curves are drawn in Fig. 7.7 corresponding to bifurcation buckling of columns with straight axes but initially imperfect flanges. The quantity $\bar{\xi}$ is the ratio of the amplitude of the initial flange waviness to the thickness h of the flange. It is seen that the greatest sensitivity to initial flange imperfections occurs for column designs such that $\sigma_E=\sigma_\ell$. Note that even for the column with initially imperfect flanges, the failure stresses plotted as solid curves in Fig. 7.7 correspond to *bifurcation* buckling in the Euler mode, not to a limit load such as point E in Fig. 2.2a. The bifurcation point is converted to a limit point only if imperfections are introduced into the axis of the column.

Optimization of Imperfect Columns and Panels in which Modal Interaction Occurs

The conventional criterion of optimization for thin elastic structures is that overall and local buckling loads should coincide. The validity of this so-called "naive" approach was originally questioned by Koiter and Skaloud[170] on the grounds that simultaneous buckling might give rise to severe imperfection sensitivity which could modify or destroy the apparent optimum.

Figures 7.8 and 7.9 pertain to the optimum design of an imperfect two-flange column in which simultaneous local and general instability might occur. All designs corresponding to various b in Fig. 7.8 and various $x=\sigma_E/\sigma_\ell$ in Figs. 7.8 and 7.9 have the same weight. The point raised by Koiter and Skaloud[170] is illustrated in Fig. 7.8: An optimum design arrived at by the bifurcation buckling analysis of a perfect structure, dimensioned such that $\sigma_E=\sigma_\ell$, corresponds to some dimension $b=b_A$. However, the imperfect structure has a maximum load-carrying capability at a different design point, $b<b_A$. Thompson and Lewis[172] found that for van der Neut's two-flange column the optimum design shifts to the left (Fig. 7.9) for small flange imperfections α and then back to the right for larger flange imperfections. The implication is that fairly well-made box columns should have dimensions such that the Euler load is a bit less than the local flange buckling load.

8. Design Method for Axially Compressed Cylinders

Almroth, Burns, and Pittner[12] suggest the following semiempirical method for evaluating designs of practical cylindrical shells which may be pressurized, stabilized by an elastic core (such as a solid propellant rocket motor), stiffened, of laminated composite wall construction, etc. An effective radius-to-thickness ratio $(R/t)_e$ is first calculated from the formula

$$(R/t)_e=[5.46(\bar{C}_{44}+\bar{C}_{55})C_{22}/(C_{11}C_{22}-C_{12}^2)]^{-1/2} \quad (13)$$

with

$$\bar{C}_{44}=C_{44}-(C_{14}^2/C_{11})$$
$$\bar{C}_{55}=C_{55}-(C_{25}^2/C_{22}) \quad (14)$$

The C_{ij} in Eq. (13) are the coefficients of the integrated constitutive law for the complex shell wall which relate the stress and moment resultants to the reference surface strains, changes in curvature and twist:

$$\begin{Bmatrix} N_1 \\ N_2 \\ N_{12} \\ M_1 \\ M_2 \\ M_{12} \end{Bmatrix} = \begin{bmatrix} C_{11} & C_{12} & 0 & C_{14} & C_{15} & 0 \\ C_{12} & C_{22} & 0 & C_{24} & C_{25} & 0 \\ 0 & 0 & C_{33} & 0 & 0 & C_{36} \\ C_{14} & C_{24} & 0 & C_{44} & C_{45} & 0 \\ C_{15} & C_{25} & 0 & C_{45} & C_{55} & 0 \\ 0 & 0 & C_{36} & 0 & 0 & C_{66} \end{bmatrix} \begin{Bmatrix} e_1 \\ e_2 \\ e_{12} \\ \kappa_1 \\ \kappa_2 \\ 2\kappa_{12} \end{Bmatrix} \quad (15)$$

Corresponding to the effective radius-to-thickness ratio $(R/t)_e$ calculated from Eq. (13), a knockdown factor ϕ is read from one of the three empirically derived curves in Fig. 8.1

†Professor van der Neut of the Delft University of Technology, in a letter to the author commenting on this section, offers the following more rigorous reasoning: "At $\sigma=\sigma_\ell$ overall buckling of the perfect structure moves one flange into the postbuckling range with stiffness reduction η whereas the other flange does not buckle. Then the bending stiffness has the reduction $\eta_b=2\eta/(1+\eta)$. With this bending stiffness neutral equilibrium exists only at one intermediate column length $L_0=\eta_b^{1/2}L_E$ (L_E being the length at which $\sigma_E=\sigma_\ell$). Columns the length of which is between L_0 and L_E are too slender for neutral equilibrium at $\sigma=\sigma_\ell$. They are unstable and consequently highly imperfection sensitive."

corresponding to isotropic cylindrical shells. (Almroth et al. recommended the 99% probability curve.) These curves were originally derived by Harris et al.[182] in 1957 from data such as shown in Fig. 3.2.

Buckling loads for the trial complex design in question are then calculated in two ways: 1) from a *wide-column formula* which includes a stabilizing contribution due to the curvature; and 2) from a computer program based on an extended version of *Koiter's special theory*[59] which is based on the assumption that the imperfection is axisymmetric and which accounts for stiffeners, orthotropic laminated skin, elastic core, and internal pressure.

Critical Load from Wide-Column Theory

The critical axial load/length of the circumference calculated from the modified wide-column formula is

$$N_{CR} = N_{WC} + \phi(N_{CL} - N_{WC}) \tag{16}$$

in which the wide-column buckling load N_{WC} is given by

$$N_{WC} = R^2 \bar{C}_{44} (\pi/L)^2 \tag{17}$$

for shells without elastic cores and

$$N_{WC} = 1.19(R^2 \bar{C}_{44})^{1/3} [E_C/(1-\nu_C^2)^{2/3}] \tag{18}$$

for shells with an elastic core of modulus E_C and Poisson's ratio ν_C. In Eq. (16) the second term on the right-hand side represents the contribution due to the curvature. N_{CL} is the classical buckling load extended to include internal pressure and an elastic core. A formula for N_{CL} is given in the appendix of Almroth, Burns, and Pittner's paper.[12] The quantity ϕ in Eq. (16) is the knockdown factor read from the appropriate curve in Fig. 8.1 corresponding to the $(R/t)_e$ calculated for the trial design from Eq. (13). This knockdown factor is applied to the difference $N_{CL} - N_{WC}$ because only that part of the axial load is sensitive to initial imperfections, the wide-column postbuckling behavior being characterized by the curves shown in Fig. 2.3a.

Critical Load from Extended Version of Koiter's Special Theory

The critical axial load/length of the circumference computed from the extended version of Koiter's special theory (axisymmetric imperfection) is the lowest real root of the equation

$$N_{CR}^3 + \alpha N_{CR}^2 + \beta N_{CR} + \gamma = 0 \tag{19}$$

in which α, β, and γ are complicated formulas that depend on the geometric and material properties of the shell wall and stiffeners, the core modulus, the internal pressure, the assumed buckling pattern wave numbers in the axial and circumferential directions, and the amplitude μ and axial wavelength λ_{imp} of the axisymmetric imperfection.

The amplitude μ of the axisymmetric imperfection is determined a priori in the following way: A knockdown factor ϕ corresponding to $(R/t)_e$ is read from the appropriate curve of Fig. 8.1. Corresponding to this value of ϕ the results of Koiter's special theory *for isotropic shells* are used to obtain μ. The actual imperfection amplitude to be used for the Koiter theory analysis of the trial design is then given by the product μt_e, where t_e is the effective thickness obtained from Eq. (13).

It is assumed in the analysis that the axial wavelength of the buckling pattern is twice the wavelength of the initial imperfection pattern. It is assumed also that the normalized imperfection amplitude μ for the equivalent monocoque cylinder is applicable to any sinusoidal pattern of imperfections whose wavelength λ_{imp} is equal to or larger than the critical wavelength λ_c for axisymmetric buckling of the perfect shell. The computer program in which the extended Koiter-type analysis is implemented first computes λ_c. (In the presence of an elastic core, iteration is required.) The critical load N_{CR} is then determined from Eq. (19) for a series of imperfection wavelengths λ_{imp} until a minimum is found. The half-wavelength of the buckling pattern, which is twice that of the imperfection, is not allowed to exceed the shell length. In addition, the critical load N_{CR} is, of course, minimized with respect to the number of circumferential waves. Formulas for the coefficients α, β, and γ in Eq. (19) are given in the appendix of Ref. 12.

Design Philosophy

The design philosophy in Ref. 12 is based on the assumption that both the wide-column method and the Koiter theory method are conservative. Consequently, in a particular case the higher of the predictions from the two methods is used as the design critical load. The computer program which generated the results to be described next is listed in Ref. 183.

Numerical Results

In Fig. 8.2 comparisons between test and theory are shown for more than 250 cylinders of different types. The reference numbers correspond to the references given in the paper by Almroth et al.[12] In Fig. 8.2a, the test results are compared with the critical load N_{CL} according to classical theory. Although all the theoretical results are for cylinders with simply supported edges, the test conditions are probably more likely to correspond to clamped edges. For most cases, it is believed that the influence of the edge conditions is insignificant, but there may be instances, especially for stringer-stiffened shells, in which the test results would have been considerably lower if the conditions of simply supported edges could have been realized. This is illustrated in the tables of Ref. 184 for some stringer-stiffened and some filament-

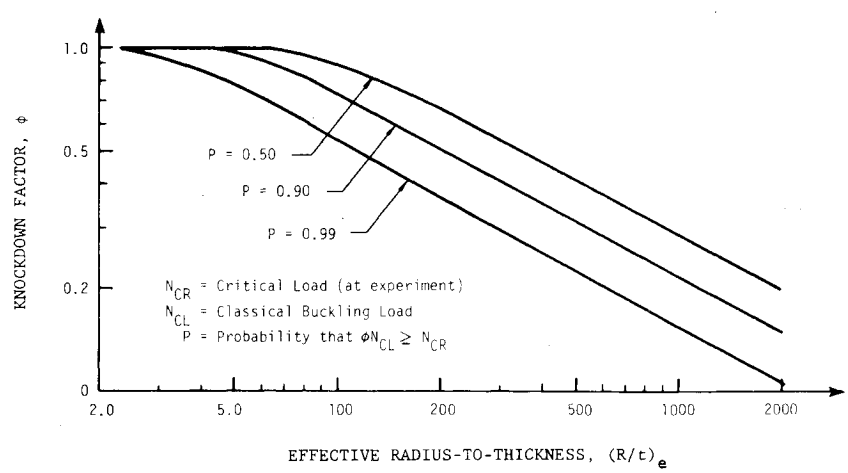

Fig. 8.1 Empirical knockdown factor ϕ for monocoque cylinders subjected to axial compression (from Almroth[70]).

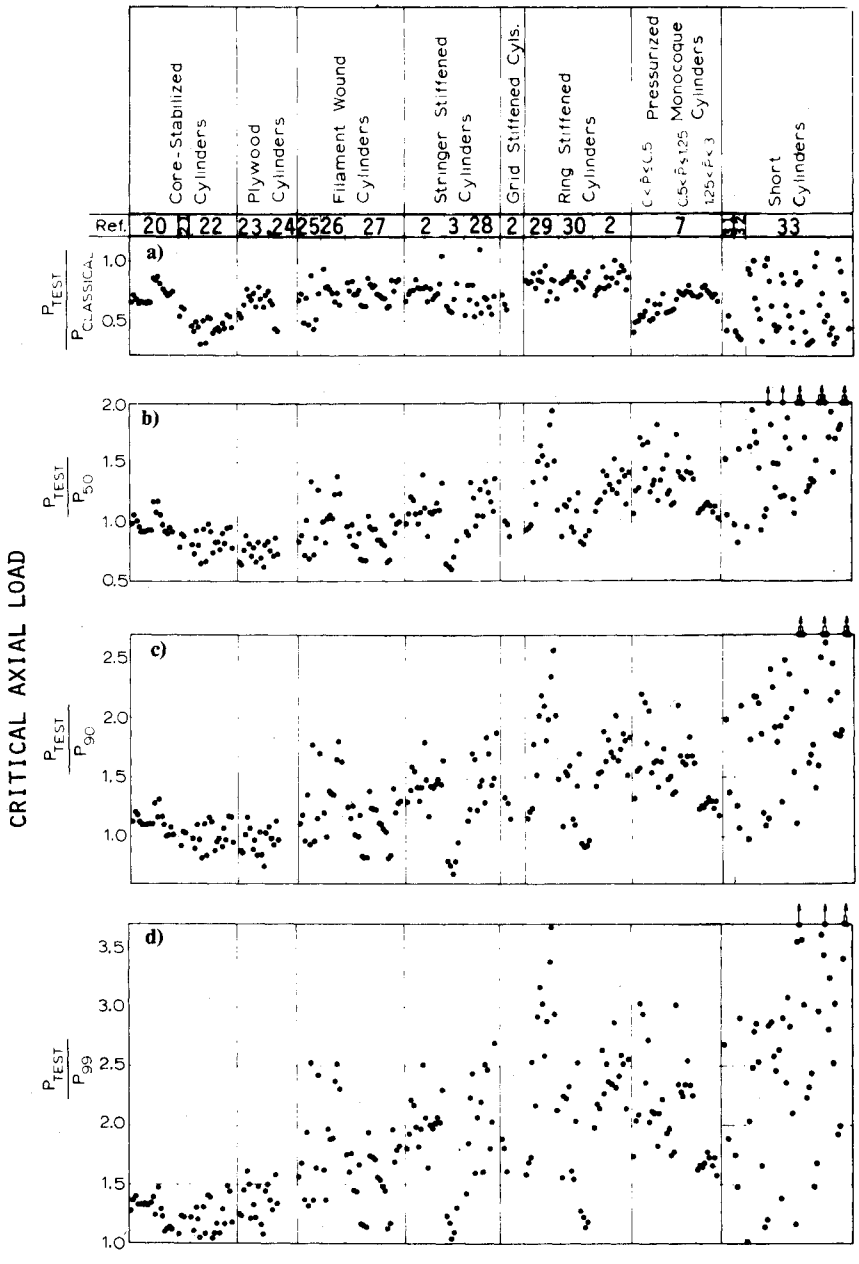

Fig. 8.2 Axially compressed cylindrical shells: correlations between test results and a) classical theory and the maximum of the wide column load [Eq. (16)] or the prediction from the extended version of Koiter's special theory [Eq. (19)] for: b) 50% probability predictions, c) 90% probability predictions, and d) 99% probability predictions (from Almroth, Burns, and Pittner[12]).

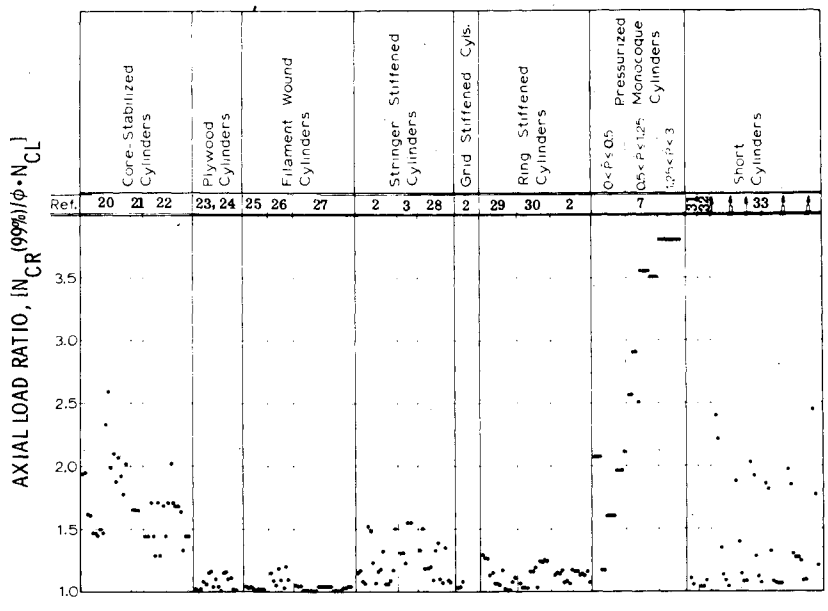

Fig. 8.3 Axially compressed cylindrical shells: Comparison of 99% probability predictions [N_{cr} (99%)] obtained with the design method of Almroth, Burns, and Pittner,[12] with predictions based on classical theory N_{CL} times ϕ for a monocoque shell with the same effective R/t ratio (from Almroth, Burns, and Pittner[12]).

wound cylinders, and it explains why three of the test results are above the classical load.

In Figs. 8.2b-d the test results are compared with the higher of the two predictions from the wide-column formula [Eq. (16)] or the Koiter-type theory [Eq. (19)]. Figure 8.2b corresponds to the use of the 50% probability curve in Fig. 8.1, while the results in Fig. 8.2c and 8.2d are based on use of the curves in Fig. 8.1 corresponding to 90 and 99% probability, respectively. It appears from Fig. 8.2c that the results based on 90% probability would not be entirely "safe" and that the 99% probability curve should therefore be recommended for design.

For pressurized cylinders, a series of test results at different values of the internal pressure was often obtained from the same test specimen. As the format of Fig. 8.2 is not suitable for such cases, comparisons between tests of this type and the theory summarized here are presented in separate figures in Ref. 12.

Conclusions

It is evident that the classical buckling load is not a suitable design limit for any of these classes of axially compressed cylinders. Although it has sometimes been stated in the literature that for one type of cylindrical shell or another the classical theory would be applicable, the designer is generally more prudent and applies conservative methods. As an example, for stringer-stiffened shells the wide-column load [Eq. (17)] is sometimes used as a design limit and in other cases a part of the "curvature effect" is added as given by Eq. (16): The present method is less conservative because the corresponding design critical load is either equal to or higher than that of Eq. (16). For other cases, it is a common procedure simply to apply to the classical load N_{CL} the same reduction factor ϕ as for the infinite monocoque shell with the same effective radius-to-thickness ratio. In Fig. 8.3 the predictions of this simple alternative method ($N_{CR} = \phi \cdot N_{CL}$) are compared with those of the method recommended here [N_{CR} obtained from the higher predictions from Eq. (16) or (19)]. It is seen that the latter method gives the same or higher values in all cases and that sometimes the difference is substantial.

It is clear, therefore, that the design principles recommended by Almroth, Burns, and Pittner[12] and summarized here will lead to more economic designs than the methods that are generally in use. At the same time, they should be entirely safe, since out of more than 250 test specimens of many different types every one failed at a value above the design load N_{CR} calculated from the higher of Eq. (16) or (19). It seems that improvements may be possible through minor modifications of the method. The choice of the curves in Fig. 8.1 and the definition of an effective radius-to-thickness ratio may, for instance, be questioned. Although it is felt that the method recommended in Ref. 12 represents a clear advantage over present design practices, it is still an interim solution that is acceptable only because totally satisfactory methods are not available.

9. Examples of Structures in which Sophisticated Buckling Analyses Affect the Design

Large Water Tank

The 1500 m^3 capacity water tank that failed in Belgium in 1972 was analyzed with use of the BOSOR4 and BOSOR5 computer programs.[2] Figure 9.1 exhibits a discretized branched shell model of the tank sketched in Fig. 1.4 and Fig. 9.2 shows axisymmetric deformations at a load factor $\lambda = 1.8$ corresponding to collapse predicted with BOSOR5. (A factor $\lambda = 1.0$ corresponds to the condition that existed when the actual tank failed.) It is necessary to include both moderately large deflection effects and nonlinear material behavior in order to obtain a sufficiently accurate prediction.

Figure 9.3a shows a new design suggested by Baltus and Massonnet.[2] The predicted deformations at collapse at the new higher load factor, $\lambda = 2.65$, are displayed in Fig. 9.3b. Again the mode of failure is axisymmetric elastic-plastic collapse.

Notched Joint in a Rocket Interstage

Rockets for launching from Earth to space are staged. The stages when consumed are separated from the remainder of the vehicle at joints with notches designed to fracture under forces generated by the explosion of a primacord contained within a cavity extending around the circumference at the plane of separation.

An example of such a joint, tested to failure in compression, is photographed in Fig. 9.4a. Figure 9.4b shows the

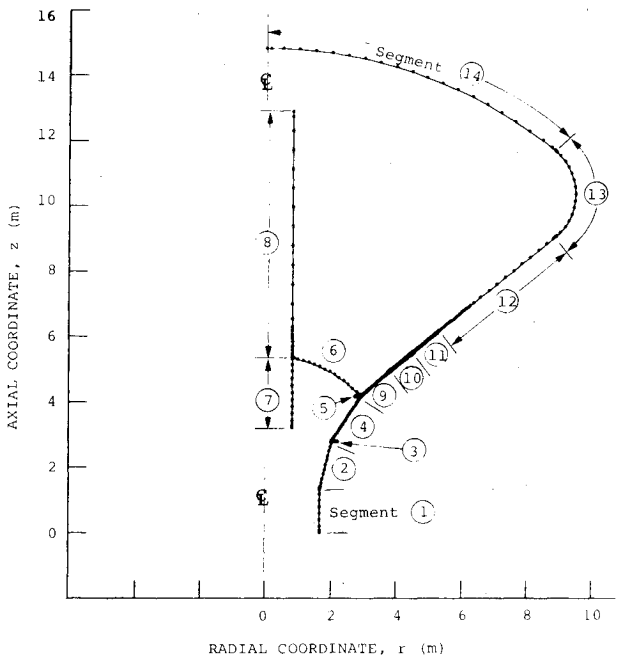

Fig. 9.1 Analysis of failure of large steel water tank shown in Fig. 1.4, segment numbering and discretization for treatment with the BOSOR5 computer program.

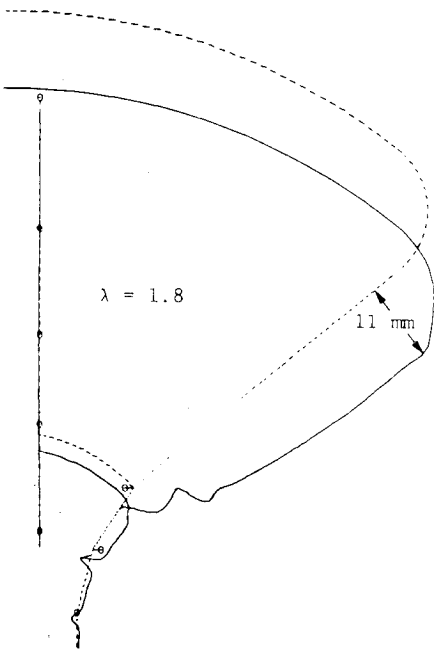

Fig. 9.2 Axisymmetric deformation of steel water tank at load factor corresponding to predicted collapse ($\lambda = 1.0$ corresponds to actual collapse conditions existing in 1972 at the time of the disaster).

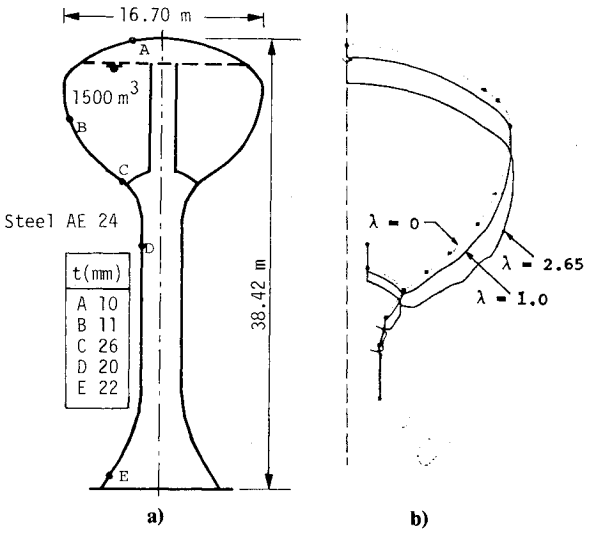

Fig. 9.3 New design of the water tank and axisymmetric deformation at load factor, $\lambda = 2.65$, which corresponds to predicted collapse (from Baltus and Massonnet[2]). a) New design; b) predicted deformation of new design at collapse.

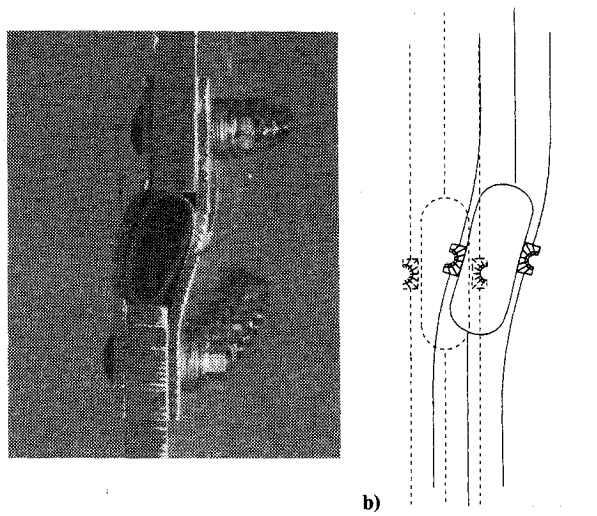

Fig. 9.4 Failure of axially compressed frangible joint typical of those used in rockets for the separation of booster stages (from Bushnell[186]). a) Test specimen, b) BOSOR6 hybrid model.

test specimen modeled as a hybrid body of revolution.[185,186] By "hybrid body of revolution" is meant a configuration in which some parts of an axisymmetric structure are modeled with the use of thin shell theory and other parts with the use of isoparametric solid elements of revolution. In Fig. 9.4b the long line segments represent reference surfaces of structural parts treated as thin shells. The behavior of the structure in the neighborhoods of the notches cannot be predicted with use of shell theory, and eight-node quadrilateral finite elements of revolution are therefore used in these limited regions.

Proper design of frangible joints is difficult because they must be strong enough to carry the launch loads but weak enough to fracture under the primacord explosion forces. If the separating joint is to fracture reliably, it must contain a circumferential notch or notches at the roots of which fracture initiates. These notches act as stress raisers under the launch loads, of course. Instability of the shell with the notched joint embedded in it results from a complicated interaction of load-path eccentricity and local plastic flow. The growth of the regions in which plastic flow occurs as the axial load is increased cannot be accurately determined from shell theory. This local plastification exacerbates the load-

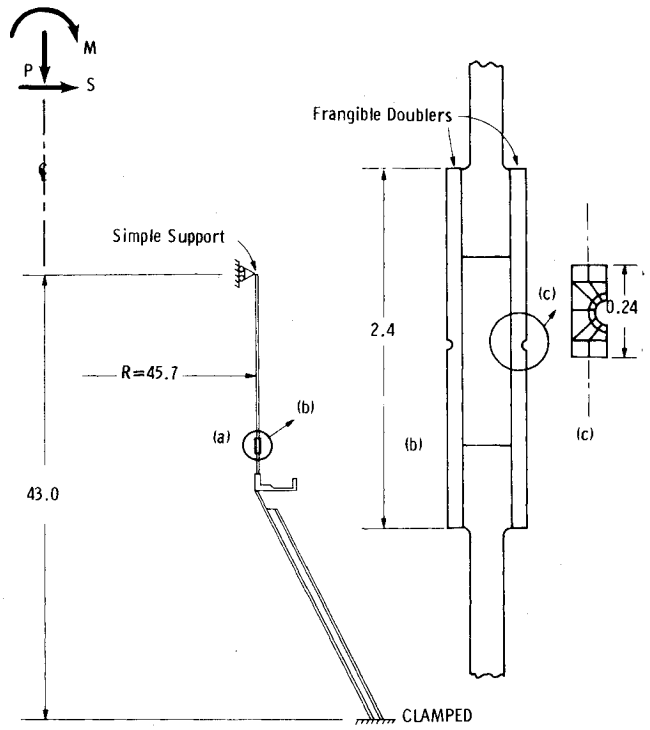

Fig. 9.5 Frangible joint embedded in a cylindrical shell near a junction between the cylinder and a conical frustrum: a) overall view; b) expanded view of notched doublers; c) expanded view of neighborhood of one of the notches, showing discretization with solid quadrilateral finite elements of revolution (from Bushnell and Yamamura[187]).

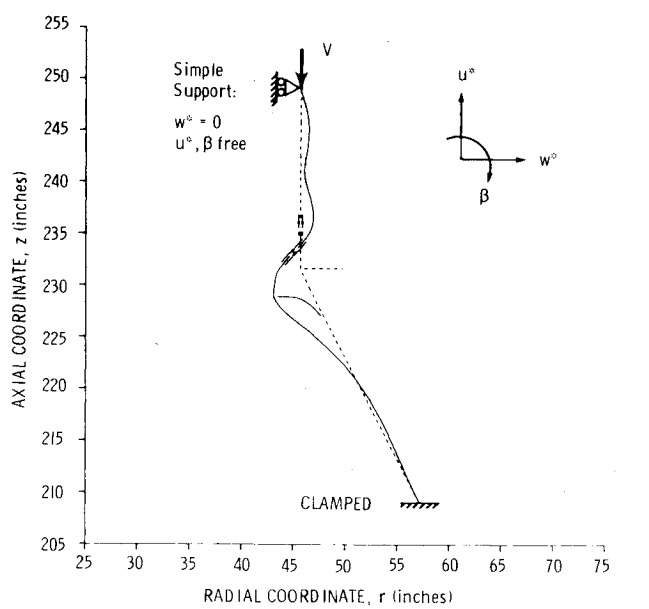

Fig. 9.6 Axisymmetric deformation of rocket interstage under uniform axial compression (the frangible joint lies within the bending region of the cylinder-cone junction).

path eccentricity caused by the notches. The increased load-path eccentricity gives rise to increased local meridional rotations that precipitate axisymmetric collapse similar to that shown in Fig. 4.7 or nonsymmetric bifurcation buckling similar to that shown in Fig. 1.9c.

Figure 9.5 shows a rocket interstage with a frangible joint similar to that displayed in Fig. 9.4, except that the primacord tube is absent. In the computerized model, the web of the large ring at the junction between the conical frustrum and the cylindrical shell is treated as a flexible shell branch, with its

flange included as a discrete ring. Axial load-path eccentricities exist in the upper part of the cylindrical shell, which is made of graphite-epoxy. The rest of the structure is made of aluminum. Details of the model are given in Ref. 187.

Certain geometrical constraints and the location of electrical equipment imposed limitations on the location of the frangible joint. The best compromise resulted in its location within the bending region in the neighborhood of the cylinder-cone junction, as demonstrated in Fig. 9.6. This behavior necessitates the use of the extensive model shown. It is not sufficient to study only the immediate region of the joint or of the notches in the frangible doublers in order to determine accurately the critical axial load. There are nonlinear interaction effects between the overall rotation, bending, and shearing of the joint region and the local bending of the frangible doublers due to the load-path eccentricities caused by the notches. The hybrid shell-solid model is ideally suited for this analysis because extensive regions in which shell theory holds can be included in the model with relatively minor increases in computer run costs.

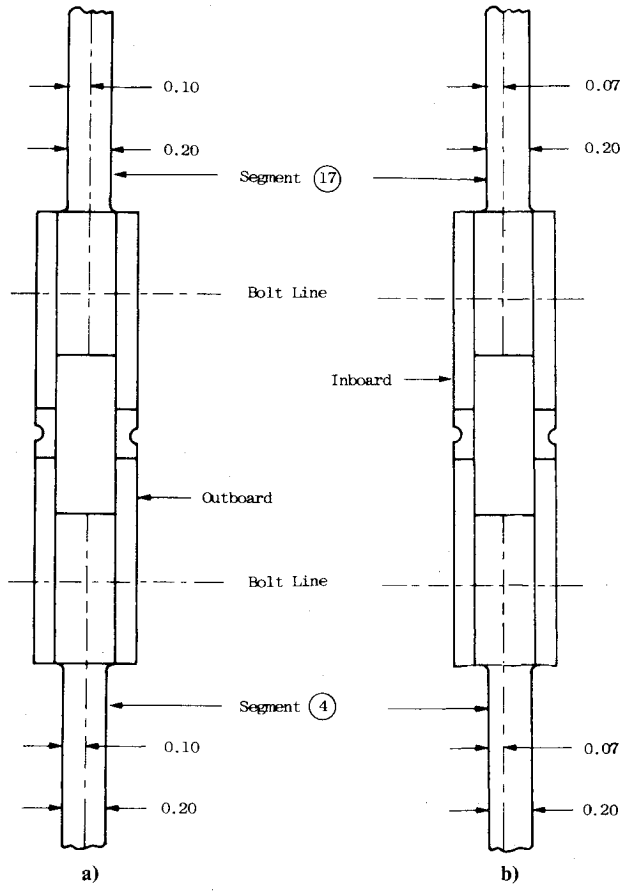

Fig. 9.7 Frangible joint detail, showing original and final designs. This minor design change raises the compressive load-carrying capability of the rocket interstage shown in Fig. 9.6 by about 10%. a) an original design; b) final design.

The actual loading on the rocket interstage consists of axial, shear, and bending components, as illustrated in Fig. 9.5. However, the local stresses in the notch areas can be predicted very accurately by an *axisymmetric* analysis in which the axisymmetric compressive axial stress resultant V_0 is set equal to

$$V_0 = P/2\pi r + (M + S\ell)/\pi r^2 \tag{20}$$

where ℓ is the distance from the axial station at which S is applied to the axial station at the notch.

Effect of Minor Design Change

Figure 9.7 shows the difference between an original joint design and the final configuration. With the original design (Fig. 9.7a) the axially loaded joint deforms in such a way that approximately 56% of the total axial load passes through the inboard frangible doubler and 44% through the outboard frangible doubler, causing the stresses at the root of the inboard notch to be higher than those at the root of the outboard notch. The changes in segments 4 and 17 shown in Fig. 9.7 shift more axial load to the outboard member such that the maximum stresses in the outboard member are slightly higher than those of the inboard member. The original design (Fig. 9.7a) leads to a predicted collapse load of 7004 N/cm (4000 lb/in.) and the redesigned joint (Fig. 9.7b) leads to a predicted collapse load of 7705 N/cm (4400 lb/in.). The 0.762 mm (0.03 in.) outboard shift of segments 4 and 17 is a bit too much. A 0.635 mm (0.025 in.) shift would probably be better. The deformations in the doublers at the collapse loads of the two configurations are illustrated in Fig. 9.8.

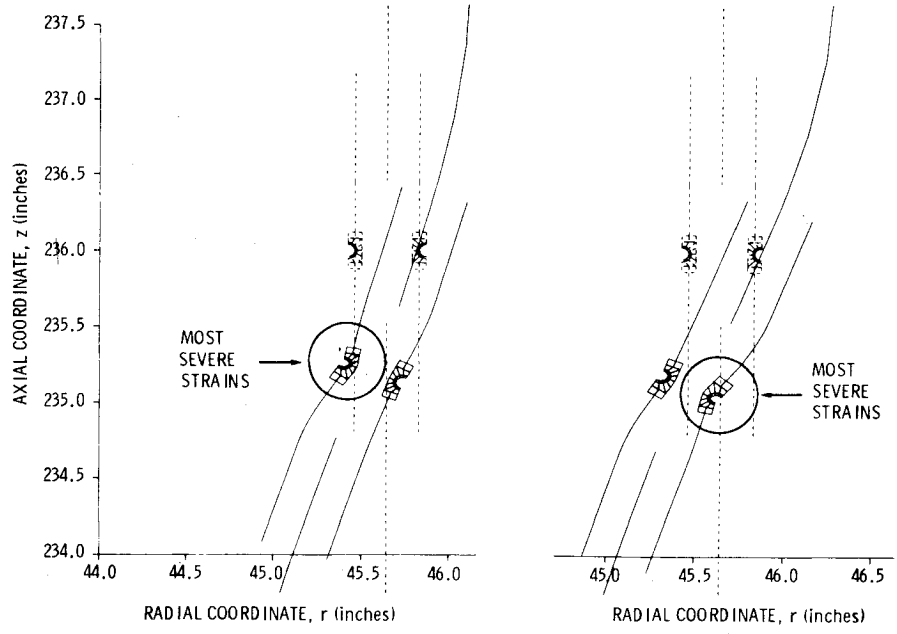

Fig. 9.8 Comparison of predicted axisymmetric deformation of the original and final designs of the frangible joint at the collapse load of each. a) Original design: $V_{cr} = 4000$ lb/in. (collapse); b) final design: $V_{cr} = 4400$ lb/in. (collapse).

10. Summary

In order to produce efficient, reliable designs of structures of which thin shells are important components, the engineer must understand the physics of shell buckling. Thus, the objective here has been to convey a "feel" for instability, whether it be due to nonlinear collapse, bifurcation, or a combination of these modes. Emphasis has been placed on practical shell structures, which may be stiffened, segmented, branched, discontinuous, and have complex wall constructions. Descriptions have been provided of some of the peculiarities of shell buckling, including nonlinear behavior caused by a combination of large deflections and plasticity, stress redistribution effects, stiffener and load-path eccentricity effects, local vs general instability, imperfection sensitivity, and modal interaction. Scattered throughout are tips on modeling that will help the engineer to discover early in the design process weak links in structures and to set up tests with properly simulated design conditions without introducing spurious failure modes. Extensive reference to earlier work is provided.

Following several dramatic examples of unexpected buckling of large, expensive shell structures, a description of the two kinds of buckling, collapse and bifurcation, is given. Examples of classical bifurcation buckling of uniformly loaded cylindrical and spherical shells are then shown, with comparisons between test and theory provided to emphasize the sensitivity of these buckling loads to initial structural imperfections. Asymptotic imperfection sensitivity theory is summarized.

A section follows in which the cause of failure is nonlinear collapse rather than bifurcation buckling. In certain of the cases the predicted nonlinear collapse load is compared to a critical load calculated from a linearized bifurcation buckling model. Included are descriptions of buckling of long tubes in bending, cylindrical panels under a normal concentrated load, and axially compressed cylinders with cutouts, noncircular cylinders, and a rocket interstage with a local axisymmetric axial load path eccentricity.

The next section provides examples of axisymmetric shells in which failure is due to bifurcation buckling and geometrical and material nonlinearity of the prebuckling behavior are important. Emphasis is first given to the nonsymmetric buckling of pressure vessels in which the prebuckled state is characterized by meridional tension and hoop compression. The effects of fabrication processes on buckling of hydrostatically compressed, ring-stiffened cylindrical shells are then described. Buckling pressures from test and theory are compared for two nominally identical specimens, one of which was carefully machined and stress relieved and the other of which was fabricated by cold bending a flat sheet into a cylindrical shell and subsequently welding rings to it.

A brief discussion follows of the effect of boundary conditions and load eccentricity on buckling. This section features an example of local crippling of a large corrugated cylindrical panel that failed in a mode different from that intended because the test specimen was not made large enough to permit the type of general instability that analysis shows is critical in the actual flight vehicle.

Next, a description of buckling of stiffened panels and shells is provided. The purpose here is to demonstrate the types of local and general buckling to which such structures are susceptible and reveal modal interaction effects that lead to lower predictions of bifurcation buckling than those obtained from simple formulas in which each type of buckling is considered separately. A number of examples is given which reveals the importance in certain cases of treating discrete stiffener webs as flexible shell branches in analytical models.

The discussion of modal interaction is continued in a demonstration of the increased imperfection sensitivity that results from buckling-constrained optimization with respect to weight of columns, panels, and shells built up of thin sections that fail in local and general instability modes at the same or almost the same load. For years specialists in buckling have called this "one-hoss-shay" approach to design naive, presuming that a different design philosophy in which the local and general instability eigenvalues are well separated would lead to lighter structures because of milder sensitivity to initial imperfections. Recent calculations tend to support the "naive" approach, however, although the proper structural dimensions must of course be arrived at with due consideration given to increased imperfection sensitivity at the optimal design.

Some details follow pertinent to a design procedure for axially compressed stiffened cylindrical panels and shells with or without internal pressure and/or an elastic core. The procedure, originally set forth by Almroth, Burns, and Pittner,[12] is based on application of a combination of a curvature-modified, wide-column formula and Koiter's special theory.[59] It yields designs which according to experimental evidence are safe, yet are less conservative than other approaches.

The paper concludes with two examples in which rather sophisticated analysis methods are required in order to identify design improvements for buckling-critical structures. In the first, an improved design for the water tank shown in Fig. 1.4 is arrived at and evaluated with a buckling analysis in which moderately large deflections and nonlinear material behavior are simultaneously accounted for.[2] In the second example the axially compressive load-carrying capability of a frangible joint in a rocket interstage is increased by approximately 10% through a hybrid analysis in which certain parts of the elastic-plastic structure must be modeled with use of solid isoparametric elements because shell theory cannot adequately predict the large-deflection, elastic-plastic behavior in the immediate neighborhoods of notches in the frangible members of the joint.

Acknowledgments

This work represents a summary of a book[5] sponsored partly by the Air Force Office of Scientific Research under Contract F49620-77-C-0122 (Lt. Col. J. D. Morgan, contract monitor) and partly by the 1979-1980 Lockheed Independent Development Program. The author wishes to express his gratitude to Bill Sable and Dick Hartung for their support and encouragement and to Bo Almroth for his many helpful comments, in particular for his contribution to the sections on buckling of composite cylindrical shells. The author also appreciates the comments of Prof. A. van der Neut of the Delft University of Technology, the Netherlands. Colleen Miller drew many of the figures and Christy Weston typed the manuscript.

References

[1] Galletly, G. D., "Torispherical Shells—A Caution to Designers," *ASME Journal for Engineering in Industry*, Vol. 81, Feb. 1959, pp. 51-66.

[2] Baltus, R. and Massonnet, C., "Use of Computer Programs BOSOR4 and 5 in the Stability Analysis of Two Civil Engineering Steel Shell Structures," *Proceedings of Stability of Steel Structures*, Liege, Belgium, April 1977, pp. 609-617.

[3] Vanderpitte, D., "Model Investigation of the Collapse of a Steel Water Tower," *Proceedings of Stability of Steel Structures*, Liege, Belgium, April 1977, pp. 599-607.

[4] Lagae, G., Laboratorium voor Modelonderzoek, Rijksuniversiteit, Gent, Belgium, private communication to D. Bushnell, Lockheed Missiles & Space Co., Palto Alto, Calif., Aug. 8, 1978.

[5] Bushnell, D., "Computerized Analysis of Shell Buckling," Lockheed Missiles & Space Co., Rept. LMSC-D681517, Dec. 1979.

[6] Shih, C. F. and Babcock, C. D., "Buckling of Cylindrical Tank under Earthquake Excitation," *ASCE Proceedings of Third Engineering Mechanics Conference*, Sept. 1979, pp. 81-84.

[7] Clough, R. W. and Niwa, A., "Static Tilt Tests of a Tall Cylindrical Liquid Storage Tank," University of California, Berkeley, Earthquake Engineering Research Center Rept. UCB/EERC-79/06, Feb. 1979.

[8] Seide, P., Weingarten, V. I., and Masri, S. F., "Buckling Criteria and Application of Criteria to Design of Steel Containment Shell," NUREG-CR 0793, March 1979.

[9] Bushnell, D., "Stress, Stability and Vibration of Complex Branched Shells of Revolution," *Computers and Structures*, Vol. 4, 1974, pp. 399-435.

[10] Bushnell, D., "Crippling and Buckling of Corrugated Ring-Stiffened Cylinders," *Journal of Spacecraft and Rockets*, Vol. 9, May 1972, pp. 357-363.

[11] Brush, D. O. and Almroth, B. O., *Buckling of Bars, Plates, and Shells*, McGraw-Hill Book Co., New York, 1975.

[12] Almroth, B. O., Burns, A. B., and Pittner, E. V., "Design Criteria for Axially Loaded Cylindrical Shells," *Journal of Spacecraft and Rockets*, Vol. 7, June 1970, pp. 714-720.

[13] Koiter, W. T., "The Nonlinear Buckling Problem of a Complete Spherical Shell under Uniform External Pressure," Nos. I-IV, *Koninklike Nederlandische Akademie van Wetenshappen*, Vol. B72, 1969, pp. 40-123.

[14] Bushnell, D., "Thin Shells," *Structural Mechanics Computer Programs, Surveys, Assessments, and Availability*, edited by W. Pilkey, K. Saczalski, and H. Schaeffer, University of Virginia Press, Charlottesville, Va., 1974, pp. 277-358.

[15] Roorda, J., "Stability of Structures with Small Imperfections," *ASCE Journal of Engineering Mechanics Division*, Vol. 91, No. EM1, 1965, pp. 87-106.

[16] Hutchinson, J. W. and Koiter, W. T., "Post-buckling Theory," *Applied Mechanics Review*, Vol. 23, 1970, pp. 1353-1356.

[17] Tvergaard, V., "Buckling Behavior of Plate and Shell Structures," *Proceedings of the 14th International Congress of Theoretical and Applied Mechanics*, edited by W. T. Koiter, North-Holland Publishing Co., New York, 1976, pp. 233-247.

[18] Hutchinson, J. W., "Plastic Buckling," *Advances in Applied Mechanics*, Vol. 14, edited by C. S. Yih, Academic Press, New York, 1974, pp. 67-144.

[19] Bushnell, D., "Plastic Buckling," Lockheed Missiles & Space Co., Rept. LMSC-D673763, April 1979 (to appear in *ASME PVP Decade of Progress*, 1981).

[20] Pilkey, W., Saczalski, K., and Schaeffer, H., (Eds.), *Structural Mechanics Computer Programs: Surveys, Assessment, and Availability*, University Press of Virginia, Charlottesville, 1974.

[21] Bushnell, D., "A Computerized Information Retrieval System," *Structural Mechanics Computer Programs: Surveys, Assessments, and Availability*, University Press of Virginia, Charlottesville, 1974, pp. 735-804.

[22] Cohen, G. A., "User Document for Computer Programs for Ring-Stiffened Shells of Revolution," NASA CR-2086, 1973; "Computer Analysis of Ring-Stiffened Shells of Revolution," NASA CR-2085, 1973; "Computer Program for Analysis of Imperfection Sensitivity of Ring-Stiffened Shells of Revolution," NASA CR-1801, 1971.

[23] Kalnins, A., "User's Manual for KSHEL Computer Programs," 1970, available from Dr. Kalnins, Lehigh University, Bethlehem, Pa., (also see "Free Vibration, Static and Stability Analysis of Thin Elastic Shells of Revolution," AFFDL-TR-68-144, March 1969).

[24] Svalbonas, V., "Numerical Analysis of Stiffened Shells of Revolution," NASA CR-2273, 1973.

[25] Koiter, W. T., "Over de Stabiliteit van het Elastisch Evenwicht," University of Delft thesis, Paris, Amsterdam, 1945 (English translation, NASA Rept. TTF-10, 1967).

[26] Biot, M. H., *Mechanics of Incremental Deformations*, John Wiley and Sons, New York, 1965.

[27] Fung, Y. C., *Foundations of Solid Mechanics*, Prentice-Hall, Englewood Cliffs, N.J., 1965.

[28] Washizu, K., *Variational Methods in Elasticity and Plasticity*, Pergamon Press, New York, 1968.

[29] Green, A. E. and Zerna, W., *Theoretical Elasticity*, 2nd Ed., Oxford University Press, London and New York, 1968.

[30] Malvern, L. E., *Introduction to the Mechanics of a Continuous Medium*, Prentice-Hall, Englewood Cliffs, N.J., 1969.

[31] Oden, J. T., *Finite Elements of Nonlinear Continua*, McGraw-Hill Book Co., New York, 1972.

[32] Przemieniecki, J. S., *Theory of Matrix Structural Analysis*, McGraw-Hill Book Co., New York, 1968.

[33] Zienkiewicz, O. C., *The Finite Element Method in Engineering Science*, McGraw-Hill Book Co., London, 1971.

[34] Desai, C. S. and Abel, J. F., *Introduction to the Finite Element Method*, Van Nostrand Reinhold Co., New York, 1972.

[35] Martin, H. C. and Carey, G. F., *Introduction to Finite Element Analysis: Theory and Applications*, McGraw-Hill Book Co., New York, 1973.

[36] Hoff, N. J., "The Perplexing Behavior of Thin Cylindrical Shells in Axial Compression," *Israel Journal of Technology*, Vol. 4, No. 1, 1966, pp. 1-28.

[37] Donnell, L. H. and Wan, C. C., "Effects of Imperfections on Buckling of Thin Cylinders and Columns under Axial Compression," *Journal of Applied Mechanics*, Vol. 17, 1950, pp. 73-83.

[38] Lorenz, R., "Achsensymmetrische Verzerrungen in dunnwandigen Hohlzylindern," *Zeitschrift des Vereines Deutscher Ingenieure*, Vol. 52, 1908, p. 1707.

[39] Timoshenko, S. P., *Theory of Elastic Stability*, McGraw-Hill Book Co., New York, 1936, p. 439.

[40] Singer, J. and Abramovich, H., "Vibration Techniques for Definition of Practical Boundary Conditions in Stiffened Shells," *AIAA Journal*, Vol. 17, July 1979, pp. 762-769.

[41] Ekstrom, R. E., "Buckling of Cylindrical Shells under Combined Torsion and Hydrostatic Pressure," *Experimental Mechanics*, Vol. 3, Aug. 1963, pp. 192-197.

[42] Harris, L. A., Suer, H. S., and Skene, W. T., "Model Investigations of Unstiffened and Stiffened Circular Shells," *Experimental Mechanics*, Vol. 1, No. 7, 1961, pp. 1-9.

[43] Kaplan, A., "Buckling of Spherical Shells," *Thin Shell Structures, Theory, Experiment, and Design*, edited by Y. C. Fung and E. E. Sechler, Prentice-Hall, Englewood Cliffs, N.J., 1974, pp. 248-288.

[44] Horton, W. H., Bailey, S. C., and McQuilkin, B. H., "An Introduction to Stability," Stanford University report version of Paper 219 presented at ASTM Annual Meeting, Atlantic City, N.J., June 1966.

[45] Carlson, R. L., Sendlebeck, R. L., and Hoff, N. J., "Experimental Studies of the Buckling of Complete Spherical Shells," *Experimental Mechanics*, Vol. 7, 1967, pp. 281-288.

[46] Koiter, W. T., "Elastic Stability and Postbuckling Behavior," *Proceedings of the Symposium on Nonlinear Problems*, edited by R. E. Langer, University of Wisconsin Press, Madison, 1963, pp. 257-275.

[47] Budiansky, B. and Hutchinson, J. W., "Buckling: Progress and Challenge," *Trends in Solid Mechanics, 1979*, edited by J. F. Besseling and A.M.A. van der Heijden, Sijthoff-Noordhoff, Amsterdam, The Netherlands, 1980.

[48] Budiansky, B., "Theory of Buckling and Post-buckling Behavior of Elastic Structures," *Advances in Applied Mechanics*, Vol. 14, Academic Press, New York, 1974, pp. 1-65.

[49] Seide, P., "A Reexamination of Koiter's Theory of Initial Post-buckling Behavior and Imperfections-Sensitivity of Structures," *Thin Shell Structures, Theory, Experiment, Design*, edited by Y. C. Fung and E. E. Sechler, Prentice-Hall, Englewood Cliffs, N.J., 1974, pp. 59-80.

[50] Masur, E. F., "Buckling of Shells—General Introduction and Review," Paper 2000 presented at ASCE National Structural Engineering Meeting, San Francisco, April 9-13, 1973.

[51] Budiansky, B. and Hutchinson, J. W., "Dynamic Buckling of Imperfection-Sensitive Structures," *Proceedings of XI International Congress of Applied Mechanics, Munich, 1964*, Springer-Verlag, Berlin, 1966, pp. 636-651.

[52] Budiansky, B., "Dynamic Buckling of Elastic Structures: Criteria and Estimates," *Dynamic Stability of Structures, Proceedings of an International Conference, 1965*, edited by G. Herrmann, Pergamon Press, New York, 1967, pp. 83-106.

[53] Budiansky, B. and Hutchinson, J. W., "A Survey of Some Buckling Problems," *AIAA Journal*, Vol. 4, Sept. 1966, pp. 1505-1510.

[54] Koiter, W. T., "The Nonlinear Buckling Problem of a Complete Spherical Shell under Uniform External Pressure," Nos. I-IV, *Koninklike Nederlandische Akademie von Wetenshappen*, Vol. B72, 1969, pp. 40-123.

[55] Arbocz, J., "The Effect of Initial Imperfections on Shell Stability," *Thin-Shell Structures: Theory, Experiment, and Design*, edited by Y. C. Fung and E. E. Sechler, Prentice-Hall, Englewood Cliffs, N.J., 1974, pp. 205-245.

[56] Hutchinson, J. W., "Axial Buckling of Pressurized Imperfect Cylindrical Shells," *AIAA Journal*, Vol. 3, Aug. 1965, pp. 1461-1466.

[57] Arbocz, J. and Babcock, C. D., "The Effect of General Imperfections on the Buckling of Cylindrical Shells," *Journal of Applied Mechanics*, Vol. 36, 1969, pp. 28-38.

[58] Arbocz, J. and Sechler, E. E., "On the Buckling of Stiffened Imperfect Cylindrical Shells," *AIAA Journal*, Vol. 14, Nov. 1976, pp. 1611-1617.

[59] Koiter, W. T., "The Effect of Axisymmetric Imperfections on the Buckling of Cylindrical Shells under Axial Compression," *Koninklike Nederlandische Akademie van Wetenshappen*, Vol. B66, 1963, pp. 265-279.

[60] Tennyson, R. C. and Muggeridge, D. B., "Buckling of Axisymmetric Imperfect Circular Cylindrical Shells under Axial Compression," *AIAA Journal*, Vol. 7, Nov. 1969, pp. 2127-2131.

[61] Hutchinson, J. W. and Amazigo, J. C., "Imperfection Sensitivity of Eccentrically Stiffened Cylindrical Shells," *AIAA Journal*, Vol. 5, March 1967, pp. 392-401.

[62] Hutchinson, J. W. and Frauenthal, J. C., "Elastic Postbuckling Behavior of Stiffened and Barreled Cylindrical Shells," *Journal of Applied Mechanics*, Vol. 36, 1969, pp. 784-790.

[63] Amazigo, J. C. and Budiansky, B., "Asymptotic Formulas for the Buckling Stresses of Axially Compressed Cylinders with Localized or Random Axisymmetric Imperfections," *Journal of Applied Mechanics*, Vol. 39, 1972, pp. 179-184.

[64] Almroth, B. O., Brogan, F. A., and Stanley, G. M., "Structural Analysis of General Shells, Vol. II: User Instructions for STAGSC," Lockheed Missiles & Space Co., Inc., Palo Alto, Calif., Rept. LMSC-D633873, Jan. 1979.

[65] Bushnell, D., "BOSOR5—Program for Buckling of Elastic-Plastic Complex Shells of Revolution including Large Deflections and Creep," *Computers & Structures*, Vol. 6, 1976, pp. 221-239.

[66] Khot, N. S., "On the Influence of Initial Geometric Imperfections on the Buckling and Post-buckling Behavior of Fiber-Reinforced Cylindrical Shells under Uniform Axial Compression," AFFDL-TR-68-136, Oct. 1968.

[67] Khot, N. S. and Venkayya, V. B., "Effect of Fiber Orientation on Initial Postbuckling Behavior and Imperfection Sensitivity of Composite Cylindrical Shells," AFFDL-TR-70-125, 1970.

[68] Tennyson, R. C., Chan, K. H., and Muggeridge, D. B., "Effect of Axisymmetric Shape Imperfections on the Buckling of Laminated Anisotropic Circular Cylinders," *Transactions Canadian Aeronautics and Space Institute*, Vol. 4, University of Toronto, Canada, Sept. 1971, pp. 131-139.

[69] Kulkarni, S. V. and Frederick, D., "Buckling of Partially Debonded Layered Cylindrical Shells," Paper presented at AIAA/ASME/SAE 14th Structures, Structural Dynamics, and Materials Conference, Williamsburg, Va., March 1973.

[70] Almroth, B. O., "Design of Composite Material Structures for Buckling," Lockheed Missiles & Space Co., Palo Alto, Calif., Rept. LMSC-D681425, Dec. 1979.

[71] Tennyson, R. C., "Buckling of Laminated Composite Cylinders: A Review," *Composites*, Vol. 6, Jan. 1975, pp. 17-24.

[72] Wilkins, D. J., "Compression Buckling Tests of Laminated Graphite-Epoxy Curved Panels," Paper presented at AIAA 12th Aerospace Sciences Meeting, Washington, D.C., Jan. 30-Feb. 1, 1974.

[73] Hutchinson, J. W., "Post-Bifurcation Behavior in the Plastic Range," *Journal of Mechanics and Physics of Solids*, Vol. 21, 1973, pp. 163-190.

[74] Tvergaard, V., "Buckling of Elastic-Plastic Oval Cylindrical Shells under Axial Compression," *International Journal of Solids and Structures*, Vol. 12, 1976, pp. 683-691, 1976 (also Errata, ibid, Vol. 14, 1978, p. 329).

[75] Tvergaard, V. and Needleman, A., "On the Buckling of Elastic-Plastic Columns with Asymmetric Cross-Sections," *International Journal of Mechanical Sciences*, Vol. 17, 1975, pp. 419-424.

[76] Hutchinson, J. W., "On the Postbuckling Behavior of Imperfection-Sensitive Structures in the Plastic Range," *Journal of Applied Mechanics*, Vol. 39, 1972, pp. 155-162.

[77] Hutchinson, J. W., "Imperfection Sensitivity in the Plastic Range," *Journal of Mechanics and Physics of Solids*, Vol. 21, 1973, pp. 191-204.

[78] Hutchinson, J. W. and Budiansky, B., "Analytical and Numerical Study of the Effects of Initial Imperfections on the Inelastic Buckling of a Cruciform Column," *Buckling of Structures*, edited by B. Budiansky, Springer-Verlag, New York, 1976, pp. 98-105.

[79] Needleman, A. and Tvergaard, V., "An Analysis of the Imperfection-Sensitivity of Square Elastic-Plastic Plates under Axial Compression," *International Journal of Solids Structures,* Vol. 12, 1976, pp. 185-201.

[80] Tvergaard, V., "Buckling of Elastic-Plastic Cylindrical Panel under Axial Compression," *International Journal of Solids Structures*, Vol. 13, 1977, pp. 957-970.

[81] Hill, R., "A General Theory of Uniqueness and Stability in Elastic/Plastic Solids," *Journal of Mechanics and Physics of Solids*, Vol. 6, 1958, pp. 236-249.

[82] Hill, R., "Some Basic Principles in the Mechanics of Solids without a Natural Time," *Journal of Mechanics and Physics of Solids*, Vol. 7, 1959, pp. 205-225.

[83] Tvergaard, V. and Needleman, A., "Mode Interaction in an Eccentrically Stiffened Elastic-Plastic Panel under Compression," *Buckling of Structures*, edited by B. Budiansky, Springer-Verlag, Berlin, Heidelberg, New York, 1976, pp. 160-171.

[84] Tvergaard, V. and Needleman, A., "Buckling of Eccentrically Stiffened Elastic-Plastic Panels on Two Single Supports or Multiply Supported," *International Journal of Solids and Structures*, Vol. II, 1975, pp. 647-663.

[85] Lee, L.H.N., "Inelastic Buckling of Initially Imperfect Cylindrical Shells Subject to Axial Compression," *Journal of Aerospace Sciences*, Vol. 29, 1962, pp. 87-95.

[86] Batterman, S. C., "Plastic Buckling of Axially Compressed Cylindrical Shells," *AIAA Journal*, Vol. 3, Feb. 1965, pp. 316-325.

[87] Sobel, L. H. and Newman, S. Z., "Plastic Buckling of Cylindrical Shells under Axial Compression," Paper presented at Third U.S. Congress on Pressure Vessels and Piping, San Francisco, June 25-29, 1979 (see also, *ASME Journal of Pressure Vessel Technology*, Vol. 102, Feb. 1980, pp. 40-44).

[88] Sewell, M. J., "A Survey of Plastic Buckling," *Stability*, edited by H. Leipholz, Chap. 5, University of Waterloo Press, Ontario, Canada, 1972, pp. 85-197.

[89] Ramsey, H., "Plastic Buckling of Conical Shells under Axial Compression," *International Journal of Mechanical Sciences*, Vol. 19, 1977, pp. 252-272.

[90] Gerard, G., "Compressive and Torsional Buckling of Thin Walled Cylinders in the Yield Region," NACA TN 3726, Aug. 1956.

[91] Murphy, L. M. and Lee, L.H.N., "Inelastic Buckling Process of Axially Compressed Cylindrical Shells Subject to Edge Constraints," *International Journal of Solids and Structures*, Vol. 7, Sept. 1971, pp. 1153-1170.

[92] Gellin, S., "Effect of an Axisymmetric Imperfection on the Plastic Buckling of an Axially Compressed Cylindrical Shell," *Journal of Applied Mechanics*, Vol. 46, 1979, pp. 125-131.

[93] Brazier, L. G., "On the Flexure of Thin Cylindrical Shells and Other 'Thin' Sections," *Proceedings of the Royal Society,* Series A, Vol. 116, 1926, pp. 104-114.

[94] Seide, P. and Weingarten, V. I., "On the Buckling of Circular Cylindrical Shells under Pure Bending," *Journal of Applied Mechanics*, Vol. 28, 1961, pp. 112-116.

[95] Stevens, W. B., Starnes, J. H. Jr., and Almroth, B. O., "Collapse of Long Cylindrical Shells under Combined Bending and Pressure Loads," *AIAA Journal*, Vol. 13, Jan. 1975, pp. 20-24.

[96] Bushnell, D., "Use of BOSOR5 for the Elastic Plastic Bending and Buckling Analysis of Pipes and Elbows," *Computers & Structures*, Vol. 13, 1981, pp. 241-248.

[97] Almroth, B. O. and Brogan, F. A., "Bifurcation Buckling as an Approximation of the Collapse Load for General Shells," *AIAA Journal*, Vol. 10, April 1972, pp. 463-467.

[98] Mescall, J., "Stability of Thin Torispherical Shells under Uniform Internal Pressure," *Collected Papers on Instability of Shell Structures*, NASA TN D-1510, Dec. 1962, pp. 671-692.

[99] Adachi, J. and Benicek, M., "Buckling of Torispherical Shells under Internal Pressure," *Experimental Mechanics*, Vol. 4, Aug. 1964, pp. 217-222.

[100] Thurston, G. and Holston, A. A. Jr., "Buckling of Cylindrical Shell End Closures by Internal Pressure," NASA CR-540, July 1966.

[101] Brown, K. W. and Kraus, H., "Stability of Internally Pressurized Vessels with Ellipsoidal Heads," Paper presented at 2nd National Congress on Pressure Vessels and Piping Technology, San Francisco, June 23-27, 1975.

[102] Bushnell, D. and Galletly, G. D., "Comparisons of Test and Theory for Nonsymmetric Elastic-Plastic Buckling of Shells of Revolution," *International Journal of Solids and Structures*, Vol. 10, 1974, pp. 1271-1286.

[103] Bushnell, D. and Galletly, G. D., "Stress and Buckling of Internally Pressurized Elastic-Plastic Torispherical Vessel Heads—Comparisons of Test and Theory," *ASME Journal of Pressure Vessel Technology*, Vol. 99, Feb. 1977, pp. 39-53.

[104] Lagae, G. and Bushnell, D., "Elastic-Plastic Buckling of Internally Pressurized Torispherical Vessel Heads," *Nuclear Engineering and Design*, Vol. 48, 1978, pp. 405-414.

[105] Galletly, G. D., "Internal Pressure Buckling of Very Thin Torispherical Shells—A Comparison of Experiment and Theory," Paper G2/3 presented at 3rd Smirt Conference, London, 1975.

[106] Galletly, G. D., "Elastic and Elastic-Plastic Buckling of Internally-Pressurized 2:1 Ellipsoidal Shells," *ASME Journal of Pressure Vessel Technology*, Vol. 100, Nov. 1978, pp. 335-343.

[107] Kirk, A. and Gill, S. S., "The Failure of Torispherical Ends of Pressure Vessels due to Instability and Plastic Deformation—An Experimental Investigation," *International Journal of Mechanical Sciences*, Vol. 17, 1975, pp. 525-544.

[108] Patel, P. R. and Gill, S. S., "Experiments on the Buckling under Internal Pressure of Thin Torispherical Ends of Cylindrical Pressure Vessels," *International Journal of Mechanical Sciences*, Vol. 20, 1978, pp. 159-175.

[109] Esztergar, E., "Development of Design Rules for Dished Pressure Vessel Heads," Welding Research Council Bulletin 215, April 1976.

[110] Ketter, R. L., "The Influence of Residual Stresses on the Strength of Structural Members," Welding Research Council Bulletin 44, Nov. 1958.

[111] Almen, J. O. and Black, P. H., *Residual Stresses and Fatigue in Metals*, McGraw-Hill Book Co., Chap. 5, 1963, pp. 46-47.

[112] Queener, C. A. and DeAngelis, R. J., "Elastic Springback and Residual Stresses in Sheet Metal Formed by Bending," *ASM Transactions Quarterly*, Vol. 61, Dec. 1968, pp. 757-768.

[113] Lunchick, M. E., "Influence of Residual Rolling Stresses on the Strength of Cylindrical Pressure Vessels under External Loading," *Transactions of ASME, Journal of Engineering for Industry*, Vol. 92, May 1970, pp. 275-280.

[114] Tacey, R. K., "A Computer Program for Calculation of the Residual Stress Distribution and the Effective Stress-Strain Curve of Cold-formed Structural Members," David W. Taylor Naval Ship Research and Development Center Rept. 76-0141, Nov. 1976.

[115] "Numerical Modeling of Manufacturing Processes," edited by R. F. Jones Jr., H. Armen, and J. T. Fong, Paper PVP-PB-025 presented at ASME Winter Annual Meeting, Atlanta, Ga., 1977.

[116] Masubuchi, K., "Report on Current Knowledge of Numerical Analysis of Stresses, Strains and other Effects Produced by Welding," *Welding in the World*, Vol. 13, No. 11/12, 1975, pp. 271-288.

[117] Hibbitt, H. D. and Marcal, P. V., "A Numerical Thermomechanical Model for the Welding and Subsequent Loading of a Fabricated Structure," *Computers and Structures*, Vol. 3, 1973, pp. 1145-1174.

[118] Nickell, R. E. and Hibbitt, H. D., "Thermal and Mechanical Analysis of Welded Structures," *Nuclear Engineering and Design*, Vol. 32, No. 1, April 1975, pp. 110-120.

[119] Friedman, E., "Thermomechanical Analysis of the Welding Process Using the Finite Element Method," *ASME Journal of Pressure Vessel Technology*, Aug. 1975, pp. 206-213.

[120] Chen, W. F. and Ross, D. A., "Axial Strength and Behavior of Cylindrical Columns," *Proceedings of 8th Annual Offshore Technology Conference*, Houston, Tex., Vol. 3, May 1976, pp. 741-754.

[121] Faulkner, D., "Effects of Residual Stresses on the Ductile Strength of Plane Welded Grillages and of Ring-Stiffened Cylinders," *Journal of Strain Analysis and Engineering Design*, Vol. 12, April 1977, pp. 130-139.

[122] Krenzke, M. A., "Effects of Initial Deflections and Residual Welding Stresses on Elastic Behavior and Collapse Pressure of Stiffened Cylinders Subjected to External Hydrostatic Pressure," David W. Taylor Model Basin, Washington, D.C., Rept. 1327, April 1960.

[123] Bushnell, D., "Effect of Cold Bending and Welding on Buckling of Ring-Stiffened Cylinders," *Computers and Structures*, Vol. 12, 1980, pp. 291-307.

[124] Kirstein, A. F. and Slankard, R. C., "An Experimental Investigation of the Shell-Instability Strength of a Machined, Ring Stiffened Cylindrical Shell under Hydrostatic Pressure Model BR-4A," David W. Taylor Model Basin, Washington, D.C., Rept. 997, April 1956.

[125] Slankard, R. C., "Tests of the Elastic Stability of a Ring-Stiffened Cylindrical Shell, Model BR-4 Subjected to Hydrostatic Pressure," David W. Taylor Model Basin, Washington, D.C., Rept. 876, Feb. 1955.

[126] Von Mises, R., "Der Kritische Aussendruck Fur Allseits Belastete Zylindrische Rohre," *Fest Zurnal 70 Geburstag von Prof. A. Stodola*, Zurich, 1929, pp. 418-430.

[127] Nash, W. A., "Buckling of Thin Cylindrical Shells Subject to Hydrostatic Pressure," *Journal of the Aeronautical Sciences*, Vol. 21, 1954, pp. 354-355.

[128] Galletly, G. D. and Bart, R., "Effects of Boundary Conditions and Initial Out-of-Roundness on the Strength of Thin-Walled Cylinders Subject to External Hydrostatic Pressure," *Journal of Applied Mechanics*, 1956, pp. 351-358.

[129] Singer, J., "The Effect of Axial Constraint on the Instability of Thin Cylindrical Shells under External Pressure," *Journal of Applied Mechanics*, 1960, pp. 737-739.

[130] Sobel, L. H., "Effects of Boundary Conditions on the Stability of Cylinders Subject to Lateral and Axial Pressures," *AIAA Journal*, Vol. 2, Aug. 1964, pp. 1437-1440.

[131] Nachbar, W. and Hoff, N. J., "The Buckling of a Free Edge of an Axially Compressed Circular Cylindrical Shell," *Quarterly Journal of Applied Mathematics*, Vol. XX, 1962, pp. 267-277.

[132] Stein, M., "The Effect on the Buckling of Perfect Cylinders of Prebuckling Deformations and Stresses Induced by Edge Support," *Collected Papers on Instability of Shell Structures—1962*, NASA TN D-1510, 1962, pp. 217-228.

[133] Fischer, G., "Uber Den Einfluss der Gelenkigen Lagerung auf die Stabilitat Dunnwandiger Kreiszylinderschalen unter Axiallast and Innendruck," *Zeitschrift fuer Flugwissenschaften*, Vol. 11, 1963, pp. 111-119.

[134] Almroth, B. O., "Influence on Edge Conditions on the Stability of Axially Compressed Cylindrical Shells," *AIAA Journal*, Vol. 4, Jan. 1966, pp. 134-140.

[135] Hoff, N. J. and Soong, T. C., "Buckling of Circular Cylindrical Shells in Axial Compression," SUDAER Rept. 204, Stanford, Calif., Aug. 1964.

[136] Cohen, G. A., "Buckling of Axially Compressed Cylindrical Shells with Ring-Stiffened Edges," *AIAA Journal*, Vol. 4, Oct. 1966, pp. 1859-1862.

[137] Leonard, R. W., Anderson, M. S., and Heard, W. L. Jr., "Design of a Mars Entry Aeroshell," *Buckling of Structures* (IUTAM Symposium, Cambridge, Mass., June 1974), Springer-Verlag, Berlin, Heidelberg, New York, 1976, pp. 346-364.

[138] Stuhlman, C. E., Deluzio, A., and Almroth, B., "Influence of Stiffener Eccentricity and End Moment on Stability of Cylinders in Compression," *AIAA Journal*, Vol. 4, May 1966, pp. 872-877.

[139] Weller, T., Singer, J., and Batterman, S. C., "Influence of Eccentricity of Loading on Buckling of Stringer-Stiffened Cylindrical Shells," *Thin-Shell Structure, Theory, Experiment and Design*, edited by Y. C. Fung and E. E. Sechler, Prentice-Hall, Englewood Cliffs, N.J., 1974, pp. 305-324.

[140] Singer, J. and Rosen, A., "Influence of Boundary Conditions on the Buckling of Stiffened Cylindrical Shells," *Buckling of Structures* (Proceedings of IUTAM Symposium, Cambridge, Mass., June 1974), Springer-Verlag, Berlin, Heidelberg, New York, 1976, pp. 227-250.

[141] Singer, J. and Abramovich, H., "Vibration Techniques for Definition of Practical Boundary Conditions in Stiffened Shells," *AIAA Journal*, Vol. 17, July 1979, pp. 762-769.

[142] Wang, R. L., "Effects of Edge Restraint on the Stability of Spherical Caps," *AIAA Journal*, Vol. 4, April 1966, pp. 718-719.

[143] Bushnell, D., "Buckling and Vibration of Ring-Stiffened Segmented Shells of Revolution—Numerical Results," *Proceedings of 1st ASME International Pressure Vessel Conference, Part 1: Design and Analysis*, 1969, ASME, New York, pp. 255-268.

[144] Reissner, E., "The Effect of Transverse Shear Deformation on the Bending of Elastic Plates," *Journal of Applied Mechanics*, Vol. 12, June 1945, pp. A69-A77.

[145] Mindlin, R. D., "Influence of Rotary Inertia and Shear on Flexural Motions of Isotropic Elastic Plates," *Journal of Applied Mechanics*, Vol. 18, June 1945, pp. 31-38.

[146] Srinivas, S. and Rao, A. K., "Buckling of Thin Rectangular Plates," *AIAA Journal*, Vol. 7, Aug. 1969, pp. 1645-1646.

[147] Noor, A. K., "Stability of Multilayered Composite Plates," *Fibre Science and Technology*, Vol. 8, 1975, pp. 81-89.

[148] Sharifi, P., "Nonlinear Buckling Analysis of Composite Shells," *AIAA Journal*, Vol. 13, June 1975, pp. 729-734.

[149] Sharifi, P. and Yates, D. N., "Nonlinear Thermo-Elastic-Plastic and Creep Analysis by the Finite Element Method," *AIAA Journal*, Vol. 12, Sept. 1974, pp. 1210-1215.

[150] Kuhn, P., *Stresses in Aircraft and Shell Structures*, McGraw-Hill Book Co., New York, 1956.

[151] Skogh, J. and Stern, P., "Postbuckling Behavior of a Section of a Section Representative of the B-1 Aft Intermediate Fuselage," AFFDL-TTR-73-63, May 1973.

[152] Baruch, M. and Singer, J., "Effect of Eccentricity of Stiffeners on the General Instability of Stiffened Cylindrical Shells under Hydrostatic Pressure," *Journal of Mechanical Engineering Science*, Vol. 5, No. 1, March 1963, pp. 23-27.

[153] Bushnell, D., "Evaluation of Various Analytical Models for Buckling and Vibration of Stiffened Shells," *AIAA Journal*, Vol. 11, Sept. 1973, pp. 1283-1291.

[154] Viswanathan, A. V., Soong, T. C., and Miller, R. E. Jr., "Buckling Analysis for Axially Compressed Flat Plates, Structural Sections, and Stiffened Plates Reinforced with Laminated Composites," NASA CR-1887, 1971.

[155] Wittrick, W. H., "A Unified Approach to the Initial Buckling of Stiffened Panels in Compression," *The Aeronautical Quarterly*,

Aug. 1968, pp. 265-283.

[156] Bushnell, D., "Stress, Buckling, and Vibration of Prismatic Shells," *AIAA Journal*, Vol. 9, Oct. 1971, pp. 2004-2013.

[157] Agarwal, B. and Davis, R. C., "Minimum-Weight Designs for Hat-Stiffened Composite Panels under Uniaxial Compression," NASA TN D-7779, Nov. 1974.

[158] Williams, F. W., "Computation of Natural Frequencies and Initial Buckling Stresses of Prismatic Plate Assemblies," *Journal of Sound and Vibration*, Vol. 21, No. 1, 1972, pp. 87-106.

[159] Przemieniecki, J. S., "Finite-Element Structural Analysis of Local Instability," *AIAA Journal*, Vol. 11, Jan. 1973, pp. 33-39.

[160] Carri, R. L. and Herring, W. H., "Compression Strength of Titanium Alloy Skin-Stringer Panels Selectively Reinforced with Boron-Aluminum Composite," AIAA Paper 72-359, San Antonio, Tex., 1972.

[161] Libove, C., "Survey of Recent Work on the Analysis of Discretely Attached Corrugated Shear Webs," AIAA Paper 72-354, San Antonio, Tex., 1972.

[162] Wittrick, W. H. and Williams, F. W., "Buckling and Vibration of Anisotropic or Isotropic Plate Assemblies under Combined Loadings," *International Journal of Mechanical Sciences*, Vol. 16, April 1974, pp. 209-239.

[163] Williams, J. G. and Stein, M., "Buckling Behavior and Structural Efficiency of Open-Section Stiffened Composite Compression Panels," *AIAA Journal*, Vol. 14, Nov. 1976, pp. 1618-1626.

[164] Anderson, M. S. and Stroud, W. J., "General Panel Sizing Computer Code and its Application to Composite Structural Panels," *AIAA Journal*, Vol. 17, Aug. 1979, pp. 892-897.

[165] Vanderplaats, G. N. and Moses, F., "Structural Optimization by Method of Feasible Directions," *Computers and Structures*, Vol. 3, July 1973, pp. 739-755.

[166] van der Neut, A., "Overall Buckling of Z-Stiffened Panels in Compression," Delft University of Technology, Delft, the Netherlands, Rept. LR-303, Aug. 1980.

[167] Bushnell, D., "PANDA—Interactive Computer Program for Preliminary Minimum Weight Design of Composite or Elastic-Plastic, Stiffened, Cylindrical Panels and Shells under Combined Loads," Lockheed Missiles & Space Co., Palo Alto, Calif., Rept. LMSC-D767794, March 1981.

[168] Tvergaard, V., "Buckling Behavior of Plate and Shell Structures," *Theoretical and Applied Mechanics*, edited by W. T. Koiter, North-Holland Publishing Co., New York, 1976, pp. 233-247.

[169] Bijlaard, P. P. and Fisher, G. P., "Column Strength of H-sections and Square Tubes in Postbuckling Range of Component Plates," NASA TN 2994, 1953.

[170] Koiter, W. T. and Skaloud, M., "Interventions," *Comportement Postcritique des Plaques Utilisees en Construction Metallique*, Colloque intern. a l'Universite de Liege, Memoires de la Societe Royale des Sciences de Liege, 5me serie, tome VIII, fasc. 5, 1962, pp. 64-68, 103, 104.

[171] van der Neut, A., "The Interaction of Local Buckling and Column Failure of Thin-walled Compression Members," *Proceedings of the Twelfth International Congress of Applied Mechanics*, edited by M. Hetenyi, and W. G. Vincenti, Springer-Verlag, Berlin, Heidelberg, New York, 1969, pp. 389-399.

[172] Thompson, J.M.T. and Lewis, G. M., "On the Optimum Design of Thin-walled Compression Members," *Journal of the Mechanics and Physics of Solids*, Vol. 20, 1972, pp. 101-109.

[173] Crawford, R. F. and Hedgepeth, J. M., "Effects of Initial Waviness on the Strength and Design of Built-up Structures," *AIAA Journal*, Vol. 13, May 1975, pp. 672-675.

[174] Maquoi, R. and Massonnet, C., "Interaction Between Local Plate Buckling and Overall Buckling in Thin-walled Compression Members," *Buckling of Structures*, edited by B. Budiansky, Springer-Verlag, Berlin, Heidelberg, New York, 1976, pp. 365-382.

[175] Graves Smith, T. R., "The Effect of Initial Imperfections on the Strength of Thin-walled Box Columns," *International Journal of Mechanical Sciences*, Vol. 13, 1971, pp. 911-925.

[176] Tvergaard, V., "Inperfection-Sensitivity of a Wide Integrally Stiffened Panel under Compression," *International Journal of Solids & Structures*, Vol. 9, 1973, pp. 177-192.

[177] Tvergaard, V., "Influence of Post-Buckling Behavior on Optimum Design of Stiffened Panels," *International Journal of Solids & Structures*, Vol. 9, 1973, pp. 1519-1534.

[178] Koiter, W. T. and Pignataro, M., "An Alternative Approach to the Interaction between Local and Overall Buckling in Stiffened Panels," *Buckling of Structures*, edited by B. Budiansky, Springer-Verlag, Berlin, Heidelberg, New York, 1976, pp. 133-148 (see also, "A General Theory for the Interaction Between Local and Overall Buckling of Stiffened Panels," *Problemi Attuali Di Meccanica Teorica e Applicata*, Torino, Italy, 1977, pp. 179-222).

[179] van der Neut, "Mode Interaction with Stiffened Panels," *Buckling of Structures*, edited by B. Budiansky, Springer-Verlag, Berlin, Heidelberg, New York, 1976, pp. 117-132.

[180] Thompson, J.M.T., Tulk, J. D., and Walker, A. C., "An Experimental Study of Imperfection-Sensitivity in the Interaction Buckling of Stiffened Plates," *Buckling of Structures,* edited by B. Budiansky, Springer-Verlag, Berlin, Heidelberg, New York, 1976, pp. 149-159.

[181] Byskov, E. and Hutchinson, J. W., "Mode Interaction in Axially Stiffened Cylindrical Shells," *AIAA Journal*, Vol. 15, July 1977, pp. 941-948.

[182] Harris, L. A., Suer, H. S., Skene, W. T., and Benjamin, R. J., "The Stability of Thin-Walled Unstiffened Circular Cylinders under Axial Compression Including the Effects of Internal Pressure," *Journal of the Aeronautical Sciences*, Vol. 24, Aug. 1957, pp. 587-596.

[183] Almroth, B. O., Burns, A. B., and Pittner, E. V., "Design Criteria for Axially Loaded Cylindrical Shells," Lockheed Missiles & Space Co., Palo Alto, Calif., Rept. 6-78-69-22, April 1969.

[184] Almroth, B. O. and Bushnell, D., "Computer Analysis of Various Shells of Revolution," *AIAA Journal*, Vol. 6, Oct. 1968, pp. 1848-1855.

[185] Bushnell, D., "Stress, Buckling, and Vibration of Hybrid Bodies of Revolution," *Computers & Structures*, Vol. 7, 1977, pp. 517-537.

[186] Bushnell, D., Holmes, A.M.C., and Loss, E. J., "Failure of Axially Compressed Frangible Joints in Cylindrical Shells," *Proceedings of 20th AIAA/ASME Structures, Structural Dynamics, and Materials Conference*, April 1979, pp. 145-157 (see also *Computers & Structures*, Vol. 12, 1980, pp. 193-210).

[187] Bushnell, D. and Yamamura, T. T., "BOSOR6 Analysis of the IUS Interstage Super-Zip Joint," Lockheed Missiles & Space Co., Palo Alto, Calif., Rept. LMSC-D626721, July 1978.